

TA7  
W34  
no.  
DRP-91-1  
rept. 1  
c. 3

Army Corps  
Engineers

# DREDGING RESEARCH PROGRAM

TECHNICAL REPORT DRP-91-1

## NMLONG: NUMERICAL MODEL FOR SIMULATING THE LONGSHORE CURRENT

Report 1

### MODEL DEVELOPMENT AND TESTS

US-CE-C PROPERTY OF THE  
UNITED STATES GOVERNMENT

by

Nicholas C. Kraus

Coastal Engineering Research Center

DEPARTMENT OF THE ARMY

Waterways Experiment Station, Corps of Engineers  
3909 Halls Ferry Road, Vicksburg, Mississippi 39180-6199

and

Magnus Larson

Department of Water Resources Engineering

Lund Institute of Technology

University of Lund

Box 118, Lund, Sweden S-221 00



June 1991

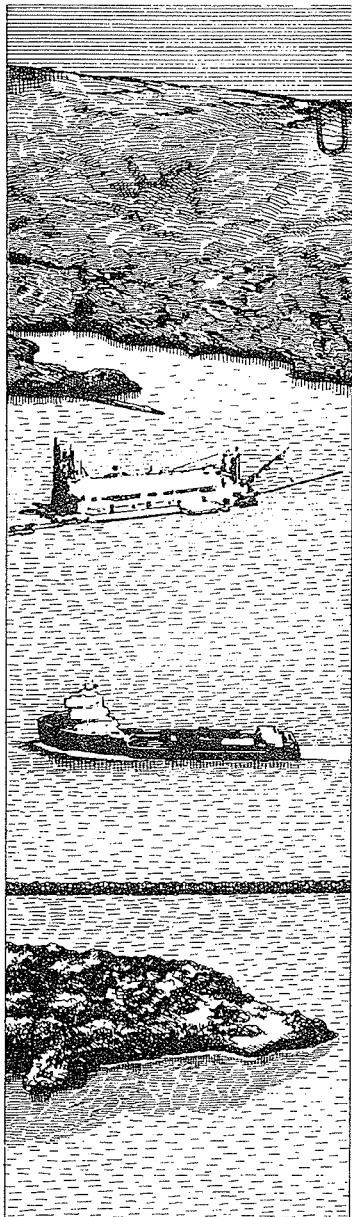
Report 1 of a Series

Approved For Public Release; Distribution Unlimited

RESEARCH LIBRARY  
US ARMY ENGINEER WATERWAYS  
EXPERIMENT STATION  
VICKSBURG, MISSISSIPPI

Prepared for DEPARTMENT OF THE ARMY  
US Army Corps of Engineers  
Washington, DC 20314-1000

Under Work Unit 32463



The Dredging Research Program (DRP) is a seven-year program of the US Army Corps of Engineers. DRP research is managed in these five technical areas:

- Area 1 - Analysis of Dredged Material Placed in Open Waters
- Area 2 - Material Properties Related to Navigation and Dredging
- Area 3 - Dredge Plant Equipment and Systems Processes
- Area 4 - Vessel Positioning, Survey Controls, and Dredge Monitoring Systems
- Area 5 - Management of Dredging Projects

Destroy this report when no longer needed. Do not return  
it to the originator.

The contents of this report are not to be used for  
advertising, publication, or promotional purposes.  
Citation of trade names does not constitute an official  
endorsement or approval of the use of such  
commercial products.

USACEWES



3 5925 00236 3221

24270503

TAY  
W3H  
no. DRP-91-1  
Sept. 1

REPORT DOCUMENTATION PAGE			Form Approved <i>C.3</i> OMB No. 0704-0188	
Public reporting burden for this collection of information is estimated to average 1 hour per response, including the time for reviewing instructions, searching existing data sources, gathering and maintaining the data needed, and completing and reviewing the collection of information. Send comments regarding this burden estimate or any other aspect of this collection of information, including suggestions for reducing this burden, to Washington Headquarters Services, Directorate for Information Operations and Reports, 1215 Jefferson Davis Highway, Suite 1204, Arlington, VA 22202-4302, and to the Office of Management and Budget, Paperwork Reduction Project (0704-0188), Washington, DC 20503.				
1. AGENCY USE ONLY (Leave blank)	2. REPORT DATE June 1991	3. REPORT TYPE AND DATES COVERED Report 1 of a Series		
4. TITLE AND SUBTITLE NMLONG: Numerical Model for Simulating the Longshore Current; Report 1, Model Development and Tests		5. FUNDING NUMBERS DRP Work Unit 32463		
6. AUTHOR(S) Nicholas C. Kraus, Magnus Larson				
7. PERFORMING ORGANIZATION NAME(S) AND ADDRESS(ES) See reverse		8. PERFORMING ORGANIZATION REPORT NUMBER Technical Report DRP-91-1		
9. SPONSORING / MONITORING AGENCY NAME(S) AND ADDRESS(ES) US Army Corps of Engineers Washington, DC 20314-1000		10. SPONSORING / MONITORING AGENCY REPORT NUMBER		
11. SUPPLEMENTARY NOTES Available from National Technical Information Service, 5285 Port Royal Road, Springfield, VA 22161.				
12a. DISTRIBUTION / AVAILABILITY STATEMENT Approved for public release; distribution unlimited		12b. DISTRIBUTION CODE		
13. ABSTRACT (Maximum 200 words) <p>This report presents the mathematical formulation and verification of a numerical model that simulates wave transformation and longshore current over a bar and trough beach profile. The model is intended for application on projects involving dredged material berms and other situations where a bar and trough topography prevents use of simple analytic or numerical solutions that are restricted to a uniformly sloping beach. The model is called NMLONG, an acronym that stands for <u>N</u>umerical <u>M</u>odel of the <u>L</u>ongshore current, and it can be conveniently run on a desk-top (personal) computer.</p> <p>The model incorporates all known features of the wave and longshore current system that appear in research-type engineering models run on mainframe computer systems. These features include wave and wind driving, wave breaking and reformation over multiple bar and trough profiles, and lateral mixing. The model also allows choice of linear or quadratic bottom friction and regular or random wave heights as options. The main restriction of the model is longshore uniformity of the waves and beach topography.</p>				
14. SUBJECT TERMS See reverse		(Continued)		
		15. NUMBER OF PAGES 166		
		16. PRICE CODE		
17. SECURITY CLASSIFICATION OF REPORT UNCLASSIFIED	18. SECURITY CLASSIFICATION OF THIS PAGE UNCLASSIFIED	19. SECURITY CLASSIFICATION OF ABSTRACT UNCLASSIFIED	20. LIMITATION OF ABSTRACT	

7. PERFORMING ORGANIZATION NAME(S) AND ADDRESS(ES) (Continued)

DEPARTMENT OF THE ARMY

Waterways Experiment Station, Corps of Engineers  
3909 Halls Ferry Road, Vicksburg, MS 39180-6199

Department of Water Resources Engineering  
Lund Institute of Technology  
Box 118, Lund, Sweden S-221 00

13. ABSTRACT (Continued)

The model was verified with several field and laboratory data sets. The wave calculation reproduced cross-shore heights of laboratory monochromatic waves on both plane-sloping and bar and trough profiles, and it also reproduced field measurements of wave height frequency of occurrence at different depths in the surf zone. The longshore current model reproduced measured currents on plane-sloping laboratory beaches and currents measured in the field or irregular bottoms. Sensitivity analyses examined linear and nonlinear bottom friction formulations, strength of lateral mixing, effect of wind on setup/setdown and the current, and wave-current interaction.

14. SUBJECT TERMS (Continued)

Breaking waves	Longshore current	Wave setup
Lateral mixing	Numerical model	Wind-generated currents
Longshore bars	Surf zone	Wind setup

## PREFACE

This study was conducted jointly at the Coastal Engineering Research Center (CERC), US Army Engineer Waterways Experiment Station (WES), and the Department of Water Resources Engineering (DWRE), Lund Institute of Technology, University of Lund (UL), Sweden. The work described herein was authorized as part of the Dredging Research Program (DRP) of Headquarters, US Army Corps of Engineers (HQUSACE), and performed under the Calculation of Boundary Layer Properties (Noncohesive Sediments) Work Unit 32463, which is part of DRP Technical Area 1, Analysis of Dredged Material Placed in Open Water. Messrs. Robert Campbell and Glenn R. Drummond were DRP Chief and TAl Technical Monitors from HQUSACE, respectively. Mr. E. Clark McNair, Jr., CERC, was DRP Program Manager (PM), and Dr. Lyndell Z. Hales, CERC was Assistant PM. Dr. Nicholas C. Kraus, Senior Scientist, Research Division (RD), CERC, was Technical Manager for DRP TAl and Principal Investigator for Work Unit 32463.

This study was performed and the report prepared over the period 1 May 1989 through 15 December 1989 by Dr. Kraus and Dr. Magnus Larson, Assistant Professor, DWRE. Initial work on this project by Dr. Larson was conducted during a 2-month study visit at the Technical University of Braunschweig, Hannover, West Germany. Professors H. Führböter and H. Dette were the hosts at the University of Braunschweig. Dr. Kraus was under the administrative supervision of Dr. James R. Houston, Chief, CERC; Mr. Charles C. Calhoun, Jr., Assistant Chief, CERC; and Mr. H. Lee Butler, Chief, RD, CERC. This report benefitted from reviews by Mr. Bruce A. Ebersole, Chief, Coastal Processes Branch (CPB), RD; Mr. Andrew W. Garcia, Prototype Measurement and Analysis Branch, Engineering Development Division, CERC; and Ms. Jane McKee Smith, Oceanography Branch, RD. Dr. William Dally, Florida Institute of Technology, provided helpful review of some sections. Ms. Holley Messing, RD, assisted in equation and text formatting. Ms. Lee T. Byrne, Information Technology Laboratory, WES, edited the final report.

COL Larry B. Fulton, EN, was Commander and Director of WES. Dr. Robert W. Whalin was Technical Director.

Additional information can be obtained from Mr. E. Clark McNair, Jr., Program Manager, at (601) 634-2070 or Dr. Nicholas C. Kraus, Principal Investigator, at (601) 634-2018.

## CONTENTS

	<u>Page</u>
PREFACE . . . . .	1
LIST OF TABLES . . . . .	4
LIST OF FIGURES . . . . .	5
SUMMARY . . . . .	6
PART I: INTRODUCTION . . . . .	7
Problem Statement and Objectives . . . . .	7
Model Design Requirements . . . . .	9
Report Contents . . . . .	10
PART II: LITERATURE REVIEW . . . . .	11
Overview . . . . .	11
Terminology . . . . .	12
Field Observations . . . . .	13
Analytic Solutions . . . . .	19
Numerical Solutions . . . . .	26
PART III: WAVE MODEL . . . . .	31
Overview of Wave Model . . . . .	31
Governing Equations for the Wave Model . . . . .	35
Numerical Solution Scheme . . . . .	42
PART IV: VERIFICATION OF WAVE MODEL . . . . .	48
Large Wave Tank Data Simulations . . . . .	48
Random Wave Simulations . . . . .	53
PART V: LONGSHORE CURRENT MODEL . . . . .	62
Governing Equations for Nearshore Currents . . . . .	62
Governing Equations for Longshore Current and Setup . . . . .	69
Evaluation of Bottom Friction . . . . .	70
Approximation to the Nonlinear Solution . . . . .	74
Evaluation of the Wind Drag Coefficient . . . . .	77
Numerical Solution of the Longshore Current Equation . . . . .	82
PART VI: VERIFICATION OF LONGSHORE CURRENT MODEL . . . . .	89
Laboratory Data from Visser (1982) . . . . .	90
Field Data from Kraus and Sasaki (1979) . . . . .	99
Field Data from Thornton and Guza (1986) . . . . .	104
Hypothetical Case from Ebersole and Dalrymple (1980) . . . . .	115
Longshore Current Driven by Wind . . . . .	117
Wave-Current Interaction . . . . .	124

PART VII: SUMMARY AND CONCLUSIONS . . . . .	130
Modeling System Capabilities . . . . .	130
Fundamental Processes . . . . .	132
Future Work . . . . .	134
REFERENCES . . . . .	135
APPENDIX A: NISHIMURA'S SQUARE-WAVE APPROXIMATION . . . . .	A1
APPENDIX B: SUMMARY OF DATA USED IN THE SIMULATIONS . . . . .	B1
Laboratory Data from Visser (1982) . . . . .	B1
Field Data From Kraus and Sasaki (1979) . . . . .	B5
Field Data From Thornton and Guza (1986) . . . . .	B5
Barred Profile of Ebersole and Dalrymple (1980) . . . . .	B9
APPENDIX C: NOTATION . . . . .	C1

LIST OF TABLES

<u>No.</u>		<u>Page</u>
1	Capabilities of Selected Analytic Longshore Current Models . . . . .	21
2	Capabilities of Selected Numerical Longshore Current Models . . . . .	27
3	Summary of Experimental Cases from Visser (1982) . . . . .	91
4	Optimal Model Parameters for the Visser (1982) Cases . . . . .	92
5	Wave Conditions from the Thornton and Guza (1986) Data . . . . .	105
6	Optimum Parameter Values for the Thornton and Guza (1986) Data . . . . .	106
B1	Visser (1982) Case 1: Slope 0.101 . . . . .	B1
B2	Visser (1982) Case 3: Slope 0.101 . . . . .	B2
B3	Visser (1982) Case 4: Slope 0.050 . . . . .	B3
B4	Visser (1982) Case 7: Slope 0.050 . . . . .	B4
B5	Kraus and Sasaki (1979) Field Data . . . . .	B5
B6	Thornton and Guza (1989) Field Measurements of 3 February . . . . .	B6
B7	Thornton and Guza (1989) Field Measurements of 4 February . . . . .	B7
B8	Thornton and Guza (1989) Field Measurements of 5 February . . . . .	B8
B9	Thornton and Guza (1989) Field Measurements of 6 February . . . . .	B9
B10	Barred Profile of Ebersole and Dalrymple (1980) . . . . .	B10

LIST OF FIGURES

<u>No.</u>		<u>Page</u>
1	Definition sketch for wave and wind direction . . . . .	36
2	Definition sketch for the numerical grid . . . . .	42
3	Comparison for CRIEPI Case 3-1 . . . . .	50
4	Comparison for CRIEPI Case 3-4 . . . . .	51
5	Comparison for CRIEPI Case 4-4 . . . . .	52
6	Comparison for CRIEPI Case 5-2 . . . . .	53
7	Monte-Carlo simulation of Rayleigh wave height distribution . . . . .	57
8	Comparison between measured and calculated $H_{rms}$ . . . . .	59
9	Calculated and measured wave height probability density functions . . . . .	60
10	Comparison of linear and quadratic bottom friction . . . . .	73
11	Correction factor for nonlinear friction term . . . . .	75
12	Wind-induced longshore current versus wind velocity . . . . .	81
13	Definition sketch for longshore current calculation . . . . .	84
14	Model simulations for Visser (1982) Case 1 . . . . .	93
15	Model simulations for Visser (1982) Case 3 . . . . .	96
16	Model simulations for Visser (1982) Case 4 . . . . .	97
17	Model simulations for Visser (1982) Case 7 . . . . .	98
18	Simulations for the Kraus and Sasaki (1979) data; linear model . . . . .	101
19	Simulations for the Kraus and Sasaki (1979) data; nonlinear model . . . . .	104
20	Simulations for Thornton and Guza (1986) data (3 February) . . . . .	108
21	Simulations for Thornton and Guza (1986) data (4 February) . . . . .	110
22	Simulations for Thornton and Guza (1986) data (5 February) . . . . .	111
23	Simulations for Thornton and Guza (1986) data (6 February) . . . . .	112
24	Influence of lateral mixing for a barred profile . . . . .	116
25	Model simulations for a barred profile . . . . .	117
26	Effect of wind on the longshore current (plane beach) . . . . .	119
27	Effect of wind on the longshore current (barred profile) . . . . .	121
28	Simulation of wind-induced setup and setdown . . . . .	123
29	Wave-current interaction on a plane-sloping beach . . . . .	125
30	Wave-current interaction on a barred beach . . . . .	127
31	Evaluation of the wave-current interaction . . . . .	128
A1	Evaluation of the square-wave approximation . . . . .	A4

## SUMMARY

This report presents the mathematical formulation and verification of a numerical model that simulates wave transformation and longshore current over a bar and trough profile. The model is intended for application on projects involving dredged material berms and other situations where a bar and trough topography prevents use of simple analytic or numerical solutions that are restricted to a uniformly sloping beach. The model is called NMLONG, an acronym that stands for Numerical Model of the LONGshore current, and it can be conveniently run on a desk-top (personal) computer.

The model incorporates all known features of the wave and longshore current system that appear in research-type engineering models run on main-frame computer systems. These features include wave and wind driving, wave breaking and reformation over multiple bar and trough profiles, and lateral mixing. The model also allows choice of linear or quadratic bottom friction and regular or random wave heights as options. The main restriction of the model is longshore uniformity of the waves and beach topography.

The model was verified with several field and laboratory data sets. The wave calculation reproduced cross-shore heights of laboratory monochromatic waves on both plane-sloping and bar and trough profiles, and it also reproduced field measurements of wave height frequency of occurrence at different depths in the surf zone. The longshore current model reproduced measured currents on plane-sloping laboratory beaches and currents measured in the field on irregular bottoms. Sensitivity analyses examined linear and nonlinear bottom friction formulations, strength of lateral mixing, effect of wind on setup/setdown and the current, and wave-current interaction.

Several time-saving algorithms were developed that enable NMLONG to run effectively on a personal computer. The model also contains an interface that allows data entry and graphical display of results similar to a commercial software product. Range checking of input data and default values of principal model parameters is also provided. The graphical output consists of the beach profile and the wave height and longshore current velocity along the profile. Output data files include the wave height, wave direction, longshore current velocity, and water surface elevation (wave- and wind-induced setup and setdown) across the beach profile.

NMLONG: NUMERICAL MODEL FOR SIMULATING THE LONGSHORE CURRENT  
MODEL DEVELOPMENT AND TESTS

PART I: INTRODUCTION

Problem Statement and Objectives

1. The longshore current is a major and pervasive flow in the near-shore, and estimates of its velocity are needed in most coastal engineering projects involving sediment transport, such as navigation channel maintenance and shore protection. The distribution of the longshore current across the nearshore zone depends on many factors that are described in detail in this report. This distribution is complex and typically has one or more peaks, for example, one peak just shoreward of the wave breaker line and another on the foreshore.

2. One of the major purposes for calculating the longshore current is to estimate the cross-shore distribution of the longshore sand transport rate. For example, the amount of sand transported around the tip of a jetty and, conversely, the amount impounded by the jetty correspond with the profile of the longshore current. If average and seasonal trends in the current and sand transport patterns at the jetty can be established, channel dredging and sand bypassing schedules and resources can be more accurately planned. In general, beach evolution is controlled by spatial and temporal changes in the longshore sand transport rate, which are directly related to changes in the longshore current velocity.

3. On many beaches, longshore bars and troughs appear at intervals offshore and follow the coast at almost fixed distances from the shore. If a coast has a rich sand supply, a large bar will tend to form at the mouths of inlets and harbor entrances. These bars are created in part by the sand transported along the coast by the longshore current and have been hypothesized to act as conduits of sand around inlets and entrances. Longshore sand transport is thus a major factor in navigation channel infilling and bypassing of sand around inlets and entrances. An estimate of the transport rate requires knowledge of the cross-shore distribution of the longshore current.

4. In recent years, the concept of placing dredged material in the nearshore in the form of shore-parallel longshore bars or "underwater berms" has been advanced as a beneficial use of dredged material for shore protection and also as a means to reduce dredging costs (Murden 1988, McLellan 1990). Such berms may act to break erosive storm waves and, possibly, serve as a source of beach nourishment. It is necessary to know the properties of the longshore current profile over these bar and trough features both to understand the nearshore hydrodynamic environment and to estimate the longshore sand transport rate and evolution of these bars.

5. The above overview of common coastal engineering situations involving longshore sand transport leads to an appreciation that realistic calculation of the longshore current can be made only under the general conditions of arbitrary bottom topography (necessarily restricted to be uniform alongshore in the present study, as is discussed in the following two chapters) and arbitrary waves, wind, and water level. Both waves and wind are driving forces of the longshore current, and both can change the water level near the shore. On a barred bottom topography, waves may break, reform, and break again, implying the existence of a multi-peaked distribution of the longshore current across the surf zone and a corresponding multi-peaked distribution of the longshore sand transport rate. The independent actions of wind and waves can either positively or negatively reinforce in generating the current, again creating a complex current profile.

6. The main objective of the present study is development of a numerical model of the longshore current applicable to nearshore dredged material placement operations involving creation of berms and coastal engineering projects involving longshore currents and longshore sand transport. An additional objective is to bring the developed technology to the desk of the engineer or planner in the form of a convenient computer program that can be easily run on a desk-top or personal computer. By use of modern mathematical and numerical procedures, the resultant program has the desired generality and reliability; yet because of its structured interface and graphical output, it is more convenient than following a handbook procedure.

## Model Design Requirements

7. The model was developed to satisfy requirements dictated by known and anticipated applications. The following is a list of those requirements:

- a. The model should calculate the longshore current profile over an arbitrary sea bottom of plane and parallel contours. Such a profile could consist of multiple longshore bars and troughs.
- b. The model solution scheme should represent the physical phenomena in the most accurate way consistent with engineering data, uses of the model, and accuracy of the governing equations.
- c. The model should require only readily available or estimated input data.
- d. Both wave and wind forcing should be represented.
- e. The change in mean water level, which enters in the longshore current calculation, should be calculated.
- f. The model should be robust, that is, be numerically stable and provide reliable answers for a wide range of conditions without requiring significant changes in empirical factors entering the model.
- g. The model should be sufficiently flexible to allow ready modification and incorporation of new developments.
- h. The model should be verified with data encompassing a wide range of wave, wind, current, and topographic conditions.
- i. The model should be sufficiently efficient to run on a desk-top computer.

8. These requirements necessarily led to development of a numerical modeling system, called NMLONG for Numerical Model of the LONGshore current, which consists of a wave transformation model and a longshore current model. The basic structure of a wave transformation model meeting the requirements was available from the literature and required minor refinements and extensions, whereas the longshore current model was developed directly from the governing equations, guided by previous work.

9. In the course of model development, a number of fundamental topics were investigated. These include the significance of the wave and current interaction, comparison of the effect of linear and quadratic bottom friction laws, and relative strength of the wind and waves in generating a longshore current.

## Report Contents

10. Part I gives the motivation and objectives of the study. An orientation to the topic of longshore current calculations and review of pertinent studies are presented in Part II. Parts III and IV describe wave model development and verification, respectively, and Parts V and VI similarly pertain to the longshore current model. A summary of main results is given in Part VII. Discussion of the numerical method used to efficiently perform the time average of the nonlinear bottom friction stress is given in Appendix A, and data sets used in model verification are listed in Appendix B.

11. The present report describes model development and tests. Report 2 in the NMLONG series will be a user's guide and description of the implementation of the model on a desk-top computer.

Presentasi ini ya  
harus report 2 esensi  
sari

## LITERATURE REVIEW

### verview

description of the longshore current, which circulation, was independently and simultaneously Longuet-Higgins (1970a, b) and Thornton (1962, 1963, 1964). Because of the importance of this subject in coastal engineering and science, over the past few years many mathematical studies and, to a lesser extent, experimental studies have been conducted to improve understanding of the processes. There is a considerable literature on the subject, which is mostly "classical" in a certain sense; yet

made of the literature on longshore currents by Longuet-Higgins and Coleman 1982, Gourlay 1982, Komar and Phillips 1982. This is so important that new analytic

solutions of the governing equations are published almost yearly. Considerable mathematical ingenuity and clever specification of idealized conditions have gone into development of these solutions. Of all the analytic solutions, the model of Longuet-Higgins (1970a, b) is remarkably insightful yet simple. This model has served as the starting point for a large number of solutions that have removed one or more restrictions from the original model or added new capabilities. As analytic solutions are made more general, however, their evaluation becomes mathematically and computationally complex. The authors believe that numerical models such as described in this report are more computationally efficient than the complex analytic or "exact" solutions and are easier to modify to incorporate improvements. In contrast, a particular analytic solution has very little flexibility to admit change owing to the conditions imposed to obtain that solution.

14. The alternative approach to analytic models of the longshore current is to solve the governing equations numerically. Indeed, in one of the original formulations, Thornton (1970) developed a numerical model and solved the governing differential equations under much less restrictive

conditions than are possible with analytic solutions. Since that time, numerous numerical models of the longshore current have been published.

15. This literature review is divided by calculation approaches, discussing analytic and numerical models separately. It begins by introducing important terminology, concepts, and field observations. The review is not comprehensive in that articles are discussed to compile results important for understanding the background of the problem and assessing the capabilities of previous models and the present model.

### Terminology

16. In this section selected terms that appear in the literature on the longshore current are introduced.

#### Velocity

17. The word "velocity" in a strict sense denotes a vector quantity that has a magnitude (speed) and a direction. In the case of the longshore current, the flow is along the coordinate axis oriented parallel to the coast, and the flow direction can be only positive or negative along this axis. Therefore, the phrase "longshore current velocity" can be used to denote speed with the understanding that the sign gives the direction, since this current is only one component of the velocity of the general two-dimensional (2-D) horizontal circulation pattern. By the same convention, vector symbols are not used in writing equations containing the longshore current velocity.

#### Profile and distribution

18. Another phrase that commonly appears in the literature is "longshore current profile," which refers to the distribution of the depth-averaged current from the mean water shoreline to a point seaward of the breaking wave zone where the wave-induced longshore current becomes negligible (typically one or two times the width of the surf zone). In contrast, referring to the distribution of the wave height across the surf zone as the "wave profile" is not appropriate, because that term normally refers to the form of an individual wave. However, the word "distribution" in reference to wave height can cause confusion because it may also describe the statistical distribution of wave height at a single point, for example, the probability density function of wave height. In this report, both uses of the word "distribution" are

necessary in discussion of the wave height, but in referring to its spatial distribution, the term "wave height distribution across the shore" or similar phrase will be employed.

#### Steady state or mean

19. The model developed in this report and in most studies on the longshore current pertains to the steady-state solution of the governing equations, i.e., time-averaged or mean quantities as opposed to instantaneous quantities. Therefore, unless otherwise stated, reference to the longshore current pertains to the steady or mean longshore current. The temporal or transient behavior of the longshore current has been little studied, although, for example, accelerations and decelerations in the water are expected to be important in mobilizing and moving sand. All modeling studies that calculate the temporal behavior of the longshore current have merely used the time-dependent term in the governing equation to step in time to a steady-state solution without detailed examination of the transient behavior of the current. In engineering approaches to calculating the longshore current, temporal changes in the current have been simulated by moving from one steady-state solution to another in discrete steps. This approach is used here, but in the future the temporal behavior of the current will need to be dealt with more rigorously.

#### Field Observations

20. In this section major concepts and processes pertaining to longshore currents observed in the field are discussed to understand the various phenomena that a mathematical model must describe and potential limitations that may be manifested in such an approach.

#### Nearshore current system

21. The term "nearshore currents" was introduced by Shepard and Inman (1950) to distinguish currents generated directly by incident waves from "coastal currents" associated with the tide and large-scale oceanic circulation systems. In this report the local wind is also taken to be a forcing mechanism of the nearshore current. The nearshore current system consists of the longshore current that flows parallel to the trend of the shore, currents that flow strongly offshore in narrow bands called "rip currents" (Shepard,

Emery, and La Fond 1941), and weaker cross-shore currents that flow onshore and offshore. The boundaries of the nearshore circulation system are dynamic: the shoreward limit is the highest runup in a time-dependent description or the mean shoreline in the case of a time-average description, and the seaward limit is in the vicinity of the seaward-most tip of rip current heads, which extend the length of about two or three widths of the surf zone. The strongest nearshore currents are located in the surf zone, which is the region of intensive depth-limited wave breaking and maximum longshore current speed, and in the throats of rip currents with their strong seaward flow. In the present situation, lateral boundaries are assumed to be located sufficiently distant so as not to influence the wave and current field in the area of interest.

22. On the basis of extensive field observations, Harris (1969) classified nearshore current patterns primarily by the angle of wave incidence as:

- a. Symmetrical and cellular, in which rip currents divide the nearshore into clear cells delineated by rip currents, tending to form under near-normal wave incidence.
- b. Alongshore system, in which the current mainly flows parallel to the shoreline, and tending to form under large oblique angles of wave incidence.
- c. Asymmetrical and cellular, an intermediate pattern between the symmetrical and cellular pattern and the alongshore system, tending to form under moderate angles of wave incidence.

23. From his synoptic field measurements of waves, currents, and bottom bathymetry, Sonu (1972) concluded that the shape of the bottom was an important factor in addition to the angle of wave incidence in controlling the pattern of the nearshore circulation. In a classification scheme similar to that of Harris (1969), Sonu defined a cellular pattern, meandering pattern, and longshore pattern. In a less strict sense, the longshore component of an asymmetrical and cellular (or meandering current) system may be approximated as an alongshore system if an average is taken over sufficiently long time.

#### Longshore uniformity

24. Conditions most favorable for the existence of a longshore current are large angles of wave incidence and relatively uniform bottom contours alongshore. If the contours are not uniform, the nearshore current will necessarily have components directed onshore or offshore. Similarly, if the wave field is not uniform alongshore, the longshore current may reverse or

weaken at points, and the nearshore current pattern may tend to form rip currents with longshore currents serving as "feeder currents" between the rips (Bowen 1969). Although it is not necessary to invoke longshore uniformity in development of a longshore current model (e.g., Komar 1975, Gourlay 1976, Keely and Bowen 1977), it is most realistic and practical to do so. The most important exception in common engineering applications where longshore uniformity is not a good approximation involves diffraction at headlands, detached breakwaters, and long jetties, which creates longshore gradients in wave height and wave angle. These gradients can produce currents of magnitude comparable to that of oblique wave incidence (Gourlay 1976).

#### "Unsteady" steady current

25. Although the concept of a steady longshore current is a convenient construct, it is only an approximate description of the longshore current existing in the field. By using tethered floats configured to reside either near the water surface or near the bottom, Inman and Quinn (1952) measured longshore currents on a Pacific Ocean beach and found that the standard deviation in the current could exceed its mean value. In nature, the forcing conditions, principally the waves but also the wind, are not stationary, and the longshore current shows significant variations in time (Inman and Quinn 1952, Wood and Meadows 1975, Meadows 1976) and along the shore (Keely and Bowen 1977). Guza and Thornton (1978) discuss temporal and spatial variability in their longshore current field measurements, review the literature on the phenomenon, and suggest that large-scale eddy motions and edge waves may be responsible.

#### Long-period waves

26. Surface gravity waves that are visibly observed to arrive at the coast may be classified as short-period waves with a typical period on the order of 10 sec. It is these waves that are taken to be one of the two driving mechanisms of the longshore current in this report, the other driving mechanism being the wind. Other types of wave motion in the nearshore not readily visible to the eye have periods longer than the incident gravity waves. The so-called infragravity waves, wave with periods longer (for example, 100 sec) than gravity waves, are associated with wave groups or surf beat, edge waves, and standing waves. These waves may modulate the longshore

current (Shepard and Inman 1950, Inman and Quinn 1952) but are not expected to greatly change the magnitude of the mean longshore current.

27. Recently, a new type of long wave, called a shear wave or far infragravity wave with a period in the range of 100 to 1,000 sec has been discovered (Bowen and Holman 1990; Oltman-Shay, Howd, and Birkemeier 1990) that may at times contribute to the total longshore current speed which is on the same order as the current produced by oblique (gravity) wave incidence. Shear waves originate from instabilities in the shear in the profile of the steady (mean) wave-induced longshore current discussed in this report. At present, knowledge of the formation and persistence of shear currents is only in its infancy. Since these waves owe their existence to the presence of a longshore current, accurate prediction of the profile of a mean current takes on even greater importance.

#### Paradox of lateral mixing

28. As in other types of hydrodynamic and circulation studies, the term "lateral mixing" refers to the exchange of fluid momentum in the horizontal plane, in the present context perpendicular to the shore. Lateral exchange of momentum mixes water particles having different longshore velocities, thereby smearing the current profile. Significant smoothing of the longshore current profile in the surf zone is expected because of the intense turbulence created by breaking waves, which is advected back and forth by oscillatory wave motion. In mathematical modeling of longshore current profiles generated in carefully performed laboratory experiments with incident waves of constant height, period, and direction, it is necessary to include lateral mixing inside the surf zone as well as outside where the tail of the profile extends substantially seaward. On the other hand, some investigators (e.g., Battjes 1972, Thornton and Guza 1986) have suggested that in the field the combination of waves of different heights and periods from different directions will produce a smooth current profile, greatly reducing the lateral mixing effect, and perhaps eliminating the necessity to include it in models. This observation leads to the "lateral mixing paradox," the fact that in most modeling studies approximately the same strength of lateral mixing has been required to describe longshore currents in the laboratory generated by regular waves as in the field with currents calculated by regular or as, in the present study, random waves.

29. A possible resolution of this paradox may lie in the recent discovery of the shear waves described in the previous section (Bowen and Holman 1990; Oltman-Shay, Howd, and Birkemeier 1990). Bowen and Holman note that the greater cross-shore length scale of a shear wave (order of 50 m) as compared with the depth-limited orbital wave motion of a gravity wave in the surf zone (order of 5 m) suggests that shear waves may be a dominant mixing mechanism, spreading the wave-induced turbulence across the nearshore. Bowen and Holman also state that "wave tank experiments (of the longshore current) may in fact be contaminated with shear wave motions" that cannot be detected by normal means. The presence of shear waves is a plausible reason for the high tails in the longshore current profile seaward of the breaker line found in some laboratory experiments. Other reasons for such high tails are circulation in a closed basin and direct wave-induced lateral mixing combined with the oscillating position of the breakers that occurs even in experiments with regular waves.

#### Effect of wind

30. The wind contributes in at least three ways as a forcing function in nearshore hydrodynamics:

- a. It creates longshore and cross-shore currents.
- b. It changes the mean water level.
- c. It changes the characteristics of the breaking waves, which feed back to the current and water surface changes.

These three processes are discussed in the following paragraphs.

31. Wind and the longshore current. Winds blowing over the sea far from a project site create a portion of the waves that arrive at the site, and these waves may generate a longshore current. Besides generating waves that break and drive currents, the local wind generates currents directly by exerting a shear on the water surface. Nummedal and Finley (1978) performed multiple regression analysis using both linear and nonlinear combinations of observed wave and wind parameters in attempted correlations with the longshore current velocity. The data set encompassed 1 year of visually obtained wind, wave, and current measurements made at Debidue Island, South Carolina, facing the Atlantic Ocean. They found that the longshore component of the wind speed (lagged by 2 to 3 hr between reversals) was the dominant parameter describing the longshore current velocity in the surf zone. Because the local wind also

generates waves, the longshore component of the current contains a contribution from obliquely incident waves, which would tend to raise the correlation. The demonstration by Nummedal and Finley of the significance of wind on the longshore current does not appear to have been adequately appreciated in the coastal engineering and science communities.

32. Everts\* described an experience of SCUBA diving in approximately 13-m depth off the Coastal Engineering Research Center's (CERC's) Field Research Facility (FRF) at Duck, North Carolina, while a fast-moving North-easter approached with a strong longshore wind component. In a matter of minutes after the wind began (order of 10 min), the current went from nondetectable to such a great speed that the divers at the bottom could not maintain position against it. This observation indicates that the lag between longshore current generation by wind and changes in the wind velocity is very short for strong winds blowing over the shallow water of the nearshore.

33. Hubertz (1986) reports measurements of wind, waves, and longshore current made at the FRF. A direct relationship between the mean longshore current and wind speed was found, and Hubertz recommended that meteorological factors be included in longshore current estimation techniques. Hubertz (1984) also performed numerical simulations of the wind- and wave-driven longshore current and found that inclusion of wind forcing significantly improved agreement with the measurements over simulations made using only wave forcing.

34. Wind and water surface elevation. The contribution to the cross-shore momentum equation governing the change in mean water level produced by an imposed wind is well known (e.g., Bretschneider 1966; DeVries and Amorocho 1980). It is included in the present model development together with wave-induced changes in mean water level. The change in water surface elevation will change the width of the surf zone and, therefore, the profile of the longshore current. High-quality correlations between the mean water surface elevation and wind velocity for the nearshore zone of an open coast are not known to the authors, but numerical surge models incorporating wind forcing can well produce water marks occurring during storm inundation. An example of

---

\* Personal Communication, June 1988, Dr. Craig H. Everts, Senior Geologist, Moffat and Nichol, Engineers, Long Beach, CA.

time-dependent change in water surface elevation was given by DeVries and Amorocho (1980) for both ends of a 9.7-km-long, 37-m-wide, and 8.4-m-deep section of the California Aqueduct, which they successfully simulated by using a numerical model. Their study developed a predictive equation for the wind drag coefficient (Amorocho and DeVries 1980) that has been used in coastal applications, but the expression may not be suitable at higher wind speeds due to the restricted fetch in their experiments. Amorocho and DeVries report that setup in the aqueduct was negligible if the wind speed at the 2-m elevation fell below approximately 4 m/sec.

35. Wind and wave breaking. The local wind can modify the characteristics of depth-limited breaking waves, such as breaker height and type (as plunging or spilling). The only quantitative work on this subject known to the authors is that of Douglas and Weggel (1988). For a certain type of wave condition in their physical model experiment, Douglas and Weggel found that a wind blowing offshore decreased the surf zone width by 43 percent due primarily to a lessening of breaking wave depth. Thus, incipient depth-limited breaking waves were able to travel farther through the "support" given by the offshore wind. This phenomenon has not gone unnoticed by surfers who pursue longer rides during days with an offshore-directed breeze. Implications of the effect of the cross-shore component of the wind on wave breaking and the longshore current are profound, since changes in breaking wave type changes the wave energy dissipation and wave height distribution across the shore, thereby changing the longshore current profile. Additionally, a change in surf zone width due to the wind correspondingly changes the width of the current profile and its location in the nearshore. The effect of the wind on wave breaker type and other breaking wave characteristics is not included in the present model.

#### Analytic Solutions

36. Starting from the first analytic solutions for the longshore current profile based on the momentum equations with wave radiation stresses, numerous approximations have been introduced to improve these solutions and extend them to more general situations. Despite the mathematical skill and physical insight that have gone into development of these models, the result

is always an exact mathematical solution of an incomplete formulation of the problem, as is seen in Table 1, which summarizes the capabilities of representative analytic models. It is clear that the analytic models satisfy only a few of the requirements of an engineering model as enumerated in Part I.

37. With proliferation of inexpensive and powerful desk-top computers, the main function of analytic models now lies in promoting understanding of the physics of the phenomenon through compact display of the relationships between the various governing parameters and how they control the current profile. The more elaborate analytic solutions are complex and require evaluation of computation-intensive special functions. Also, matching conditions are required since solutions must be obtained separately seaward and shoreward of the wave break point, the result of an assumed discontinuity in the wave driving force at the break point. Numerical solutions, described in the next section, automatically compute across the breaker line.

38. In the following, selected analytic solutions based on momentum flux concepts are discussed to introduce the important phenomena and to present model capabilities. The discussion is summarized in Table 1, which compares the capabilities of the analytic models ranging from the oldest to the more recent. A similar table will be given for numerical models in the next section. Familiarity with basic surf zone hydrodynamics is assumed, and Part III can be consulted for a review of the governing equations.

39. Discussion is omitted of closed-form solutions for only the mean longshore current velocity, which are obtained by averaging the current profile across the surf zone. Such calculations have been presented by Longuet-Higgins (1970b) for oblique wave incidence, and Komar (1975) and Gourlay (1976, 1982) for oblique wave incidence and longshore variation in wave height (and in wave angle, Keely and Bowen 1977).

40. To obtain closed-form or analytic solutions, truncated power series and perturbation techniques are universally employed, principally to linearize the form of the quadratic bottom friction stress, which is the main retarding force of the current. These procedures introduce mathematical limitations on the range of validity of the solution, since the depth and expansion parameters should formally remain small. Shallow-water approximations to linear-wave theory must also be used to eliminate hyperbolic functions appearing in the equations. Thus, analytic solutions are not only exact solutions of a

Table 1  
Capabilities of Selected Analytic Longshore Current Models

<u>Capability</u>	Model by Author*							
	<u>B</u>	<u>L-H</u>	<u>L&amp;D</u>	<u>K&amp;S</u>	<u>D</u>	<u>T&amp;G</u>	<u>S&amp;K</u>	<u>M&amp;H</u>
Concave beach	--	--	--	--	--	--	--	Yes
Barred beach	--	--	--	--	--	--	--	--
Large wave angles	--	--	Yes	Yes	--	--	Yes	--
Wave refraction	--	--	Yes	Yes	Yes	--	Yes	--
Nonuniform wave height decay	--	--	--	--	--	--	Yes	--
Linear bottom friction (weak current)	Yes	Yes	Yes	Yes	Yes	Yes	Yes	Yes
Nonlinear bottom friction (strong current)	--	--	Yes**	--	--	--	--	--
Lateral mixing	Yes	Yes	--	Yes	--	--	Yes	Yes
Wave-current interaction	--	--	--	--	Yes	--	--	--
Wind driving	--	--	--	--	--	--	--	--
Random wave height	--	--	--	--	--	Yes	--	--
Random wave direction	--	--	--	--	--	--	--	--

\* Key to authors and models: B = Bowen (1969); L-H = Longuet-Higgins (1970a, b); L&D = Liu and Dalrymple (1978); K&S = Kraus and Sasaki (1979); D = Dalrymple (1980); T&G = Thornton and Guza (1986); S&K = Smith and Kraus (1987); M&H = McDougal and Hudspeth (1989).

\*\* Weak current and strong current solutions are different models.

limited-scope problem, but also a mathematically approximate description of the included processes.

41. With reference to Table 1 and for comparison of the capabilities of both analytic and numerical models, limitations found in most analytic models may be summarized as:

- a. Small incident wave angle (approximately less than 20 deg at the breaker line).
- b. Linearized bottom friction stress.
- c. Regular waves (fixed wave height, direction, and period).
- d. Plane-sloping beach.
- e. Wave height proportional to the water depth in the surf zone (for broken waves).
- f. No refraction in the surf zone.
- g. No wind forcing.

Use of shallow-water wave theory, although reducing computation time, is not convenient for general engineering applications because the surf width and depth will vary. In the following discussion, improvements removing one or more restrictions will be noted.

42. The earliest analytic models (Bowen 1969; Longuet-Higgins 1970a, b) demonstrated that the momentum-based formulation led to qualitatively and quantitatively correct shapes and magnitudes of the wave-induced longshore current profile. The leading-order processes were identified as bottom friction and the excess momentum flux or radiation stresses of the waves, with lateral mixing acting primarily to adjust the shape of the profile. The formulation of the bottom friction force was validated with laboratory data, and the order of magnitude of the bottom friction coefficient was determined to be  $10^{-2}$ . In these and in almost all analytic and most numerical models, the time-averaged bottom friction stress is linearized by assuming that the magnitude of the longshore current is much smaller than that of the wave-induced horizontal water particle orbital velocity. Other approximations used in the original models of Bowen (1969) and Longuet-Higgins (1970a, b) include restriction of the waves to small angles, omission of wave refraction in the surf zone, and simplified formulations of the eddy viscosity coefficient. Also, the driving force of wind and the wave-current interaction were omitted.

43. In the Bowen (1969) model, the bottom friction stress was linearized in the longshore current velocity, and both the wave orbital velocity in the bottom friction stress and the eddy viscosity in the lateral mixing term were constant. The resultant solution of the second-order differential equation for the longshore current as a function of the distance across the shore pertains to a uniformly (plane) sloping beach. The solution is expressed in terms of modified Bessel functions and is not easily evaluated without a computer.

44. Longuet-Higgins (1970a) solved for the current profile inside the surf zone by assuming no lateral mixing, obtaining a triangular distribution for the current with a peak at the breaker line. In a companion paper (Longuet-Higgins 1970b), lateral mixing was included with an eddy viscosity coefficient proportional to the distance offshore and the wave orbital speed. A linearized bottom friction stress was used with the wave orbital velocity expressed by shallow-water wave theory. Solution of the resultant second-order ordinary differential equation for the current resulted in a power series of only two terms inside the surf zone and one term for the region seaward of the breaker line. An important dimensionless parameter that emerged controlled the shape of the profile and can be interpreted as expressing the relative strength of lateral mixing and bottom friction.

45. A surprising result in longshore current modeling has been that a linearized friction term provides a good quantitative solution of the current profile even though the assumption is violated in the verification data. Thornton and Guza (1986) and the present work as discussed below have shown that the success of the linear model in describing virtually all field and laboratory data sets owes to the fact that the bottom friction and wave driving force dominate, leading to an approximate correspondence in linear and nonlinear solutions by a reduction in the value of the friction coefficient in the nonlinear friction model as compared with the linear model. Presumably, the value of the bottom friction coefficient pertaining to the nonlinear model is more physically correct.

46. Liu and Dalrymple (1978) examined the functioning and mathematical range of validity of the linear or weak-current and nonlinear or strong-current bottom friction formulations through closed-form solutions for the current profile inside the breaker line, including wave-induced setup but

omitting lateral mixing. Weak-current and strong-current approximations were treated independently to obtain two different solutions. Although the formal validity of the linear and nonlinear bottom friction approximations was demonstrated, their results did not explain the robustness of the linear model achieved by simple scaling of the value of the friction coefficient. Also, the weak-current case of Liu and Dalrymple contains an error producing values of the current at the breaker line that are too small by a factor of about 0.5 (Kraus and Sasaki 1979, Baum and Basco 1986, Miller 1987).

47. Kraus and Sasaki (1979) extended the Longuet-Higgins (1970a, b) solution to include large wave angles, refraction in the surf zone, and the improved lateral mixing description of Madsen, Ostendorf, and Reyman (1978). The model was verified with four laboratory cases of Mizuguchi, Oshima, and Horikawa (1978) and their own field data. By matching the position of the maximum current velocity, the value of the bottom friction coefficient found in the field verification was 0.0061, smaller than the values ranging from 0.011 to 0.024 found for the laboratory cases.

48. Dalrymple (1980) investigated the wave-current interaction in the surf zone associated with wave refraction and larger incident wave angles in an analytic model that omitted lateral mixing. The wave-current interaction was included in Snell's Law governing refraction (wave direction), but was omitted in calculating wave height decay because a simple linear decrease in wave height in constant proportion to the water depth was assumed. Dalrymple found that the interaction lowered the magnitude of the current and noted that conservation of the force on the bottom by the waves implies that the width of the surf zone must correspondingly increase. Dalrymple concluded that the wave-current interaction by refraction was significant (order of 10 percent) only for large incident wave angles. Similarly, Thornton and Guza (1986) found that the refractive effect of the mean current was less than 1 percent for their calculated cases.

49. Thornton and Guza (1986) derived an analytic solution under the conditions of a plane beach, small wave angle, no mixing, and linear bottom friction, but using an analytic random wave height model. Their paper introduces randomness in the wave height in the longshore current calculation in an efficient way and compares model predictions to a high-quality field data set. The model successfully reproduced the measurements of one case of their field

measurements (2 February 1980) by adjustment of the value of the bottom friction coefficient. Thornton and Guza also present numerical models with linear and nonlinear bottom friction representations, discussed in the next section.

50. Smith and Kraus (1987) extended the Kraus and Sasaki (1979) model to include a power law form of the wave height decay (concave up, concave down, or linear with water depth) depending on an empirical coefficient related to the breaker index (ratio of wave height and water depth at incipient breaking) and beach slope. The power law provides a more realistic representation of the wave height distribution across the shore than a simple linear dependence on water depth and was found to control the shape of the current profile in the surf zone similar to lateral mixing. This result indicates that more accurate representation of wave height decay will change the values of the bottom friction coefficient and lateral mixing strength. Miller (1987) developed a similar capability in a more complex analytic solution using an exponential wave height decay. Smith and Kraus (1988) investigated wind driving in an analytic wave- and wind-generated longshore current model, but found it infeasible because of a discontinuity in the solution at the shoreline.

51. Leont'ev (1988) developed analytic solutions for random wave height decay in the surf zone and the resultant longshore current for both plane-sloping beaches and beaches having a bar and trough. Previous analytic models of wave breaking and longshore currents were also reviewed. Leont'ev verified his random height model against the bar-trough laboratory data of Battjes and Janssen (1978).

52. McDougal and Hudspeth (1989) developed an analytic solution for a planar slope on the foreshore joining to a concave bottom profile. A concave-sloped beach, which is more realistic representation of the typical beach profile, was found to have the peak in the longshore current located more shoreward than on a planar slope. Their solution is relatively complicated and is expressed in terms of special functions involving matching conditions both at the slope intersection and the breaker line.

## Numerical Solutions

53. A large number of numerical models of the wave-induced nearshore circulation have been developed since the first comprehensive model of this type introduced by Noda (1974). These models solve for the horizontal circulation and water surface elevation on a 2-D grid by using either a finite-difference or finite-element solution approach. Two-dimensional models are extremely expensive to run as compared with one-dimensional (1-D) models such as presented here, but are necessary to calculate wave and current conditions on irregular sea bottoms. Two-dimensional models are computation expensive for two reasons. First, calculations must be performed for  $N^2$  grid points as opposed to  $N$  points for a 1-D model, where  $N$  is the representative number of grid points in the x- and y-directions. Second, 2-D models typically reach the steady-state solution by stepping through time, requiring on the order of 200 to 500 iterations over the grid for a general, new condition. ("Hot starts" can be made if the solution for a similar condition is available, which reduces the number of iterations somewhat, although instabilities can sometimes occur with this procedure.) In contrast, 1-D solutions can operate directly with the steady-state equations of motion, requiring as little as one pass or iteration on  $N$  grid points with the particular solution scheme for a linearized model or, for example, typically 4 to 8 iterations for the present model in nonlinear form. In the following, discussion will focus on representative models listed in Table 2.

54. Thornton (1970) developed a numerical model that included lateral mixing and the bottom friction coefficient of Jonsson (1966). Although the model in principle could be applied to an arbitrary bottom topography, in practice it was limited by a simple wave height decay model that depends on a constant wave-height to water-depth ratio in the surf zone. There was only one empirical parameter, the bottom roughness, and model predictions agreed with laboratory measurements and approximate field measurements. Details of the numerical solution method were not given.

55. Jonsson, Skovgaard, and Jacobsen (1974) developed a numerical model with a sophisticated numerical solution scheme that is probably not warranted for engineering application considering the empiricism of the formulation and the accuracy of input data. An interesting feature of the development was use

Table 2

Capabilities of Selected Numerical Longshore Current Models

<u>Capability</u>	<u>Model by Author*</u>							<u>Present Model</u>
	<u>T</u>	<u>JSJ</u>	<u>V</u>	<u>WTG</u>	<u>BB</u>	<u>H</u>	<u>S</u>	
Barred beach	--	--	--	Yes	Yes	--	?	Yes
Large wave angles	Yes	Yes	Yes	Yes	Yes	Yes	Yes	Yes
Wave refraction	Yes	Yes	Yes	Yes	Yes	Yes	Yes	Yes
Nonuniform wave height decay	--	--	--	--	Yes	--	?	Yes
Nonlinear bottom friction	--	Yes	Yes	--	--	Yes	Yes	Yes
Lateral mixing	Yes	Yes	Yes	Yes	Yes	--	--	Yes
Wave-current interaction	--	--	Yes	--	--	--	Yes	Yes
Wind driving	--	--	--	--	--	Yes	--	Yes
Random wave height	--	--	--	--	--	Yes	Yes	Yes
Estimate of calc. efficiency	?	Med	Med	Low	Med	Low	Med	High

\* Key to authors and models: T = Thornton (1970); JSJ = Jonsson, Skovgaard, and Jacobsen (1974); V = Visser (1984a); Wu, Thornton, and Guza (1985); BB = Baum and Basco (1986); H = Hubertz (1987); S = Southgate (1989).

of a combined wave and current friction factor.

56. Visser (1984a, b) presented a numerical model "aimed to be more reliable than existing ones" through calibration with his careful laboratory measurements (Visser 1982) involving seven cases. Four of the cases are used in model testing in the present study. The Visser model includes a nonlinear bottom friction term formulated for combined waves and current, lateral mixing, and refraction in the surf zone. It has limitations in using

shallow-water linear-wave theory and constant wave-height to water-depth ratio in the surf zone. Rather than allow wave energy dissipation to begin at the break point (point of highest wave height), the dissipation is started at the measured plunge point based on his observation that measured setdown was greatest at the plunge point, not at the break point. The numerical model gave an overall excellent fit to the data with the same value of the empirical mixing coefficient, individually determined bottom friction coefficients (roughness lengths), and the measured plunge point. Details of the numerical solution scheme were not given except that iteration was used.

57. Wu, Thornton, and Guza (1985) applied their 2-D finite-element model to simulate the alongshore current system measured at Leadbetter Beach, California (Thornton and Guza 1986, 1989). These measurements are also used here. Their model included linearized bottom friction terms, lateral mixing after Longuet-Higgins (1970b), and nonlinear convective terms. The wave model in the surf zone used a constant wave-height to water-depth ratio, and the measured root-mean-square (rms) wave height was input as a monochromatic regular wave. Fitting parameters were the bottom friction coefficient, mixing coefficient, and a wave-height to water-depth ratio of 0.44 determined in one case, which was held constant through the other four cases. Use of the small value of 0.44 is inconsistent with the treatment of the rms wave as a monochromatic wave, and this subject is pursued further in Part IV. The mean value of the (linear) bottom friction coefficient was 0.01. Running of the model with and without the nonlinear convective terms gave about the same agreement with the measurements by modification of the calibration parameters.

58. Baum and Basco (1986) presented a numerical model similar to the model developed here in emphasizing calculation of the longshore current profile on a bar and trough bottom. The wave decay model of Dally (1980) and Dally, Dean, and Dalrymple (1985), which allows multiple wave breaking and reformation, provided the wave driving forces. Shallow-water linear-wave approximations were used everywhere in the calculation domain. Other features were large-wave angle, linearized bottom friction stress, and lateral mixing. Model predictions agreed well with the laboratory data of Mizuguchi, Oshima, and Horikawa (1978) for a plane-sloping beach, and reasonable agreement was found with the field data of Kraus and Sasaki (1979) for an irregular profile. Numerical efficiency for this linear model is not optimal because iteration is

used to determine the mean water surface elevation and an iterative "shooting" method to calculate the current.

59. Recognizing the importance of wave randomness and the wind in determining the longshore current profile in the field, Hubertz (1987) developed a model incorporating these effects to provide a more realistic and accurate alternative to handbook-type calculations. Wave randomness was calculated with a spectral wave propagation model that transforms the spectrum accounting for changes in direction, height, and peak frequency. The drag coefficient of Amorocho and DeVries (1980) was used in the wind driving term. The model contains a quadratic bottom friction law, but lateral mixing was omitted and a constant wave-height to water-depth ratio applied in the surf zone. Model calculations were verified with field data involving both waves and wind, including the current seaward of the surf zone arising mainly from the wind. The model was developed as a special case of a 2-D model with a time-stepping solution to the steady state; therefore, several hundred iterations are required to obtain the solution.

60. The most recent numerical longshore current model found in the literature review is part of a larger 1-D modeling system for calculating waves, wave-induced longshore current, and tidal current (Southgate 1989). The model was developed with the same pragmatic philosophy as the present study, that engineering situations may involve thousands of runs and large quantities of data, necessitating use of 1-D models. Features included in the model are random wave breaking through the truncated Rayleigh distribution method of Battjes and Janssen (1978), nonlinear bottom friction law, wave-current interaction, and inclusion of the tidal current as calculated from another model or data. Lateral mixing was evidently not taken into account to increase calculation efficiency, and wind driving was not included. It is believed that the model as presented is not applicable to barred beaches. In the monochromatic (single-wave) mode, agreement of the current prediction for Visser (1982) Case 1 was not good because of the omission of lateral mixing. It was argued that for field application use of random wave heights decreased the need for lateral mixing. Details of the numerical solution scheme were not given but, because of the necessity of performing time integration of the bottom friction stress and an apparent absence of a skillful first

approximation for the iteration, efficiency of the Southgate model is judged to be medium.

61. Finally, this review concludes with mention of two longshore current models that employed nonlinear-wave theory under simple conditions of a plane-sloping beach, those of James (1974) and Pechon (1987). James employed a hybrid hyperbolic wave theory to calculate waves and current in the surf zone, but such an approach no longer seems reasonable with accurate and efficient calculation schemes for cnoidal waves. Pechon (1987) used the shallow-water wave theory of Serre (1953; according to Pechon 1987) and gave examples of differences in wave height transformation, radiation stresses, and longshore current calculated with linear- and nonlinear-wave theory. Because only one comparison case with the Visser (1982) data was shown, it is difficult to judge superiority of results. A problem in use of nonlinear-wave theories is matching at the boundary between shallower and deeper water, where discontinuities in some quantities will occur (Hardy and Kraus 1988). Also, it has not been proved that any nonlinear-wave theory is superior to linear-wave theory in the surf zone. Once special conditions are imposed, such as use of nonlinear-wave theory to calculate shoaling, but not refraction, modification of the group speed inside the surf zone, but not outside, and other such inconsistent simplifications, generality of the model is probably degraded.

### PART III: WAVE MODEL

62. This chapter describes the wave model used to drive the longshore current model. Wave model selection and development are first discussed, followed by introduction of the governing equations and a description of the numerical implementation. Randomization of the wave model output is accomplished using a Monte-Carlo input simulation technique, making it possible to calculate properties of the wave height probability density function at any location across the shore on a multiple bar and trough profile. The wave model is verified with laboratory and field measurements in Part IV. Additional wave model verification is presented in conjunction with the longshore current simulations given in Part VI, as interpretation of the current calculation results requires consideration of the wave input.

#### Overview of Wave Model

63. Calculation of the longshore current as a function of distance across the shore requires knowledge of the driving wave characteristics at intervals inside and outside the surf zone. As a predictive tool, the wave model must calculate the change in height, direction, and length of the waves as they propagate onshore starting from wave conditions specified at the seaward end of the grid. Such a calculation involves the major wave transformation processes of shoaling, refraction, breaking with energy dissipation, and wave reformation. Wave diffraction does not enter in the applications considered in this report since it produces wave height and direction gradients perpendicular to the direction of wave propagation, violating the basic assumption of longshore uniformity used in the present model. Wave dissipation seaward of the surf zone is neglected for the sake of computational speed, but could be easily incorporated if warranted, such as for calculation of waves and currents over a muddy bottom.

64. In the development of the wave model, certain requirements were imposed to define a numerically stable, cost-effective engineering model with minimal computer memory demands:

- a. The model should accept arbitrary wave input (time series of representative wave height, period, and direction) and complex

bottom topographies (which exhibit uniformity alongshore as, for example, beaches with multiple bars and troughs).

- b. The calculation accuracy of the wave transformation should be compatible with engineering data available for the wave input and calculation accuracy of the current distribution.
- c. The model should contain a minimum number of empirical parameters, preferably with values that have been well established with data for general wave and bottom topography conditions.
- d. The execution time of the model should be sufficiently short and memory requirements minimal to allow it to run efficiently on a personal computer.

65. One representation of the wave transformation that satisfies the criteria is linear-wave theory for calculating shoaling and refraction seaward of the break point, connecting to a modified version of the breaker decay model developed by Dally (1980) (see also Dally, Dean, and Dalrymple 1985) to calculate wave properties in the surf zone. Linear-wave theory has been successful in many applications for predicting wave propagation even under conditions where it is formally violated, such as in the vicinity of the break point and in the surf zone, and it requires minimal computer memory and execution time as compared with nonlinear-wave theories. At the present state of knowledge on surf zone dynamics, it seems difficult to significantly improve the predictive capabilities and reliability of engineering wave models using more complicated wave theories, although efficient calculation routines are available for the region seaward of the break point (e.g., Kraus, Cialone, and Hardy 1987; Hardy and Kraus 1988).

66. The Dally (1980) breaker decay model is one of several models available for calculating wave transformation in the surf zone. Similar models have been developed by Goda (1975), Battjes and Janssen (1978), Mizuguchi (1980), Thornton and Guza (1983), and Svendsen (1984). The main difference among these models is the formulation of the energy dissipation term, where one common approach uses the analogy between wave breaking and a moving hydraulic bore for estimating the rate of energy dissipation (Le Mehaute 1962). Some models employ a probabilistic approach (Goda 1975, Battjes and Janssen 1978, Thornton and Guza 1983) for describing the transformation of a representative statistical wave height, usually the rms wave height. A discussion of the differences between probabilistic models and deterministic models is given later in this chapter.

67. The Dally model was selected for use in the present study because of the extensive verification that has been made for a variety of wave conditions and bottom topographies. Both small-scale (Dally, Dean, and Dalrymple 1985) and large-scale laboratory (Larson and Kraus 1989) measurements have been employed in the verification process, as well as field measurements (Ebersole 1987, Dally 1990). An appealing feature of the model is the demonstrated reliability of the values of its two empirical parameters, although a small and, as yet, unquantified dependence on beach slope has been noted (Dally, Dean, and Dalrymple 1985; Larson and Kraus 1989). Thus, a satisfactory description of wave height transformation in the surf zone using average parameter values is expected without additional calibration effort. The Dally model is formulated in terms of wave energy flux and is, therefore, general. In applications to date, including the present report, the flux is expressed by means of linear-wave theory.

68. The question arises whether other wave-related quantities are accurately described by the model, in particular, the radiation stresses, which are of importance in calculating the longshore current, even if the wave height is well predicted. Roelvink and Stive (1989) distinguished between turbulent energy production and dissipation, the latter governing changes in radiation stresses and thus quantities such as the setup and the longshore current. This topic is discussed in Part VI where longshore current model predictions are compared with laboratory measurements made by Visser (1982). Indirect evaluation of the model can be made by comparing measured and calculated quantities, such as the mean water surface elevation and longshore current profile, which depend on different components of the radiation stress.

69. In the model, wave transformation seaward of the break point for an individual wave is calculated using the wave energy flux equation without bottom or surface dissipation (although dissipation could be included if warranted), with quantities determined from linear-wave theory. Once wave breaking takes place, a dissipation term representing breaking is activated in the energy flux equation. Wave refraction throughout the calculation domain is given by Snell's Law under the condition of straight and parallel bottom contours. An empirical relationship is used to predict the critical ratio between wave height and water depth at incipient breaking. The mean displacement of the water surface (setup or setdown) is calculated using the

cross-shore momentum equation. Importantly, the model has the desirable feature of allowing wave reformation; wave breaking can cease, and a wave can again begin to shoal if the wave-height to water-depth ratio falls below a critical value.

70. All equations in the wave model involve variables regarded as time averages; that is, changes in the offshore wave conditions must occur sufficiently slowly to allow a quasi-stationary approach. In principle, the restriction of slowly varying conditions should apply to the calculation of setup and setdown as well as the current, because establishment of a mean water surface elevation requires a certain number of identical waves before the time-averaged momentum equations are valid. The wave energy flux equation has been shown to be applicable for individual waves propagating across the surf zone in the field (Ebersole 1987), exhibiting a surprising degree of robustness that works in favor of the approach taken here.

71. In a laboratory environment with monochromatic (constant period) and regular (constant height) waves, or in the field when clean swell-type wave conditions occur, the choice of a representative wave height is unambiguous, and the break point will be relatively stable on a fixed bed. However, if large variability in the wave conditions exists (which is typically the case in the field with waves of different generating sources, characteristics, and breaking locations), it is more difficult to determine a representative wave height, period, and direction. A probabilistic approach is thus reasonable for describing wave transformation in the surf zone under these conditions.

72. There are two generic approaches for probabilistically describing surf zone wave properties: integration of the wave energy flux equation with respect to an existing probability density function (characteristics of the probability density function must be known at each point cross-shore, such as the percentage of broken waves), and simulation of the transformation of each wave component from a known probability density function prescribed in deeper water. The latter approach is computationally more intensive and rests on the validity of linearly superimposing the response from each wave component, but will yield information about the local wave height probability density function without *a priori* assumptions about the shape of the function. The individual-component approach is also expected to more accurately describe the wave height distribution on an irregular bottom where wave reformation can

occur and both breaking and reformed waves coexist. Dally (1990) has recently developed closed-form solutions describing random wave breaking on a planar beach using the individual-component approach, and these solutions reproduce trends reported in laboratory and field measurements. The analytic work of Dally for planar beaches both supports and complements the computer-intensive approach taken here for barred beach profiles.

73. A strict limitation of the wave and longshore current models presented in this report arises from the requirement of alongshore uniformity in forcing conditions. This limitation allows a 1-D approach to be taken in which the wave (current) distribution along a single cross-shore transect is sufficient to describe the local wave (current) conditions. In situations violating longshore uniformity, such as in the vicinity of structures where significant three-dimensionality in waves occurs or in areas having highly irregular bathymetry, the present model may not be suitable.

#### Governing Equations for the Wave Model

74. For the 1-D case with straight and parallel bottom contours along-shore (but allowing the depth to be nonmonotonic with distance offshore, such as in the case of multiple bars and troughs), wave characteristics across the profile are determined by four fundamental equations:

- a. The wave energy flux equation.
- b. The cross-shore momentum equation.
- c. The wave number equation (Snell's Law).
- d. The wave dispersion relation.

75. Figure 1 is a definition sketch introducing the axes convention and notation to be used in equations governing wave transformation and the longshore current. Angle definitions giving positive orientations are also shown. In particular, the symbol  $\theta^*$  is used in all governing equations to denote the incident wave angle. However, the sign convention, although common, is not intuitive because a positive angle will generate a longshore

---

\* For convenience, symbols and abbreviations are listed in the Notation (Appendix C).

current directed along the negative y-axis. Therefore, as input to the numerical model, the mirror-image angle  $\theta'$  is used, which is defined as

$$\theta' = -\theta \quad (1)$$

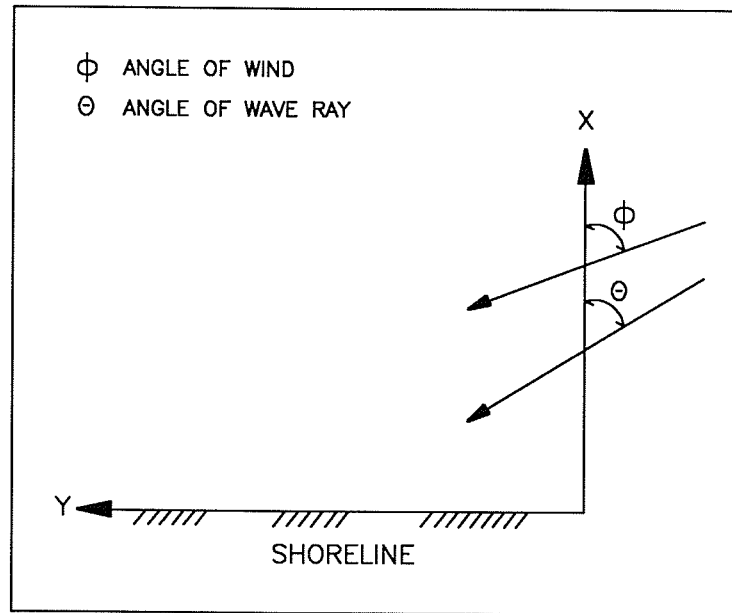


Figure 1. Definition sketch for wave and wind direction

### Energy flux

76. By generalizing the breaker decay model of Dally (1980) originally developed for normal wave incidence (see Ebersole, Cialone, and Prater 1986 for a similar treatment), in the absence of currents, the 2-D equation for conservation of energy flux incorporating energy dissipation produced by wave breaking is,

$$\frac{\partial}{\partial x} (F \cos\theta) + \frac{\partial}{\partial y} (F \sin\theta) = \frac{\kappa}{d} (F - F_s) \quad (2)$$

where

$x$  = cross-shore coordinate positive in the seaward direction (m)

$F$  = wave energy flux (Nm/m/sec)

$\theta$  = wave angle with respect to shore normal

$y$  = longshore coordinate (m)

$\kappa$  = wave decay coefficient (nondimensional empirical coefficient)

$d$  = total water depth (m)

$F_s$  = stable wave energy flux (Nm/m/sec)

The wave energy flux is given by,

$$F = EC_g \quad (3)$$

where

$E$  = wave energy density (Nm/m<sup>2</sup>)

$C_g$  = wave group speed (m/s)

The wave energy density is written using linear-wave theory as,

$$E = \frac{1}{8} \rho g H^2 \quad (4)$$

where

$\rho$  = density of water (kg/m<sup>3</sup>)

$g$  = acceleration produced by gravity (m/sec<sup>2</sup>)

$H$  = wave height (m)

The total water depth  $d$  is the sum of the still-water depth  $h$  and the change in mean water level  $\eta$  produced by waves and wind:

$$d = h + \eta \quad (5)$$

77. Assuming the waves to be uniform alongshore and the bottom contours to be straight and parallel, Equation 2 reduces to:

$$\frac{d}{dx} (F \cos\theta) = \frac{\kappa}{d} (F - F_s) \quad (6)$$

Equation 6 is the main equation used in this report to describe the transformation of wave height in the absence of a current.

78. If a mean current is present, there is an interaction between the waves and the current, and an additional term appears in the wave energy flux equation (Equation 6) to express the work done by the radiation stress on the current. Inclusion of the wave-current interaction gives (Mei 1983),

$$\frac{d}{dx} (F \cos\theta) + S_{xy} \frac{dV}{dx} = \frac{\kappa}{d} (F - F_s) \quad (7)$$

where

$S_{xy}$  = shoreward-directed radiation stress alongshore (N/m)

$V$  = longshore current speed (m/sec)

79. Because of the inclusion of the  $dV/dx$  term in Equation 7, the wave and current distributions must be solved for simultaneously (iteratively) if waves contribute to current generation. The importance of the radiation stress or wave-current interaction term for the wave height and the across-shore distribution of the longshore current will be discussed in Part VI.

80. The radiation stress component  $S_{xy}$  is given by linear-wave theory as,

$$S_{xy} = \frac{n}{16} \rho g H^2 \sin 2\theta \quad (8)$$

where

$$n = \frac{1}{2} \left[ 1 + \frac{\frac{4\pi d}{L}}{\sinh\left(\frac{4\pi d}{L}\right)} \right] \quad (9)$$

81. In Equation 7, the wave decay coefficient  $\kappa$  controls the rate of energy dissipation, whereas the stable energy flux  $F_s$  controls the amount of energy dissipation necessary for stable waves to exist once breaking is initiated. The "stable wave condition" refers to a state where energy dissipation produced by wave breaking ceases, permitting waves to reform. The stable energy flux is expressed as,

$$F_s = E_s C_g \quad (10)$$

where  $E_s$  is the wave energy density corresponding to a wave that has decayed to a stable form. The stable wave energy flux corresponds to a stable wave height  $H_s$ , which is a function of the water depth (Horikawa and Kuo 1966, Dally 1980),

$$H_s = \Gamma d \quad (11)$$

where  $\Gamma$  is a nondimensional empirical coefficient.

82. Two empirical coefficients, therefore enter in the breaker decay model,  $\kappa$  and  $\Gamma$ . Values of these coefficients have been found to vary little over a wide range of wave and bottom conditions in the laboratory and on natural beaches. Dally, Dean, and Dalrymple (1985) recommend the values  $\kappa = 0.15$  and  $\Gamma = 0.40$  for a varying bottom slope on the basis of favorable comparison of model predictions to laboratory and prototype-scale tank data. These values are used as defaults in modeling results presented here. Ebersole (1987) evaluated the performance of the breaker decay model using field measurements and found good results for engineering applications. He also tested the breaker decay model developed by Svendsen (1984) and found it to be comparable but slightly inferior in minimizing the rms error between measurements and calculation.

#### Dispersion relation

83. The wave group speed  $C_g$  is related to the phase speed of an individual wave  $C$  through the factor  $n$ , which is a function of the water depth and the wavelength  $L$  (or wave period  $T$ ):

$$C_g = nC \quad (12)$$

The phase or form speed of a wave is determined through the dispersion relation,

$$C = C_o \tanh\left(\frac{2\pi d}{L}\right) \quad (13)$$

where

$$C_o = \frac{gT}{2\pi} \quad (14)$$

The quantity  $C_o$  is the wave speed in deep water. Equation 13 is one form of the dispersion relation for linear waves; it is an implicit equation that is solved numerically since  $C$  depends on the wavelength,  $C = L/T$ .

#### Cross-shore momentum equation

84. As waves propagate over a sloping bottom, a variation in the flux of momentum (variation in radiation stress) arises because of shoaling, refraction, and breaking and alters the mean water elevation. Wave shoaling prior to breaking produces an increase in wave height and a corresponding increase in momentum flux. This flux increase is balanced by lowering of the mean water elevation, called setdown (Longuet-Higgins and Stewart 1962, 1963). Inside the surf zone, as waves break and decrease in height, the momentum flux decreases and an increase in mean water elevation occurs, known as setup.

85. The displacement of the mean water surface (setup or setdown) produced by waves (neglecting wind for present discussion) is determined from the momentum equation,

$$\frac{dS_{xx}}{dx} = -\rho g d \frac{d\eta}{dx} \quad (15)$$

where  $S_{xx}$  = radiation stress in the direction of the waves (N/m). The radiation stress component  $S_{xx}$  is given by linear-wave theory for an arbitrary wave angle of incidence as:

$$S_{xx} = \frac{1}{8} \rho g H^2 \left[ n(\cos^2 \theta + 1) - \frac{1}{2} \right] \quad (16)$$

### Snell's Law

86. The energy flux conservation equation (Equation 6, or Equation 7 if the wave-current interaction is included), the wave dispersion relation (Equation 13), and the cross-shore momentum equation (Equation 15) are not sufficient to specify the wave height if the waves arrive at an oblique (nonzero) angle with respect to the bottom contours. In this case an additional equation expressing the conservation of wave number is needed to obtain the wave angle. The wave number conservation equation is written in general form as:

$$\frac{\partial}{\partial x} \left( \frac{\sin \theta}{L} \right) - \frac{\partial}{\partial y} \left( \frac{\cos \theta}{L} \right) = 0 \quad (17)$$

87. For straight and parallel bottom contours, as assumed throughout this report, there is no longshore variation in wave properties, and Equation 17 simplifies to:

$$\frac{d}{dx} \left( \frac{\sin \theta}{L} \right) = 0 \quad (18)$$

If Equation 18 is integrated, Snell's Law is obtained, which states that the quantity  $\sin \theta / L$  is constant. Equations 6 (or 7), 13, 15, and 18 determine the wave height distribution after appropriate boundary conditions are established. If the wave-current interaction is included, Equation 18 is modified to describe additional refraction produced by the mean current. In this case Snell's Law becomes:

$$\frac{d}{dx} \left( \frac{C}{\sin \theta} + v \right) = 0 \quad (19)$$

## Numerical Solution Scheme

88. An explicit finite-difference scheme is used to numerically solve the governing equations determining the wave height as a function of distance across the shore. The following presents the solution scheme and the difference equations employed. Figure 2 gives a definition sketch of the grid and defines quantities entering the difference equations.

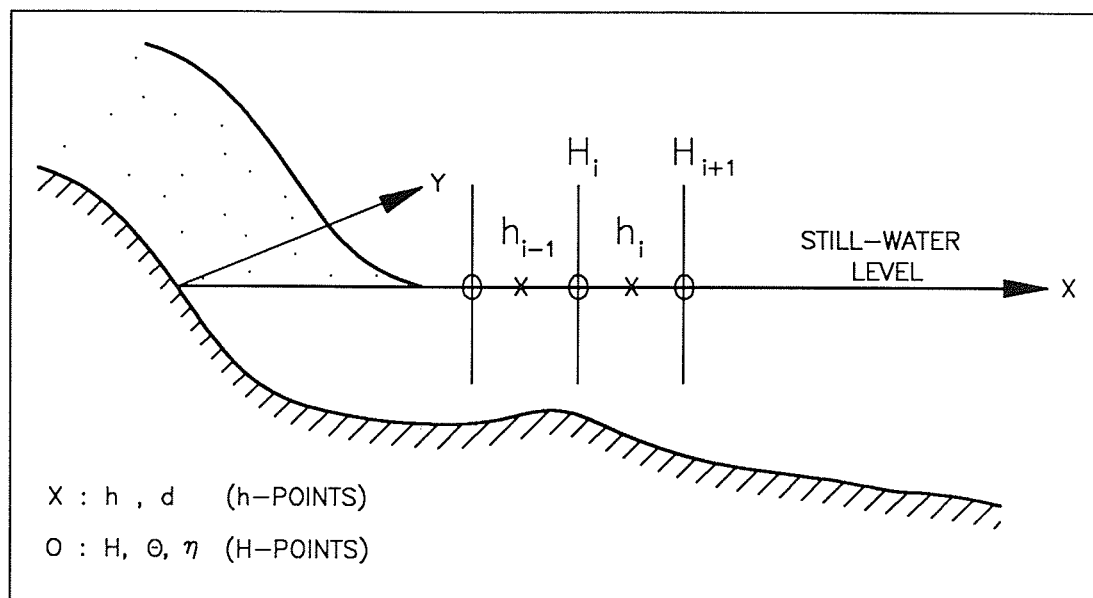


Figure 2. Definition sketch for the numerical grid

89. The numerical calculation starts at the most seaward point on the grid and proceeds onshore, where quantities known at one grid point are used to determine corresponding quantities at the next grid point closer to shore. In the difference equations, the index  $i$  denotes the number of a specific grid point. A staggered grid is used with quantities defined at either points in the middle of a calculation cell or at the boundaries between cells (Figure 2). The fundamental quantity in the middle of a cell is the water depth, and these grid points will be referred to as "h-points" (depth points). At the boundaries of calculation cells, the main quantity is the wave height, and grid points located here are known as "H-points" (wave points). All wave-related quantities are defined at H-points. The numbering convention is such that the wave height  $H_i$  is defined on the left boundary of calculation cell

number  $i$ . Finally, it is noted that if the grid contains  $N$   $h$ -points, it will have  $N+1$   $H$ -points.

90. The incident wave height, period, and direction must be available at the most seaward grid point (directly specified or calculated from some reference depth offshore) prior to starting the calculation. From knowledge of the wave properties at the seaward-most grid point (an  $H$ -point), wave setdown at the seaward-most point is determined from the analytic solution to Equation 15 first presented by Longuet-Higgins and Stewart (1962):

$$\eta = \frac{-\pi H^2}{4L \sinh\left(\frac{4\pi h}{L}\right)} \quad (20)$$

The mean water surface elevation is calculated at  $H$ -points, and depths at cell boundaries are obtained by linear interpolation, except for the first and last  $H$ -point where the depth at the nearest cell is used. Similarly, the energy flux and the radiation stress in the direction of the waves are determined from depth and wave quantities at the first  $H$ -point, proceeding shoreward.

91. In going from one  $H$ -point to the next, wave refraction is first determined if the incident wave approaches at a nonzero angle to the bottom contours. From Equation 18, the angle  $\theta_i$  between wave crests and bottom contours at the next shoreward  $H$ -point is given by:

$$\theta_i = \arcsin\left(\frac{L_i}{L_{i+1}} \sin\theta_{i+1}\right) \quad (21)$$

Note that the grid point numbering decreases in the shoreward direction since the  $x$ -axis points offshore. The water depth at grid point  $i$  in Equation 21 is corrected with the setdown or setup value calculated at  $H$ -point  $i+1$  (half a cell seaward) in order to eliminate the need for iteration (Dally 1980). Wavelengths are calculated using the dispersion relation (Equation 13), numerically solved by a Pade' approximation (Hunt 1979). Wave angles in Equation 21 are defined at  $H$ -points.

92. The next step in the calculation is to determine the change in energy flux and thus the wave height. Equation 6 is written in difference form as,

$$F_i = \frac{F_{i+1} (\cos\theta_{i+1} - 0.5A_{ci}) + A_{ci}F_{si}}{\cos\theta_i + 0.5A_{ci}} \quad (22)$$

where

$$A_{ci} = \frac{\kappa\Delta x}{h_i + \eta_{i+1}} \quad (23)$$

in which  $\Delta x$  is the length step or grid cell length (meters). The stable wave energy flux is determined from:

$$F_{si} = \frac{1}{8} \rho g [\Gamma(h_i + \eta_{i+1})]^2 \frac{(C_{gi} + C_{gi+1})}{2} \quad (24)$$

An average value of the group speed over a cell is used since this quantity is defined at  $H$ -points, whereas the stable wave energy flux is evaluated at  $h$ -points. Seaward of the break point,  $\kappa$  should be set to zero, implying that  $A_{ci}$  is also zero, because energy dissipation by breaking does not occur.

93. After the energy flux has been calculated at a specific point, the corresponding wave height is determined from Equations 3 and 4:

$$H_i = \left( \frac{F_i}{\frac{1}{8} \rho g C_{gi}} \right)^{\frac{1}{2}} \quad (25)$$

Using this wave height, the radiation stress is calculated from Equation 16, and the mean water surface displacement is given from Equation 15 expressed in difference form:

$$\eta_i = \eta_{i+1} + \frac{(S_{xx})_{i+1} - (S_{xx})_i}{\rho g (h_i + \eta_{i+1})} \quad (26)$$

As before,  $\eta$  is evaluated at an  $H$ -point half a cell seaward of the  $h$ -point in calculating the depth to avoid use of an implicit scheme.

94. The alongshore radiation stress component  $S_{xy}$  is calculated at  $H$ -points from Equation 8 for use in the longshore current model. Thus, if the wave-current interaction is neglected all wave quantities needed to calculate the wave height can be computed by a single pass with an explicit solution scheme as described above. However, if the influence of a steady current cannot be neglected, the wave and current distributions have to be solved for simultaneously or iteratively. To include the wave-current interaction, the numerical representations of the wave energy flux equation and Snell's Law must be modified. Equation 21 describing wave refraction is replaced by the following equation according to Equation 19:

$$\theta_i = \arcsin \left[ \frac{L_i}{\frac{L_{i+1}}{\sin \theta_{i+1}} - \frac{T}{2}(V_{i-1} - V_{i+1})} \right] \quad (27)$$

Longshore current speeds are evaluated at  $h$ -points (see Part V) and are interpolated to obtain values at  $H$ -points for the refraction calculation. To modify the difference form of the energy flux equation, an extra term appears in the numerator of Equation 22, according to Equation 7:

$$S_{xy} \frac{dV}{dX} \approx [(S_{xy})_{i+1} + (S_{xy})_i] \left( \frac{V_{i+1} - V_{i-1}}{4\Delta X} \right) \quad (28)$$

(The  $\Delta x$  factor in the denominator of Equation 28 will be canceled by the corresponding factor from the right side of Equation 7.)

95. Because the longshore current velocity, initially unknown if it has a wave-induced contribution, occurs both in the refraction calculation and the energy flux equation, independent solution of the wave height distribution is

not possible. An iterative scheme must be employed. The calculation is started by assuming no current; thereafter, the current distribution is determined and the wave computation updated, proceeding in this manner until the wave and current calculations converge with some specified accuracy (typically, 1 percent) at every grid point. The influence of the wave-current interaction is small for all but extremely high current speeds, as will be discussed in Part VI, so convergence is rapid.

96. At every calculation step, a check is made to determine if depth-limited wave breaking has occurred according to a criterion that specifies the maximum permissible ratio between wave height and water depth  $\gamma_b$  (called the breaker index) for an unbroken wave. This index typically varies between 0.7 and 1.2, with the values 0.78 and 1.0 most commonly used in modeling. A dependence of  $\gamma_b$  on wave steepness and beach slope has been reported by several authors (e.g., Galvin 1969, Weggel 1972, Singamsetti and Wind 1980, Sunamura 1980, Larson and Kraus 1989, Smith and Kraus 1990). Beach slope and wave steepness may be combined to yield the surf similarity parameter  $\xi$  (Battjes 1974) used to form a predictive equation for  $\gamma_b$ , as reported by Sunamura (1980) and Larson and Kraus (1989),

$$\gamma_b = \frac{H_b}{d_b} = 1.14 \xi^{0.21} \quad (29)$$

where the surf-similarity parameter is defined as:

$$\xi = \tan\beta \left( \frac{H_o}{L_o} \right)^{-\frac{1}{2}} \quad (30)$$

In Equations 29 and 30, the subscripts  $b$  and  $o$  denote breaking and deepwater conditions, respectively, and  $\tan\beta$  is the average slope of the sea bottom along approximately one-third of the local wavelength seaward of the break point.

97. Once breaking is initiated, the wave decay coefficient,  $\kappa$  is assigned the value 0.15, and energy dissipation takes place. Also, if

breaking has occurred and if the wave energy flux falls below the stable energy flux, a check is made for wave reformation. The stable wave height coefficient is set to  $\Gamma = 0.40$  and, if there is wave reformation,  $\kappa$  is set to zero. An arbitrary number of break points with intermediate zones of wave reformation can be represented by the numerical model.

#### PART IV: VERIFICATION OF WAVE MODEL

98. The Dally (1980) breaker decay model has been extensively verified with laboratory and field data and demonstrated to provide a good description of wave height decay in the surf zone (Dally, Dean, and Dalrymple 1985, Ebersole 1987). Another positive feature of the model is that variability in the two empirical coefficients for different wave and topographic conditions is small. In this section, model performance for complex bathymetries involving bar and trough formations is evaluated using data from a large wave tank experiment (Kajima *et al.* 1983a, b). Also, the capability of the model to reproduce changes in the statistical characteristics of a wave height probability density function is demonstrated. Additional wave model verification for laboratory and field data sets for cases involving longshore current measurements is presented together with verification of the longshore current model in Part VI.

##### Large Wave Tank Data Simulations

99. The accurate and controlled measurements reported by Kajima *et al.* (1983a, b) are well suited for verifying simulation models of waves transforming over complex bottom bathymetries. The measurements were made in the large wave tank of the Central Research Institute for Electric Power Industry (CRIEPI) in Japan. The tank is 205 m long, 3.4 m wide, and 6 m deep, and wave measurements were made using resistance wave gages. The primary objective of the CRIEPI program was to investigate beach profile change under wave action. Most tests were started from a plane slope (1/50 to 1/10), and profile evolution caused by the regular breaking waves was measured through time. Twenty-four tests were made with wave periods ranging from 3 to 12 sec and wave heights from 0.3 to 1.8 m in the horizontal portion of the flume. Tests were performed separately with two grain sizes, 0.47 and 0.27 mm (quartz sand).

100. Because the initial beach profile was not in equilibrium with the imposed waves, wave action redistributed the sand to approach a stable profile over the course of the run. Most of the tests exhibited offshore sand movement and corresponding bar formation with the waves breaking on the bar.

These tests thus constitute an excellent source for evaluating the performance of the wave model for barred profiles, one of the main requirements entering model development in the present study.

101. Larson and Kraus (1989) used a portion of the CRIEPI data set to investigate the sensitivity of the wave model to the two empirical parameters  $\kappa$  and  $\Gamma$  in Equations 6 and 11. A slight dependence on beach slope was noted (Dally, Dean, and Dalrymple 1985), but a predictive relationship could not be developed with any level of significance. In the present report, the values  $\kappa = 0.15$  and  $\Gamma = 0.40$ , as recommended by Dally, Dean, and Dalrymple (1985), were employed to test the model. The reasoning was that if these values determined for plane beaches hold well for complex bottom profiles and prototype-scale waves, then the recommended parameter values could be confidently used as default values.

102. Wave height measurements made at the end of the runs were used in the present study since the profile was close to equilibrium (changing little), and the bars and troughs were most prominent. A large number of cases were simulated to test the wave model in the present study; here, typical cases showing the predictive capability of the model are described. The numbering of the cases follows the notation of Kajima *et al.* (1983a). The elapsed times bracketing the wave height measurements and the time of the bottom profile measurement input to the wave model are given for each case. The grid spacing was 0.5 m.

#### Case 3-1

103. This case exhibited bar development with material composing the bar removed from the foreshore and from the area seaward of the bar. The wave period was relatively long ( $T = 9.1$  sec,  $H = 1.07$  m), promoting development of a broad, flat bar. Figure 3 shows the comparison between measured (67.1 to 67.6 hr) and calculated wave height together with the bottom profile measured at 71 hr. The model reproduces the bipeaked wave height distribution across the shore. Equation 29, developed with all the CRIEPI breaking wave data (Larson and Kraus 1989), was used to determine the breaker index and gave a good prediction of the location of the break point for this case.

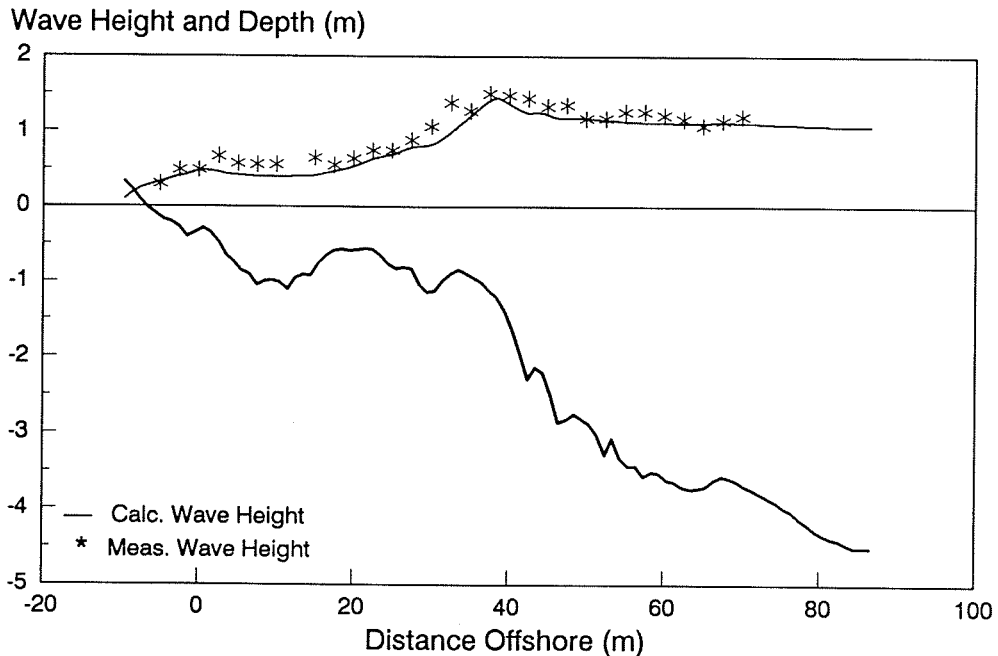


Figure 3. Comparison for CRIEPI Case 3-1

#### Case 3-4

104. Extremely steep waves were applied in this case with a generated wave height of 1.54 m and a period of 3.1 sec. A very peaked bar developed in the offshore with much steeper flanks than are formed in the field under varying waves and water level, and a second small bar was created near the shoreline. This bottom profile provides a severe test of the wave model for which steep shoaling is required at the outer bar followed by wave reformation in the trough and second breaking on the inner bar.

105. Figure 4 compares the measured (69.6 to 70.1 hr) and calculated wave height distributions along the tank, displayed with the profile measured after 76.1 hr. The measured wave height distribution is typical of the extremely peaked bottom profile cases. The model reproduces the location of the break point and the initial, steep portion of the wave height decay after breaking. However, the calculated waves reformed earlier in their travel across the trough landward of the sharp bar, the model underpredicting the energy dissipation and wave decay. An improved simulation can be obtained without modifying model parameter values by calculating with a smoothed

profile (Larson and Kraus 1989) or by requiring wave dissipation to occur over a minimum distance before reformation can take place (introducing an additional empirical parameter). Both of these modifications can be physically justified.

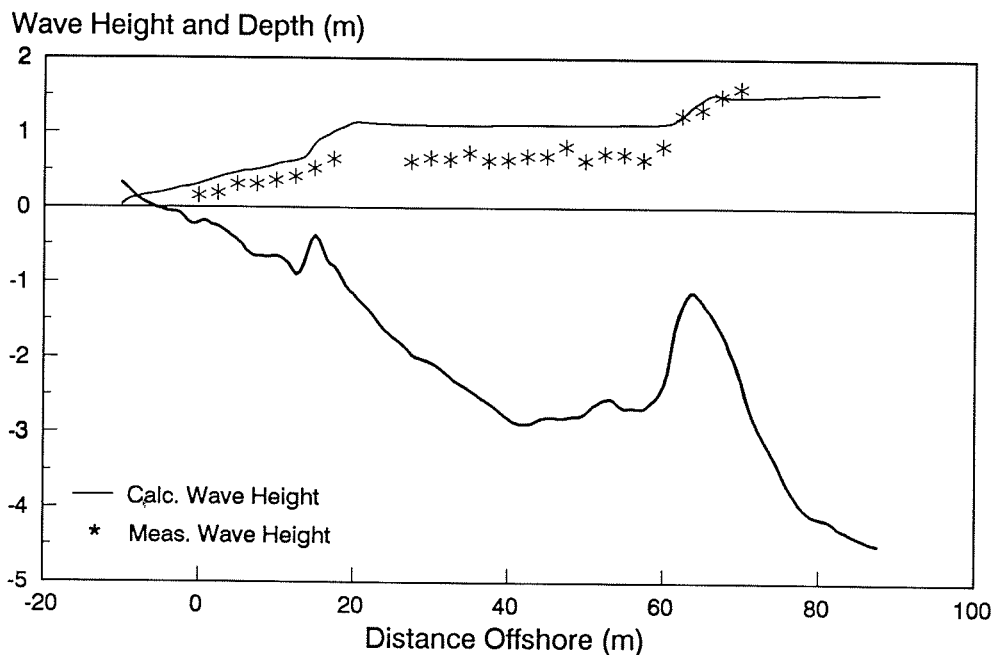


Figure 4. Comparison for CRIEPI Case 3-4

#### Case 4-4

106. The initial profile for this case was the final profile from a previous case involving steep waves, in which a peaked bar developed in the seaward part of the profile. Milder (accretionary) wave conditions ( $H = 1.0$  m,  $T = 9.0$  sec) were employed in Case 4-4, which flattened the offshore bar considerably, and the break point was located at a smaller double-bar feature that formed inshore. The result of the model simulation is illustrated in Figure 5, which plots the measured wave height (8.6 to 9.0 hr), the profile measured after 10 hr of wave action, and the calculated wave height distribution across the tank. The overall model prediction is in good agreement with the measurements at and shoreward of the break point. Differences occur, however, at the two peaks in the measurements appearing at

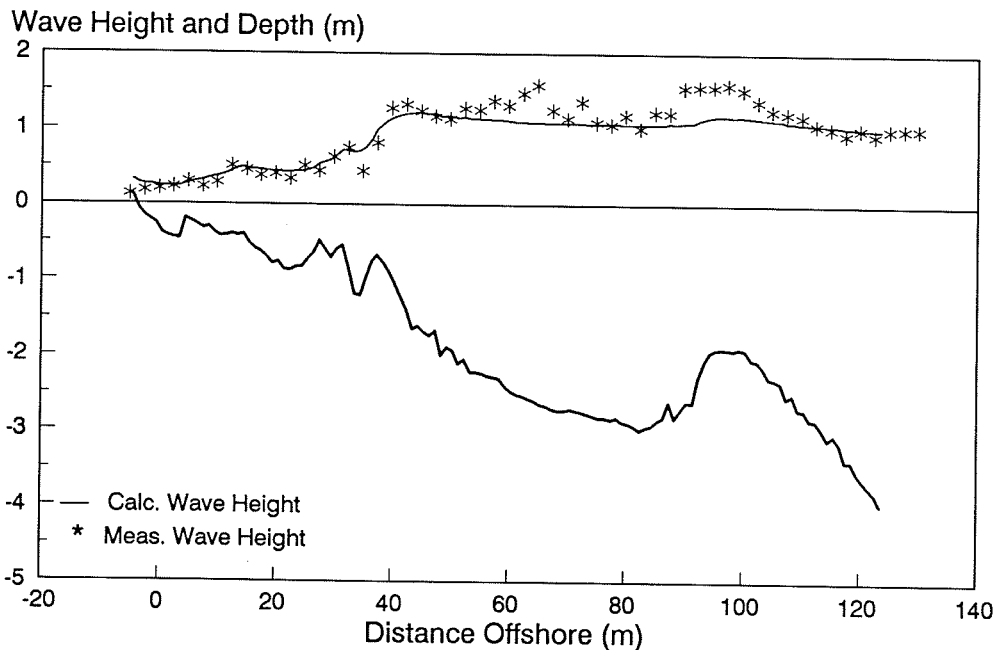


Figure 5. Comparison for CRIEPI Case 4-4

about 65 and 95 m. These local maxima are believed to be a result of wave reflection on the relatively steep bottom slope; reflection is not described in the wave model.

#### Case 5-2

107. This case is an example of a beach with a mild slope (1/50) exposed to moderately steep waves ( $H = 0.74$  m,  $T = 3.1$  sec), causing a small bar to develop under the breaking waves. Figure 6 displays the results of the model simulation by comparing the measured waves (97.7 to 98.4 hr), bottom profile after 103 hr, and the calculated wave height across the tank. Agreement is good overall, with small differences between calculation and measurements appearing in the intermediate region where wave reformation took place. These differences are caused by the peaked bar, which induces rapid wave reformation in the model as was described for Case 3-4.

#### Summary

108. The wave model satisfactorily reproduced measured wave heights over the barred bathymetry generated in a large tank. For some cases with very steep waves, reformation was predicted too early (too far seaward) in the wave

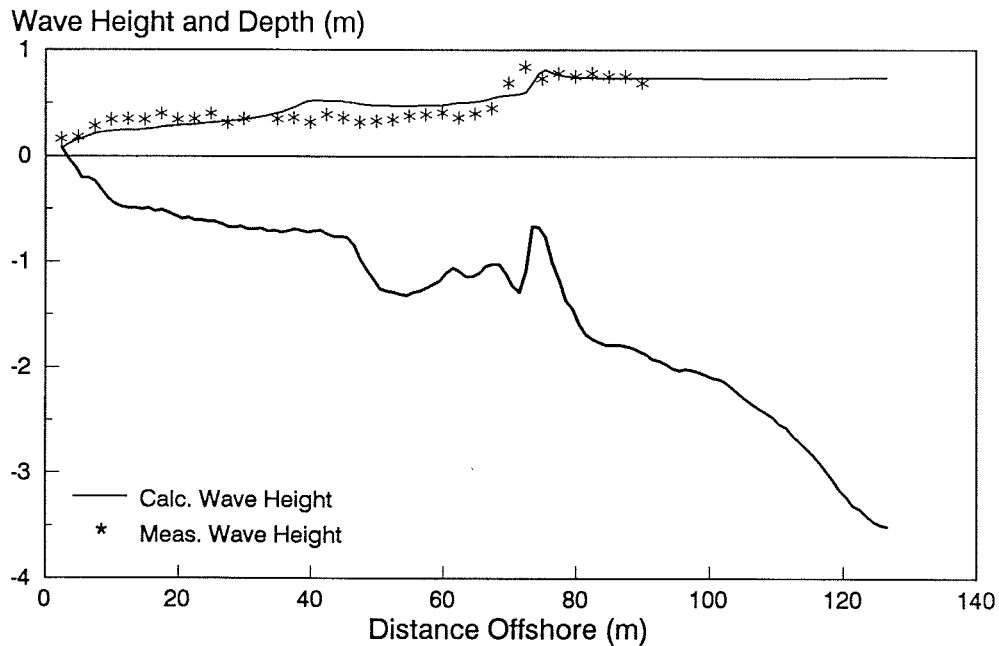


Figure 6. Comparison for CRIEPI Case 5-2

model, resulting in overprediction of the wave height in zones of reformation. Premature reformation could be eliminated by slight smoothing of the profile, which is physically justified because a real wave probably responds over a certain length of the bottom and not to abrupt, highly localized changes in bathymetry.

#### Random Wave Simulations

109. Two different approaches may be taken to simulate the transformation of random waves. Both approaches employ a deterministic description of the wave transformation process itself, but the input to the calculation procedure or model is a wave height probability density function with known statistical properties specified by different procedures. It is assumed here that the waves are narrow banded in frequency and direction so that a single frequency and direction are sufficient to characterize the sea state. Thus, randomness in the waves only enters through variability in wave height. Because the wave height variability is described by a probability density

function, the waves are assumed to be independent and have no correlation with precedent or antecedent waves. This procedure can be extended to an arbitrary number of wave direction and period bins if the directional frequency spectrum is known.

#### Modified probability density approach

110. This method was introduced by Goda (1975) and further developed by Battjes and Janssen (1978), Thornton and Guza (1983), and Leont'ev (1988). The wave energy flux equation is integrated with respect to the probability density function for the wave height, in which the rms wave height  $H_{rms}$  is used as the single statistical descriptor. If the wave energy dissipation term is integrated to yield the average dissipation rate, an independent procedure or criterion must be applied to specify the percentage of broken waves at each calculation point across the shore. Battjes and Janssen (1978) truncated a Rayleigh distribution above the height of the breaking wave and equated the percentage of broken waves to the truncated probability mass. Thornton and Guza (1983) assumed that the waves break in proportion to the distribution for all waves and introduced an empirical weighting function which depends on the ratio of wave height to water depth. Earlier, Goda (1975) introduced a model in which breaking occurred over a small range of water depths with redistribution of waves in a truncated probability density function.

#### Monte-Carlo approach

111. The other approach is to randomly select offshore waves according to height from a known wave height distribution and transform each as an individual wave with a propagation and breaker decay model. A wave height probability density function is obtained at each calculation point across the shore from transformation of a large number of waves randomly selected from the distribution. The percentage of broken waves is automatically given as the number of broken waves at the specific location in relation to the total number of waves. Because each wave component is calculated separately, a breaker criterion such as Equation 29 may be used without appeal to further assumptions as required by the truncated probability density approach. The disadvantage of the Monte-Carlo method is the computational intensiveness, because a large number of waves (order of 100) must be simulated to obtain an accurate representation of the probability density function. A more efficient

but less accurate way of constructing the probability density function at points across the shore is to discretize it with respect to typical wave heights and transform each such bin with appropriate weighting (Dally 1987, 1990; Nairn 1988).

112. The Monte-Carlo approach will be used here instead of the modified probability density approach because limited information exists on weighting functions suitable for describing the proportion of broken waves and how they vary across the surf zone, particularly for an irregular or barred profile. Thornton and Guza (1983) demonstrated using field data that the Rayleigh distribution holds as a good approximation primarily in deep water, and in some cases also surprisingly well in shallow water. Ebersole and Hughes (1987) and Hughes and Borgman (1987) examined deviations from the Rayleigh distribution of the wave height in and just outside the surf zone using a data set obtained with an accurate photogrammetric technique to measure the water surface elevation. Portions of the data sets of Thornton and Guza (1983) (as given in Thornton and Guza 1989) and Ebersole and Hughes (1987) will be used here to evaluate the accuracy of the Monte-Carlo approach using the Dally (1980) breaker decay model to predict characteristic changes in the statistical properties and distribution of wave height across the profile.

#### Verification of Monte-Carlo approach

113. It is assumed that the Rayleigh distribution is an adequate description of the input wave height distribution at the most seaward grid point, presumed to be in relatively deep water (depth-limited breaking does not occur). If  $p$  is a uniformly distributed random number having a value between zero and one, the Rayleigh-distributed wave height corresponding to this level of probability is given by,

$$H_p = H_{rms} \left[ \ln \left( \frac{1}{1-p} \right) \right]^{\frac{1}{2}} \quad (31)$$

in which  $H_p$  = wave height threshold associated with the exceedance probability of  $1 - p$ , and  $\ln$  = natural logarithm.

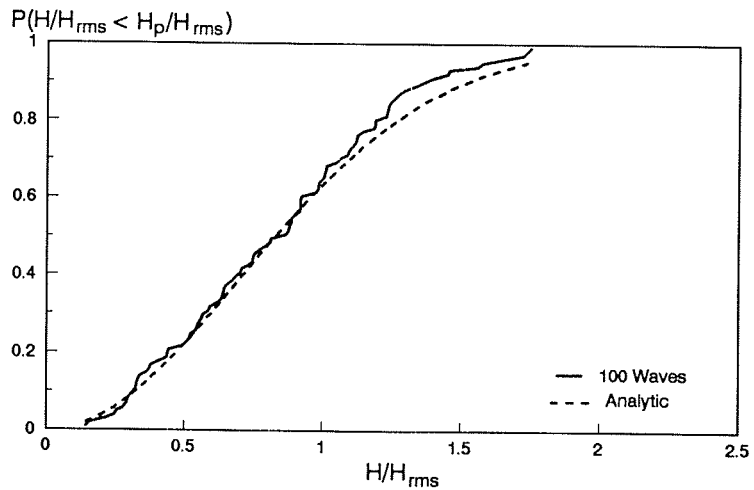
114. By numerical experimentation using a random-number generator, it was established that approximately 100 wave selections are necessary to reasonably reproduce the Rayleigh distribution, and 500 waves give good

agreement. Typical Monte-Carlo simulations of the cumulative probability distributions for 100, 200, and 500 waves selected randomly are shown in Figure 7. In the figure, the simulated distribution was plotted using the Weibull plotting position formula. A sufficiently large selection of random numbers will yield an accurate representation of a target Rayleigh cumulative distribution once the rms wave height is specified.

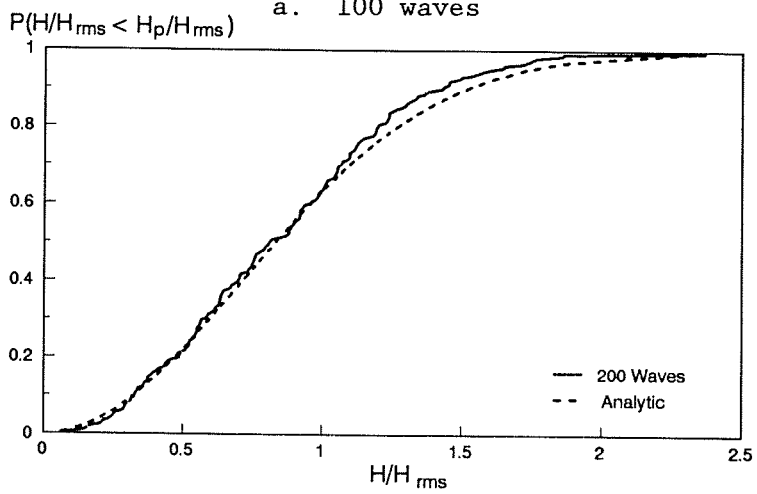
115. Field data on the wave height transformation across the surf zone collected by Ebersole and Hughes (1987) at CERC's FRF in Duck, North Carolina, were used to test the Monte-Carlo simulations. Ebersole and Hughes filmed, with 16-mm synchronized movie cameras, the water surface elevation at 14 poles installed at nominal 6-m intervals across the surf zone of a near-planar beach. This method, called the "photopole" method by CERC researchers, provides a direct measurement of the wave height and period and does not rely on a transfer function as is necessary if the sea surface elevation is inferred from another measured variable such as pressure or wave orbital velocity. Photopole data collection runs lasted approximately 12.5 min with film exposures made every 0.2 sec.

116. Ebersole (1987) verified the applicability of the Dally breaker decay model with field data. His study concerned tracking of individual waves through the surf zone, and he did not apply the breaker decay model in a probabilistic context to investigate the transformation of the probability density function or statistical wave parameters such as  $H_{rms}$ . Hughes and Borgman (1987) noted that measured wave heights in the surf zone tend to be skewed toward higher values than predicted by the Rayleigh distribution. They proposed a "Beta-Rayleigh" distribution to describe the deviation from the pure Rayleigh distribution in shallow water in terms of three empirical parameters. Such a distribution could easily be incorporated in the present model if further research indicates the correction is warranted.

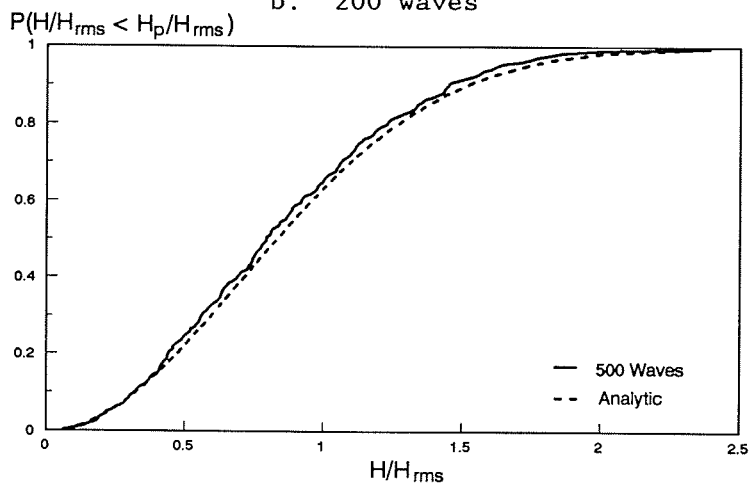
117. To evaluate the Monte-Carlo approach, photopole run 859041510 (4 September 1985 at 15:10) from Ebersole and Hughes (1987) was chosen as a typical case for simulation. Also, the data provided the opportunity to determine the degree to which the probability density function could be predicted across the shore. As mentioned previously, use of the Monte-Carlo technique requires no *a priori* assumptions about the shape of the probability density function at locations along the profile. However, the probability



a. 100 waves



b. 200 waves



c. 500 waves

Figure 7. Monte-Carlo simulation of Rayleigh wave height distribution

density function must be specified at some seaward location for input to the model.

118. The beach profile had a step-type shape with a steep foreshore. Quantitative information on the local incident wave angle is not available, but visual observation indicated that the waves arrived at a small angle to the shore (taken to be zero in the present work) as long-crested swell. The energy-based significant wave height measured at FRF Gage 630 located at 18-m depth was 0.60 m, and the peak spectral wave period was 11.3 sec.

119. Two different approaches were taken in the simulations of the field data. The first method used the waves measured at the most seaward photopole during the run and transformed them individually across the shore. Sixty-three waves were identified at this pole during the 12-min run. The other approach, the true Monte-Carlo technique as would be used in a typical engineering application, used the measured rms wave height at the seaward-most photopole to define a Rayleigh distribution from which a large number of waves were randomly selected and transformed across the shore. The main difference between the two approaches is that a number of very small waves are expected to appear in the selection process from the Rayleigh distribution; these waves will produce lower values of statistically determined wave heights at some locations along the profile.

120. Parameters in the breaker decay model were set to the default values of  $\kappa = 0.15$  and  $\Gamma = 0.40$ , and the breaker index was set to 1.0 for all waves because the random wave height simulation can produce unreasonably high wave steepness values in Equation 29 (breaker criterion). Wave heights measured at the most seaward photopole (Pole 13) located in 1.44-m depth were transformed seaward to 3-m depth by linear-wave theory for starting the calculation. It is noted that a few of the waves at Pole 13 had already broken, introducing a small error in the calculations. The depths available from the photopole record, which are total depths, were entered directly in the governing calculations, so that no prediction of setup or setdown was made.

121. Figure 8 shows a comparison between the calculated and measured rms wave height across the shore at the photopoles. The difference in results of the two simulation approaches is minor, with the actual measured waves giving a larger  $H_{rms}$  than the random selection procedure seaward of the area where

most waves break. The maximum in the measured  $H_{rms}$  is located shoreward of the calculated maxima, but the general trend in the wave height decrease is well reproduced. Use of a larger breaker index would give improved agreement in the location of the maxima, but this procedure is considered artificial since the discrepancy is probably related to factors not included in the model, in particular, nonlinear-wave shoaling.

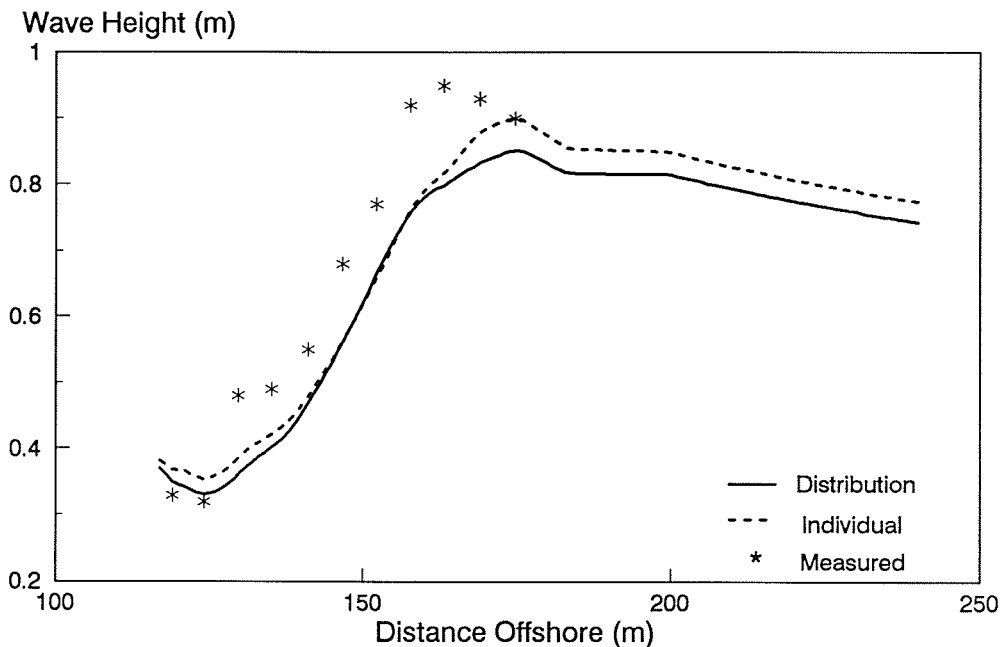
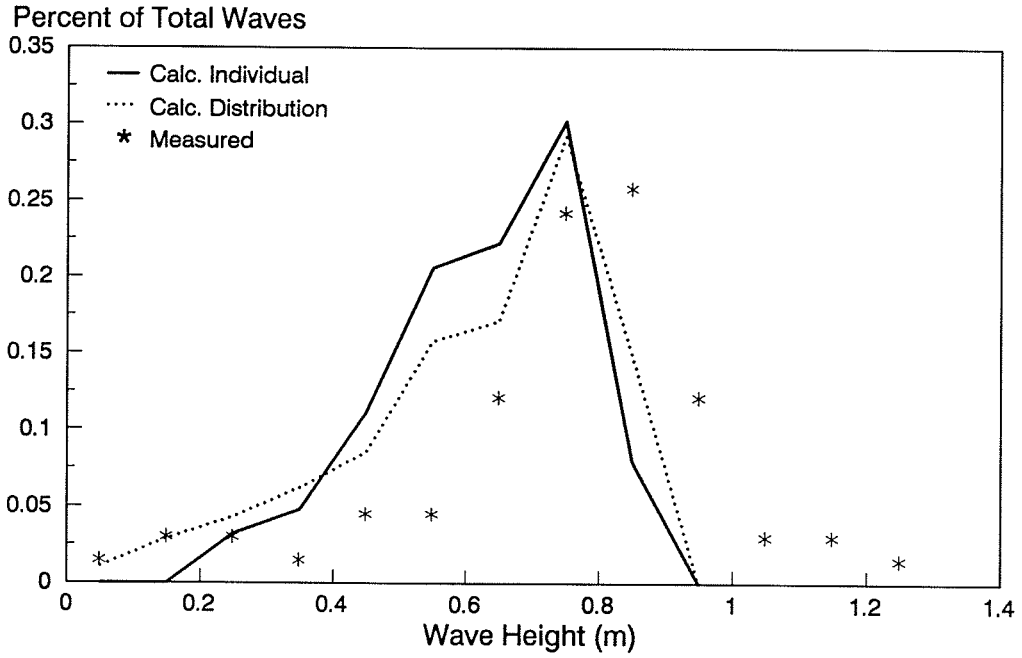


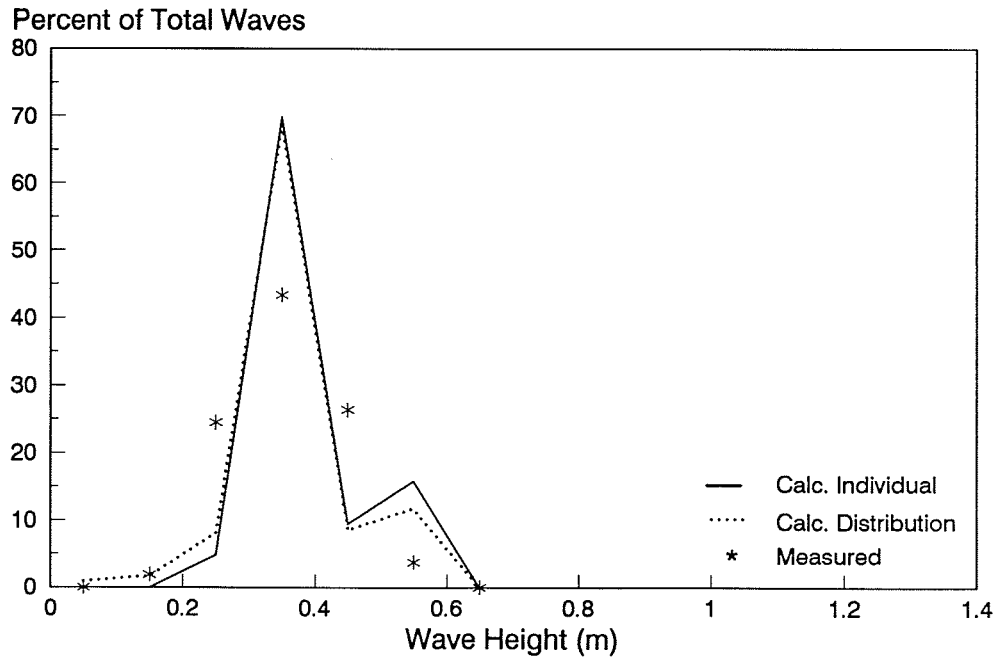
Figure 8. Comparison between measured and calculated  $H_{rms}$ .

122. Output from the wave model can be used to calculate statistical quantities at any point on the calculation grid, such as the percentage of broken waves and the ratio of the rms wave height to the average water depth. The empirical probability density function or normalized wave height histogram is also readily constructed from the individual wave heights at each point for comparison to the measured density function at any photopole.

123. Figures 9a and b respectively give comparisons of measured and calculated probability density functions at photopoles 9 and 3; Pole 9 was located just shoreward of the area where the higher waves began breaking, and Pole 3 was located close to shore where almost all waves had broken. Because most waves were calculated to break farther from shore, the calculated wave



a. Pole 9 (0.95-m depth)



b. Pole 3 (0.44-m depth)

Figure 9. Calculated and measured wave height probability density functions

heights at Pole 9 are smaller than the measured heights, and the maxima in the calculated probability density functions are displaced toward the lower waves. At Pole 3, located close to the shoreline, the maxima in the measured and calculated probability functions coincide, but the shape of the calculated function is more peaked. Figures 9a and b show that the calculations well reproduce the overall shape and range of the measured probability density function at the two very different regions of breaking waves in the surf zone.

#### Summary

124. The Monte-Carlo technique of transforming individual wave components was successful in reproducing the rms wave height measured in the field on an irregular bottom topography. The main deviation between calculation and measurements appeared at the location of the maximum height, for which the calculated waves tended to break seaward of the actual region of significant wave breaking. The two calculation approaches of propagating individual waves from the 3-m depth and randomly selecting waves from a Rayleigh distribution defined by the rms wave height gave almost the same results. It is concluded that the Rayleigh wave height distribution is an adequate descriptor of waves entering the surf zone, and specification of the rms wave height or similar statistical wave height at a location seaward of the first breakers is sufficient for accurately estimating random wave transformation over a surf zone with irregular bottom topography.

## PART V: LONGSHORE CURRENT MODEL

125. This chapter presents the numerical model of the longshore current developed in this study. The model calculates the longshore current across a barred profile under forcing by arbitrary combinations of waves arriving at an oblique angle to shore and a steady wind blowing over the sea surface at an arbitrary angle. The longshore components of the wave and wind forces generate a longshore current, and the shore-normal components change the mean water surface elevation, resulting in setup and setdown. The main restriction of the model is that the beach contours must be uniform alongshore.

126. First, the theoretical background is given, and the governing equations of the model are derived starting from the time-averaged and depth-integrated equations of motion. The formulation of the bottom friction term in the alongshore momentum equation is examined with various degrees of approximation to determine the accuracy of simplifications made to increase computational efficiency. Two mathematical descriptions of the bottom friction are presented, resulting in a linear and a nonlinear longshore current model. Representation of lateral mixing is also discussed, and an eddy viscosity coefficient is proposed for calculating currents generated over a barred profile. Finally, the discretization procedure for the governing equations and the numerical solution scheme are described, leading to the computationally efficient double-sweep implicit technique for obtaining the velocity. The current model is verified in Part VI.

### Governing Equations for Nearshore Currents

127. The vertically integrated, time-averaged momentum equations may be written (Mei 1983),

$$U \frac{\partial U}{\partial x} + V \frac{\partial U}{\partial y} = -g \frac{\partial \eta}{\partial x} + F_{bx} + L_x + R_{bx} + R_{sx} \quad (32)$$

$$U \frac{\partial V}{\partial x} + V \frac{\partial V}{\partial y} = -g \frac{\partial \eta}{\partial y} + F_{by} + L_y + R_{by} + R_{sy} \quad (33)$$

where

- $U$  = time-averaged (mean) cross-shore current (m/sec)
- $V$  = time-averaged (mean) longshore current (m/sec)
- $F_{bx}$  = cross-shore component of bottom friction term (m/sec<sup>2</sup>)
- $F_{by}$  = longshore component of bottom friction term (m/sec<sup>2</sup>)
- $L_x$  = cross-shore component of lateral mixing term (m/sec<sup>2</sup>)
- $L_y$  = longshore component of lateral mixing term (m/sec<sup>2</sup>)
- $R_{bx}$  = cross-shore component of the wave driving term (m/sec<sup>2</sup>)
- $R_{by}$  = longshore component of the wave driving term (m/sec<sup>2</sup>)
- $R_{sx}$  = cross-shore component of the wind (surface) driving term (m/sec<sup>2</sup>)
- $R_{sy}$  = longshore component of the wind (surface) driving term (m/sec<sup>2</sup>)

Equation 32 is a more general form of the momentum equation in the x-direction than Equation 15 used in the wave model in Part III to compute setup and setdown. After a number of simplifying assumptions, Equation 15 is obtained from Equation 32 as described below. In the wave-related terms, the subscript "b" is used to denote the force produced by shoaling and breaking waves, since the more natural notation "w" might cause confusion between waves and wind.

#### Wave-driving terms

128. The wave-driving terms are a function of the change in radiation stresses that takes place as waves propagate toward shore and transform by shoaling, refraction, and breaking. They are expressed as,

$$R_{bx} = \frac{-1}{\rho d} \left( \frac{\partial S_{xx}}{\partial x} + \frac{\partial S_{xy}}{\partial y} \right) \quad (34)$$

$$R_{by} = \frac{-1}{\rho d} \left( \frac{\partial S_{xy}}{\partial x} + \frac{\partial S_{yy}}{\partial y} \right) \quad (35)$$

where the radiation stress components  $S_{xx}$  and  $S_{xy}$  are given by Equations 16 and 8, respectively. By linear-wave theory, the radiation stress component alongshore  $S_{yy}$  is:

$$S_{yy} = \frac{1}{8} \rho g H^2 \left[ n(\sin^2 \theta + 1) - \frac{1}{2} \right] \quad (36)$$

### Bottom friction terms

129. Bottom friction is expressed as a quadratic stress law in the total local fluid velocity and is produced by the combination of steady motion from the mean wave- and wind-induced current and unsteady motion from oscillatory waves. The instantaneous shear stress components at the bottom are written,

$$\tau_{bx} = C_f \rho \sqrt{u^2 + v^2} u \quad (37)$$

$$\tau_{by} = C_f \rho \sqrt{u^2 + v^2} v \quad (38)$$

where  $C_f$  is an empirical bottom friction coefficient, and the x-component  $u$  and y-component  $v$  of the total current velocity (evaluated at the bottom) are given by:

$$u = U + u_b \quad (39)$$

$$v = V + v_b \quad (40)$$

The horizontal velocity components  $u_b$  and  $v_b$  of oscillatory wave motion at the bottom are given from linear-wave theory as,

$$u_b = u_m \cos\left(\frac{2\pi t}{T}\right) \cos\theta \quad (41)$$

$$v_b = u_m \cos\left(\frac{2\pi t}{T}\right) \sin\theta \quad (42)$$

where the amplitude of the horizontal component of the wave orbital velocity is

$$u_m = \frac{gHT}{2L \cosh\left(\frac{2\pi d}{L}\right)} \quad (43)$$

130. From Equations 37 and 38, the bottom friction terms in the x- and y- momentum equations (Equations 32 and 33) may be obtained, noting that  $F_{bx}$  and  $F_{by}$  are not identical to the shear stress but are by definition the shear stress components divided by water density and total depth:

$$F_{bx} = -\frac{C_f}{d} \langle \sqrt{u^2 + v^2} u \rangle \quad (44)$$

$$F_{by} = -\frac{C_f}{d} \langle \sqrt{u^2 + v^2} v \rangle \quad (45)$$

In these equations and elsewhere in this report, triangular brackets denote a time-averaging operation over the interval of a wave period.

131. As seen from the equations for the oscillatory velocity components (Equations 41 and 42),  $u$  and  $v$  are time dependent, and a time average will produce a nonzero value because of the existence of the steady current. Thus, in solving the governing equations to obtain the current velocity, intensive numerical computations are required not only because of the nonlinear (quadratic) stress law, but also to perform the time-averaging operation.

#### Lateral mixing terms

132. The lateral mixing terms describe the diffusion of momentum and are related to the turbulent Reynolds stresses. Lateral mixing, which is not well understood in the nearshore, is modeled using an eddy viscosity approach. The mixing terms may be expressed in general form as

$$L_x = \frac{1}{d} \left[ \frac{\partial}{\partial x} \left( \epsilon_{xx} d \frac{\partial U}{\partial x} \right) + \frac{\partial}{\partial y} \left( \epsilon_{xy} d \frac{\partial U}{\partial y} \right) \right] \quad (46)$$

$$L_y = \frac{1}{d} \left[ \frac{\partial}{\partial x} \left( \epsilon_{yx} d \frac{\partial V}{\partial x} \right) + \frac{\partial}{\partial y} \left( \epsilon_{yy} d \frac{\partial V}{\partial y} \right) \right] \quad (47)$$

where the  $\epsilon_{i,j}$  ( $i, j = x, y$ ) are the components of an eddy viscosity tensor.

133. Knowledge of momentum diffusion in the surf zone by turbulence is limited, but observations of the growth of a point source of dye injected in

the surf zone show that its dimensions increase much more rapidly across-shore as compared with alongshore, indicating that the magnitudes of the viscosity components involving the cross-shore component are much greater than that of  $\epsilon_{yy}$  (Kraus, Mimura, and Horikawa 1980). In the present case involving homogeneity alongshore and no cross-shore current in the steady-state case ( $U = 0$ ), the only eddy viscosity component of interest is  $\epsilon_{yx}$ , abbreviated as  $\epsilon$  hereafter.

134. Many forms of the eddy viscosity coefficient  $\epsilon$  have been proposed, as summarized by Kraus, Mimura, and Horikawa (1980); McDougal and Hudspeth (1986); and O'Conner and Yoo (1987). Traditionally, a Prandtl approach is taken in which the eddy viscosity coefficient is assumed proportional to appropriate velocity and length scales. Longuet-Higgins (1970b) set  $\epsilon \sim x(gh)^{1/2}$ , which is an intuitively reasonable representation in the surf zone and on a uniformly sloping beach, since the eddy size should increase with distance offshore (or, equivalently, with the wave height, which is depth-limited and proportional to distance offshore), and the velocity scale should be related to  $u_m$ , which is proportional to  $(gh)^{1/2}$  in shallow water. Madsen, Ostendorf, and Reyman (1978) introduced the form  $\epsilon \sim xu_m$  to give the eddy viscosity coefficient a decreasing value seaward of breaking waves; otherwise, for the surf zone their form of  $\epsilon$  is similar to that of Longuet-Higgins.

135. Kraus, Mimura, and Horikawa (1980) and McDougal and Hudspeth (1986) developed generalized analytic solutions of the longshore current profile as a function of the form of the eddy viscosity coefficient. Both groups concluded that the current profile on a plane beach was insensitive to the form of the coefficient. On a barred profile, parameterization of  $\epsilon$  with the cross-shore distance  $x$  is not logical because wave breaking in the vicinity of bars located at different distances from the shore will create local areas of agitated white water (strong turbulence), with possible quiescent green water (weak turbulence) in between bars where wave reformation can occur. Based on their measurements of the longshore current profile on a barred beach in the Great Lakes, Greenwood and Sherman (1986) concluded that lateral mixing was enhanced by current velocity gradients in the vicinity of bars.

136. In this report, the local bottom orbital velocity is taken as the characteristic velocity and the local wave height as the typical length scale to give,

$$e = \Lambda u_m H \quad (48)$$

where  $\Lambda$  is an empirical coefficient. In this formulation the eddy viscosity has two rational properties:

- a. It decays with distance seaward of the surf zone as the mean depth increases.
- b. It is sensitive to local wave conditions as exist in breaking over bars and reformation over troughs, in that larger waves will produce greater mixing.

#### Wind-driving terms

137. The local wind is another important driving force in the nearshore. Birkemeier and Dalrymple (1975) were among the first to consider the wind in nearshore circulation numerical modeling. If a wind blows over a water surface, a current will be generated, and the surface will tilt in adjustment of the water body to the transfer of momentum at the air-sea interface. Wind-generated currents have been detected at depths on the order of 100 m (Long and Hubertz 1988), and strong wind can produce significant setup and setdown at the shoreline during storms, depending on the direction of its cross-shore component (e.g., Bretschneider 1966).

138. The wind stress appears as a forcing term in the momentum equations and is expressed by a quadratic drag law. For a wind blowing over a water surface, the shear stress  $\tau_s$  at the air-water interface is written,

$$\tau_s = C_D \rho_a W^2 \quad (49)$$

where the subscript  $s$  refers to forcing by wind at the water surface. The shear  $\tau_s$  has the units of  $N/m^2$ , and

$C_D$  = drag coefficient

$\rho_a$  = density of air ( $kg/m^3$ )

$W$  = wind speed (m/sec)

If the wind blows at an angle to the shoreline, the wind-induced shear stress in Equation 49 is expressed as a cross-shore component  $\tau_{sx}$  and a longshore component  $\tau_{sy}$ ,

$$\tau_{sx} = C_D \rho_a |W| W \cos \phi \quad (50)$$

$$\tau_{sy} = C_D \rho_a |W| W \sin \phi \quad (51)$$

where  $\phi$  is the incident angle of the wind. The angle definition employed in Equations 50 and 51 is shown in Figure 1.

139. In the general case of a wind blowing at a nonzero angle to the shoreline, the driving terms describing the wind in the momentum equations, Equations 32 and 33, are:

$$R_{sx} = -\frac{C_D \rho_a}{\rho d} |W| W \cos \phi \quad (52)$$

$$R_{sy} = \frac{C_D \rho_a}{\rho d} |W| W \sin \phi \quad (53)$$

In a strict sense, in the wind-driving terms the velocity difference between the wind and the water surface  $W - V$  should be used instead of  $W$  alone. The speed of a coastal current induced by a persistent wind is about 3 percent of the mean wind speed (e.g., Hsu (1988) and the discussion in the next chapter). Because the condition  $W \gg V$  is expected to hold in all applications,  $V$  can be neglected in comparison to  $W$ . Inclusion of  $V$  in the wind-driving term would add another nonlinearity and complicate the numerical solution, although the iterative solution scheme used in the nonlinear model could accommodate such an expression, but at greater computational overhead. From discussion in Part III, the uncertainty in the value of the drag coefficient appears to obviate further any practical need to account for the relative speed of the wind and current in the wind-driving terms.

140. If a steady wind blows over the open-ocean surface, it is well known (Pond and Pickard 1977, Bishop 1984) that the resultant equilibrium current will not be in the direction of the wind, but an angle to the right (left) in the Northern (Southern) Hemisphere because of the Coriolis force. The Coriolis force is not included in the equations of motion used in this

report because of the relatively narrow seaward extent of the longshore current, but the possible necessity of including the Coriolis force in the offshore boundary condition is noted.

141. At some sites, the coastal wind boundary layer (Hsu 1988) should be considered to account for changes in the local wind speed and direction. Further research on this subject is planned.

#### Governing Equations for Longshore Current and Setup

142. The full governing equations, Equations 32 and 33, are reduced based on the following assumptions:

- a. Linear-wave theory is applicable everywhere, both inside and outside the surf zone.
- b. The time-averaged cross-shore current  $U$  is zero.
- c. The bottom contours are straight and parallel, indicating uniformity in the  $y$ -direction ( $\partial/\partial y = 0$ ).
- d. Bottom friction in the cross-shore direction is small in comparison with  $\partial S_{xx}/\partial x$ . (Retaining the cross-shore friction term couples the momentum equations.)

These assumptions imply that all convective acceleration terms in Equations 32 and 33 are zero. The friction and lateral mixing terms vanish from the momentum equation in the  $x$ -direction (Equation 32), leaving:

$$\rho g d \frac{d\eta}{dx} = - \frac{dS_{xx}}{dx} - C_D \rho_a |W| W \cos \phi \quad (54)$$

Neglecting wind, this equation reduces to Equation 15 used in the wave model to compute setup and setdown. Because the variables in Equation 54 depend only on the  $x$ -coordinate, the partial derivatives in Equation 32 were changed to full derivatives.

143. After simplifications based on the above-listed assumptions, the remaining terms in the  $y$ - or longshore component momentum equation are wave driving, wind driving, bottom friction, and lateral mixing. Equation 33 may thus be written, using Equation 35 for the wave-driving term and Equation 47 for the lateral mixing term,

$$\frac{d}{dx} \left( \epsilon d \frac{dV}{dx} \right) - f_{by} = \frac{1}{\rho} \frac{dS_{xy}}{dx} - C_D \frac{\rho_a}{\rho} |W| W \sin \phi \quad (55)$$

where  $f_{by}$  is defined as:

$$f_{by} = - F_{by} d \quad (56)$$

Equation 55 is a second-order nonlinear ordinary differential equation in the current velocity. The assumptions decouple the momentum equations (if the wave-current interaction is neglected), eliminating the need for simultaneous solution of the waves and longshore current, significantly reducing computational time and improving stability. The nonlinearity enters through the bottom friction term containing a dependence on current velocity squared. The next section discusses different simplifications and procedures for evaluating the bottom friction terms, and their validity.

#### Evaluation of Bottom Friction

144. The computational difficulty in evaluating the bottom friction term lies not only in its dependence on the current velocity squared, introducing a strong nonlinearity, but also in the time-average that has to be calculated at each model grid point across the shore because of the oscillatory motion of the waves (Equation 45). From Equations 41 and 42 for the orbital velocities, the y-component of the friction term may be expressed as:

$$f_{by} = c_f \left\{ \left[ u_m^2 \cos^2 \left( \frac{2\pi t}{T} \right) + v^2 + 2V u_m \cos \left( \frac{2\pi t}{T} \right) \sin \theta \right]^{1/2} \left[ V + u_m \cos \left( \frac{2\pi t}{T} \right) \sin \theta \right] \right\} \quad (57)$$

145. Evaluation of  $f_{by}$  at each model grid point through the surf zone is computation intensive; a 16-point Simpson integration or an 8- or 16-point Gauss integration is typically used to perform the time average. In analytic treatments and in many numerical circulation models, simplifying approaches have been taken to linearize Equation 57 by putting restrictions on the ratio

of the magnitude of the current velocity to the wave orbital velocity, as well as restricting the incident wave angle.

146. As discussed in the literature review in Part II, reliable theoretical formulas for the friction factor  $c_f$  are lacking for the surf zone, although the value in the field seems to be fairly well established in the range of approximately 0.005 to 0.01. Numerical experimentation with NMLONG did not produce improved agreement between measurements and calculations using the wave-dependent friction factor of Jonsson (1966), although the Jonsson factor did provide values of the correct order of magnitude. To reduce model calculation time, a constant value of  $c_f$  is used that can be a default value or a value determined in calibration.

#### Weak-current (linear) approximation

147. The most common approximation to Equation 57 (Bowen 1969, Longuet-Higgins 1970a) results from the assumptions that the current is weak with respect to the magnitude of the wave orbital velocity and that the incident wave angle is small. With these restrictions Equation 57 can be expanded in a Taylor series and time-averaged term by term; after higher order terms are dropped, a linear form of  $f_{by}$  in  $V$  is obtained:

$$f_{by} = \frac{2}{\pi} c_f u_m V \quad (58)$$

A higher order approximation was presented independently by Liu and Dalrymple (1978) and Kraus and Sasaki (1979), still assuming a weak current, but allowing large incident wave angles. The time-averaged friction term becomes:

$$f_{by} = \frac{2}{\pi} c_f u_m V (1 + \sin^2\theta) \quad (59)$$

#### Strong-current approximation

148. The case of a strong current and small waves is simple and reduces Equation 57 to a quadratic velocity dependence on the current according to:

$$f_{by} = c_f |V| V \quad (60)$$

Square-wave approximation

149. A more applicable approach for numerical modeling was introduced by Nishimura (1982, 1988), who approximated the sinusoidal time variation in wave orbital velocity by a square wave with the same area. This construct allows an explicit solution of Equation 57 to be obtained with respect to the time-averaging procedure, the details of which are given in Appendix A. For negligible cross-shore current ( $U = 0$ ), Nishimura's expression for the time-averaged friction term is,

$$f_{by} = c_f \left( Z + \frac{w^2}{Z} \sin^2 \theta \right) V \quad (61)$$

where the auxiliary quantities  $Z$  and  $w$  are defined as:

$$Z = \frac{1}{2} \left( \sqrt{V^2 + w^2 + 2wV \sin \theta} + \sqrt{V^2 + w^2 - 2wV \sin \theta} \right) \quad (62)$$

$$w = \frac{2}{\pi} u_m \quad (63)$$

150. According to Nishimura (1988) the maximum relative error in this approximation is 10 percent as compared with high-order numerical integration of Equation 57. (The accuracy of Equation 61 is investigated in Appendix A.) Equation 61 significantly reduces the computation time for the longshore current because the time averaging was performed analytically; also, the necessity of invoking the assumptions of a weak longshore current and small wave angles is eliminated. A quadratic dependence on the velocity in Equation 55 still remains, requiring an iterative approach to solve for the current.

151. In the development of NMLONG, both a linear (Equation 59) and a nonlinear (Equation 61) bottom friction law were considered, yielding two different numerical solution schemes or models. To investigate the validity of the different approximations of the bottom friction term, Equation 57 was

integrated numerically using 20-point Gauss quadrature, yielding a quantity  $(f_{by})_{non}$  accurate to about the fourth decimal place. The bottom friction term given by Equation 57 was normalized with the linearized bottom friction  $(f_{by})_{lin}$  according to Equation 58. The ratio  $(f_{by})_{non}/(f_{by})_{lin}$  depends on two nondimensional variables as shown in Figure 10, the ratio of magnitudes of the current and the wave orbital velocity  $V/u_m$ , and the incident wave angle  $\theta$ .

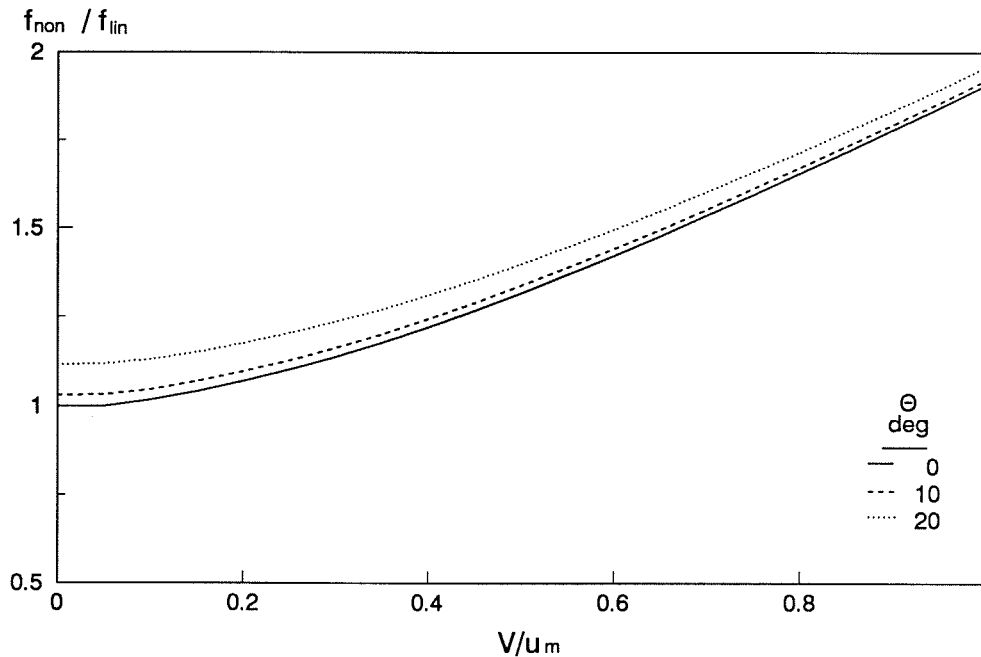


Figure 10. Comparison of linear and quadratic bottom friction

152. Figure 10 displays the deviation between the numerically evaluated (complete) friction term and the linearized term as a function of  $V/u_m$  and  $\theta$ . The linear friction formulation gives errors as great as 50 percent for strong currents and large wave angles. The influence of the angle is more effective at small values of  $V/u_m$ , because the term  $V^2$  dominates for strong currents. If the magnitude of the current velocity equals that of the wave orbital velocity, the bottom friction stress for the linearized formulation is only half the correct value if the same value of  $c_f$  is applied in both cases. This discrepancy can be avoided in the pragmatic sense by calibrating the linear current model with a larger value of  $c_f$ . Thus linearized models have been applied successfully at  $V/u_m$ -ratios well beyond the strict limit of mathematical validity of the weak-current approximation.

### Approximation to the Nonlinear Solution

153. If lateral mixing is omitted it is possible to derive a correction factor to be applied to the solution of the linearized model to obtain the current velocity from the nonlinear model. This factor, called  $\alpha$ , is a function of  $V/u_m$  and  $\theta$ , and must for the general case be represented in tabular or graphical form. Omitting mixing in Equation 55, the driving force is balanced by bottom friction. Therefore, for a certain driving force (waves and/or wind), the bottom friction force will be identical whether a linear or a quadratic friction law is used. By equating the friction formulations specified by Equations 57 and 58, a relation is derived between the velocity predicted by the nonlinear model, numerically evaluated as  $V_{non}$ , and that predicted by the linear model  $V_{lin}$ . An equation for  $\alpha$  is obtained,

$$\alpha \int_{-1}^1 \sqrt{\cos \pi z (\cos \pi z + 2\alpha \psi \zeta) + \alpha^2 \psi^2} \left( 1 + \frac{\zeta \cos \pi z}{\alpha \psi} \right) dz = \frac{4}{\pi} \quad (64)$$

where  $z = 2t/T$  is a dummy integration variable for the transformation made to obtain convenient limits for Gauss integration, and

$$\alpha = \frac{V_{non}}{V_{lin}} \quad (65)$$

$$\psi = \frac{V_{lin}}{u_m} \quad (66)$$

$$\zeta = \sin \theta \quad (67)$$

154. A Newton-Raphson technique was employed to find the solution of Equation 64. In Figure 11 the factor  $\alpha$  is displayed as a function of  $V_{lin}/u_m$  and  $\theta$ . As also seen in Figure 10, the incident wave angle is only important for small values of  $V_{lin}/u_m$ , because the solution approaches the strong-current case for large values on  $V_{lin}/u_m$ .

155. As previously stated,  $\alpha$  may be used to correct the solution obtained with a linearized friction term in the absence of lateral mixing. Without mixing, the current velocity at any point across the shore is independent of the velocity at neighboring points and may be solved for independently

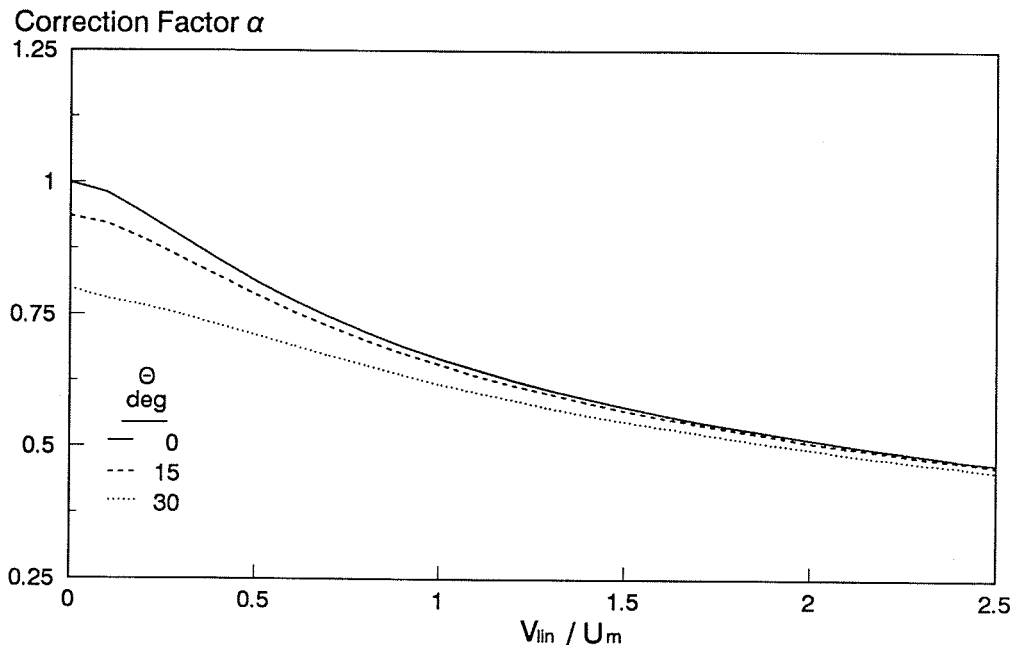


Figure 11. Correction factor for nonlinear friction term

once local wave and wind properties are known. The factor  $\alpha$  is determined by local wave properties that enter through the wave orbital velocity and wave angle.

156. The factor  $\alpha$  may be interpreted in another way, namely, as a function of the bottom friction coefficient  $c_f$ . Identical current velocities may be obtained from the nonlinear and linear models if different values of the friction coefficient  $(c_f)_{non}$  and  $(c_f)_{lin}$  are employed in the respective models (still neglecting lateral mixing) such that  $(c_f)_{non} = \alpha (c_f)_{lin}$ , with  $\alpha$  defined as before. It is noted that even if  $(c_f)_{lin}$  is taken as a constant, the apparent  $(c_f)_{non}$  will vary in accordance with the local wave properties because  $\alpha$  is a function of those properties.

157. Limiting cases of Equation 64 provide insights to previous work. If  $\psi$  approaches zero (weak-current assumption), the limiting value is:

$$\alpha = \frac{1}{1 + \zeta^2} \quad (68)$$

If dimensional quantities are reintroduced, the solution for the current will be (dropping the index "non" for the improved solution of the current):

$$V = \frac{R_{by} + R_{sy}}{\frac{2}{\pi} C_f u_m (1 + \sin^2 \theta)} \quad (69)$$

Equation 69 is identical to the solution obtained with the large-angle and weak-current friction formulation used by Liu and Dalrymple (1978) and Kraus and Sasaki (1979), omitting the wind-driving term. This expression for the bottom friction involves no restrictions in terms of the wave angle, but only depends on the assumption of a weak current with respect to the magnitude of the bottom wave orbital velocity and is, in that sense, exact.

158. The other limiting case of Equation 64 to consider is  $\Psi \rightarrow \infty$ , the so-called strong-current approximation. In this case, Equation 64 may be solved to yield:

$$\alpha = \left( \frac{2}{\pi \Psi} \right) \quad (70)$$

Expressed in dimensional quantities, Equation 70 simplifies to:

$$V = \left( \frac{R_{by} + R_{sy}}{C_f} \right)^{\frac{1}{2}} \quad (71)$$

This solution corresponds to the formulation given in Equation 60.

159. Lateral mixing is expected to enter in applications, which eliminates the possibility of using a simple approach with a correction factor to obtain a rapid solution of the nonlinear current equation. However, computation time is reduced by applying the correction factor to improve the initial estimate in an iterative scheme involving the quadratic bottom stress term.

## Evaluation of the Wind Drag Coefficient

160. Two problems are associated with applying Equation 49 for the wind stress, determining the value of the drag coefficient  $C_D$  and choosing a proper wind speed. These problems are related because  $C_D$  is expected to vary with the reference height of the wind according to the variation of the wind speed with elevation. In most applications the drag coefficient is referenced to the wind speed given at a level of 10 m. The drag coefficient is a bulk description of the flow resistance offered by the water surface and is composed of two parts, frictional drag and form resistance. Frictional drag is caused by the shear along the water surface, and form drag is produced by pressure differences associated with the shape of the surface. Thus  $C_D$  is expected to be a function of several parameters including a representative roughness length scale of the surface and the general air flow conditions. A difficulty in determining the value of the drag coefficient at an air-sea interface is the mobility of the water surface and the ease in which it deforms. Strong winds create waves and thus increase the surface roughness as compared with more moderate winds.

161. A large number of studies have been performed with the objective of determining the drag coefficient over a water surface (or roughness length scale of the surface). Garratt (1977) and Long and Hubertz (1988) review such studies and summarize measured values of  $C_D$ . Typical values are in the range of  $1 \cdot 10^{-3}$  to  $3 \cdot 10^{-3}$  with the associated wind speed in the interval 5 to 20 m/sec, although large scatter in the data is common. Long and Hubertz (1988) reported a factor of 32 between the lowest ( $0.2 \cdot 10^{-3}$ ) and highest ( $6.4 \cdot 10^{-3}$ ) value of  $C_D$  found in the literature. A dependence of  $C_D$  on the wind speed is also found (Garratt 1977, Large and Pond 1981, Amorocho and DeVries 1980, The WAMDI Group 1988), at least for higher wind speeds, and some recent studies also attempt to quantify the influence of waves (Huang *et al.* 1986).

162. The classical method for determining the drag coefficient is based on a logarithmic velocity profile above the water surface,

$$W(z) = \frac{u_*}{\kappa} \ln\left(\frac{z}{z_0}\right) \quad (72)$$

where

$u_*$  = shear velocity ( $= (\tau_s/\rho)^{1/2}$  (m/sec)

$\kappa$  = von Karman's constant (about 0.41)

$z$  = elevation above water surface (m)

$z_0$  = roughness length scale (or location where  $W = 0$ ) (m)

From measured wind velocity profiles, it is possible to empirically determine  $u_*$  and  $z_0$ , and, thus,  $C_D$ . The drag coefficient is written using Equation 49 and the definition of shear velocity,

$$(C_D)_{10} = \frac{u_*^2}{(W_{10})^2} \quad (73)$$

where the subscript "10" denotes values evaluated at the 10-m elevation.

163. The logarithmic wind velocity profile represented by Equation 72 is valid for neutral (adiabatic) atmospheric stability. Under non-neutral conditions of either stable and unstable thermal stratification, the wind profile departs from logarithmic form. However, the effect of thermal stratification diminishes with increasing wind speed, more so for stable than unstable conditions. Hsu (1972) measured the vertical wind profile at three locations in the surf zone over a 2-week period and obtained nearly 1,500 15-min average profiles. Analysis of the profile data under adiabatic and onshore wind conditions showed that more than 90 percent of the wind measurements were logarithmic. This result and others referenced by Hsu (1972) indicates that stress laws developed from logarithmic wind profiles are adequate for routine applications of engineering models.

164. Most investigations of  $C_D$  transform the calculated drag coefficient to neutral or stable atmospheric conditions using environmental data at the measurement site. In the simulations presented here, it is assumed that the atmospheric conditions are stable and that values of  $C_D$  from the literature

may be applied without corrections. Also, all wind velocities and drag coefficients refer to the 10-m elevation if not otherwise stated.

165. To establish the order of magnitude of the drag coefficient within the context of longshore current modeling and to qualitatively investigate the relationship between the transfer of momentum at the air-sea interface and the resulting current, the simple situation without lateral mixing and wave driving was examined. From the momentum equation, Equation 55, it is seen that the wind stress is balanced by bottom friction. Since the momentum equation is vertically integrated, the wind effectively acts on the entire water body and generates an average current velocity  $V$ . In the nearshore region with comparably shallow water, this conceptual model should provide a good first approximation. Thus, equating the wind stress to the bottom friction stress yields the following relationship between wind speed and wind-generated current velocity (which is a general velocity and not just the longshore current velocity) in the situation of equilibrium momentum transfer:

$$V = \left( \frac{\rho_a}{\rho} \right)^{\frac{1}{2}} \frac{C_D}{C_f} W \quad (74)$$

The ratio between the density of air ( $\rho_a = 1.2 \text{ kg/m}^3$ ) and density of seawater ( $\rho = 1.03 \cdot 10^3 \text{ kg/m}^3$ ) is approximately 1/850. With a ratio of  $C_D/C_f = 0.2$ , the magnitude of the wind-generated current velocity is approximately 1.5 percent that of the wind speed, whereas for a ratio of 1.0 the corresponding value is 3.5 percent. In the presence of waves, the generated current for a specific ratio of  $C_D/C_f$  will be smaller because of the additional friction force contributed by the wave bottom orbital velocity.

166. To obtain quantitative information on the ratio  $C_D/C_f$ , field data from the FRF as described in Hubertz *et al.* (1987) and Birkemeier *et al.* (1987) were used. These studies describe results of a comprehensive study of nearshore waves and currents conducted during September 1985 in which the current was measured at 11 locations in the nearshore together with a large number of other oceanographic and meteorological parameters. The longshore current data set was not used in the present modeling on longshore currents since most of the current meters were outside the surf zone during the

measurement time (although a storm with high waves passed the area on 12 to 14 September, providing some potentially useful data). Also, it was difficult to obtain reliable information on the incident wave angle defining conditions favorable to current modeling; the times currents were generated only by local winds were not known. However, the data do provide the capability of evaluating wind-generated currents in an approximate fashion.

167. The objective of the present analysis is to obtain a rough estimate of the ratio  $C_D/c_f$  from wind and current measurements through regression analysis. A data record from 7 to 14 September 1985 containing hourly averages of wind speed and direction, longshore current velocity, wave height, and wave period was analyzed. On or after 14 September, a rip current appeared at the location of the main array of the current meters, making the measurements after that date inappropriate for the present purpose. The current was taken from the most seaward current meter (Gage SD25) in the array (in an average water depth of 6.1 m) to minimize the influence of currents generated by breaking waves. At this location the current was measured at three vertical stations, and averages of those stations were used. The wind speed and direction were measured at the end of the FRF pier at elevations of 14.02 m (Gage 682) and 12.97 m (Gage 683), respectively. No effort was made to transform the wind measurements to the 10-m level or correct for instability in the atmosphere.

168. Although the current was measured outside the breaker zone with presumably little contamination by the wave-generated longshore current, the wave orbital velocity was still an important factor determining the bottom friction because the current meter was situated in relatively shallow water. Wave information from Gage 640 in 8 m of water was used to calculate the bottom orbital velocity. Because reliable information on the incident wave angle was lacking, a small-angle assumption was made, meaning the wave angle was neglected in determining the bottom friction. The mean wave height was chosen as a representative measure for calculating the bottom orbital velocity, and the bottom friction was computed from the Nishimura (1982) square-wave approximation (Equation 61).

169. The empirical relationship between  $V[V^2 + (2/\pi)u_m^2]^{1/2}$  and  $|W|W_y$  is determined from the trend in the 153 available data points obtained under the aforementioned assumptions and plotted in Figure 12, for which  $W_y = |W|\sin\phi$  is

the longshore component of the wind. The least-squares fitted straight line through the measurement points is also shown. Although considerable scatter is present (partly due to simplifications introduced in the analysis), a clear trend indicates that stronger currents are associated with stronger winds. The slope of the straight line represents the ratio  $\rho_a/\rho C_D/c_f$ , from which an average value can be evaluated. Assuming a density ratio between air and seawater of 1/850, the slope of the line in Figure 12 gives  $C_D/c_f = 1.2$ . Thus, according to this exploratory analysis, the drag and bottom friction coefficients were approximately equal for the conditions studied. This result is within the range of variability of the parameter values as reported in the literature, but higher than typical values reported. Most values of  $C_D$  given in the literature are considerably smaller than values of  $c_f$ .

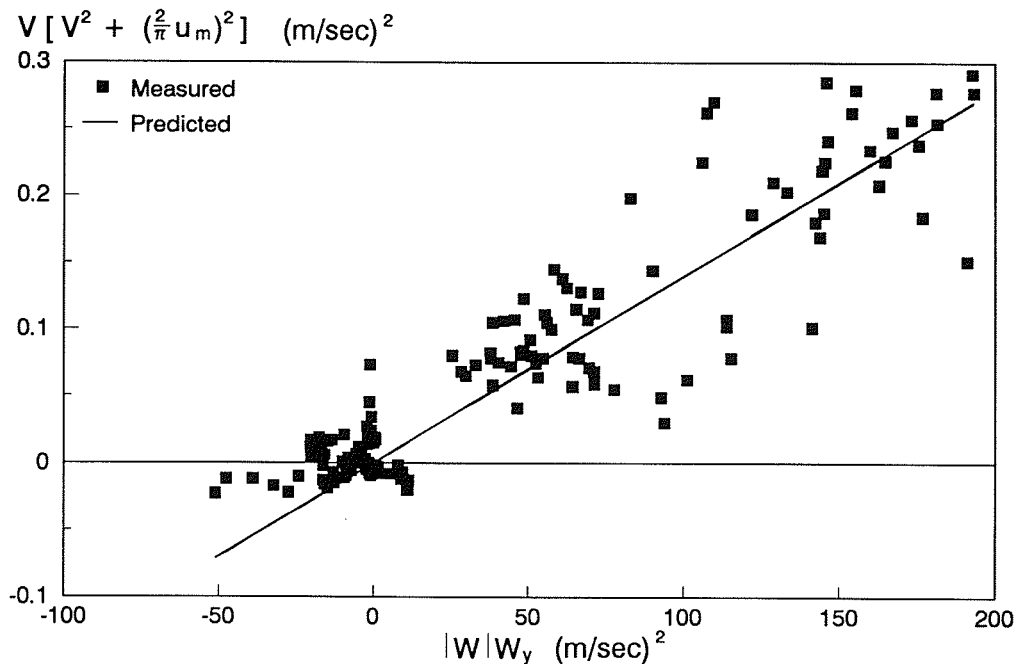


Figure 12. Wind-induced longshore current versus wind velocity

170. Although the above analysis was crude, it shows that  $C_D$  and  $c_f$  have the same order of magnitude. The coefficient of determination for the regression line in Figure 12 is  $r^2 = 0.82$ , indicating that more than 80 per cent of the variation in the measured data is explained by the regression model. Inclusion of an intercept in the regression only marginally improved

the fit ( $r^2 = 0.84$ ), thus supporting the assumption that the wind is the dominant driving force for the currents studied in this analysis. However, although a simple linear regression model between wind and current provides a reasonable description according to the data analysis, the cause and effect process between wind and current is complex. Other factors are involved, such as the contribution to the current from obliquely incident breaking waves which were in part or entirely generated by the wind at the site.

171. The WAMDI Group (1988) found that their hindcast of waves in the North Sea was sensitive to the value of the drag coefficient for high wind speeds and developed the following expression used in NMLONG:

$$C_D(W) = \begin{cases} 1.2875 \cdot 10^{-3}, & |W| < 7.5 \text{ m/sec} \\ (0.8 + 0.065|W|) \cdot 10^{-3}, & |W| \geq 7.5 \text{ m/sec} \end{cases} \quad (75)$$

172. Hsu\* compared predictions of Equation 75 with his field measurements in the Gulf of Mexico made at both low wind speeds and at very high wind speeds in a hurricane. Equation 75 fit his data well through the range of wind speeds. This independent agreement provides validation of the WAMDI drag coefficient formula at a site with very different wind and wave characteristics, but both sites are relatively shallow-water basins, a situation occurring in nearshore applications involving longshore currents in and near the surf zone.

#### Numerical Solution of the Longshore Current Equation

173. If the wave-current interaction is neglected, iteration between the wave and current calculations is not necessary, and all wave properties can be determined prior to solving for the current. These wave properties enter in the current calculation through the wave driving term  $dS_{xy}/dx$ , the bottom friction term that depends on  $u_m$  and  $\theta$ , and the lateral mixing term that depends on  $H$  and  $u_m$ . The x-component momentum equation yields the mean displacement of the water surface and thus the time-averaged mean water depths

---

\* Personal Communication, November 1989, Dr. S. A. Hsu, Professor, Coastal Studies Institute, Louisiana State University, Baton Rouge, LA.

used in calculation of the current. The numerical grid for the current calculation is superposed with the wave model grid as discussed next.

Finite-difference equations

174. Figure 13 is a definition sketch for the discretization and numerical solution scheme used in the longshore current models. (A corresponding sketch for the wave model is given in Figure 2.) The same approach is used for the linear and nonlinear current models, except that the nonlinear model requires iteration between the current and bottom stress. The numerical solution will first be described for the linear model and additional comments given regarding modifications necessary for solving the nonlinear model equations.

175. For convenience, the quantities  $A$  and  $B$  are defined to simplify notation:

$$A = ed \tag{76}$$

$$B = \frac{2}{\pi} C_f u_m (1 + \sin^2 \theta) \tag{77}$$

Equation 55 is written, using the bottom friction term from Equation 59,

$$A \frac{d^2 V}{dx^2} + \frac{dA}{dx} \frac{dV}{dx} - BV = \frac{1}{\rho} \frac{dS_{xy}}{dx} - C_D \frac{\rho_a}{\rho} |W| W \sin \phi \tag{78}$$

Equation 78 is expressed in difference form in Equation 79 for each calculation cell running from number 2 to  $N - 1$  for a grid encompassing  $N$  cells. Boundary conditions on  $V$  must be provided at cells 1 and  $N$ . Difference equation representations of Equation 78 are coupled by the mixing terms (terms in Equation 78 involving  $A$ ) and form a system of  $N - 2$  equations with  $N - 2$  unknown current velocities  $V$ .

176. The system of equations is tridiagonal and can be solved with a double-sweep (implicit solution scheme) technique. In the following, the subscript  $i$  denotes (as before) the number of a specific calculation cell, and a staggered grid will be used with certain quantities evaluated in the middle

of a cell and others at the cell boundaries, according to Figure 13. The current velocity is given in the middle of a cell ( $h$ -point) together with the quantity  $B_i$ , whereas  $A_i$  and  $(S_{xy})_i$  are evaluated at the boundaries of calculation cells ( $H$ -points). Because  $B$  contains the wave orbital velocity and wave angle, its value is interpolated from neighboring  $H$ -points. A staggered grid of this type, which involves averaging and overlapping of calculated quantities, enhances the stability of the numerical scheme by calculating derivatives at the most appropriate position.

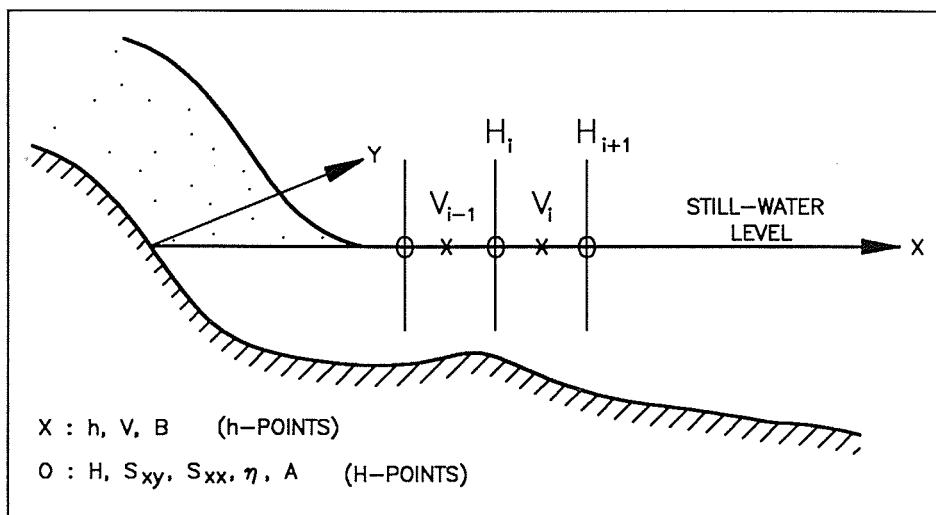


Figure 13. Definition sketch for longshore current calculation

177. The canonical form of the difference equation for calculation cell number  $i$  is,

$$-AH_iV_{i-1} + BH_iV_i - CH_iV_{i+1} = RH_i \quad (79)$$

where the coefficients are defined as:

$$AH_i = - \frac{A_i}{(\Delta X)^2} \quad (80)$$

$$BH_i = - \left[ B_i + \frac{(A_{i+1} + A_i)}{(\Delta X)^2} \right] \quad (81)$$

$$CH_i = - \frac{A_{i+1}}{(\Delta X)^2} \quad (82)$$

$$RH_i = \frac{1}{\rho} \frac{(S_{xy})_{i+1} - (S_{xy})_i}{\Delta X} - C_D \frac{\rho_a}{\rho} |W| W \sin \phi \quad (83)$$

Analogous to the wave model,  $H$ -point number  $i$  lies on the left boundary of the corresponding calculation cell.

178. By introducing two auxiliary coefficients,  $EE_i$  and  $FF_i$ , a double-sweep solution scheme may be derived. It is assumed that a recursive solution to the system of equations exists of the form:

$$V_i = EE_i V_{i+1} + FF_i \quad (84)$$

By substituting Equation 84, written for index  $i-1$ , into Equation 79 the following expressions are obtained for the double-sweep coefficients,

$$EE_i = \frac{CH_i}{DN_i} \quad (85)$$

$$FF_i = \frac{AH_i FF_{i-1} + RH_i}{DN_i} \quad (86)$$

where

$$DN_i = BH_i - AH_i EE_{i-1} \quad (87)$$

The solution procedure is to determine  $EE_i$  and  $FF_i$  starting from  $i = 2$  through the whole grid in a forward sweep from knowledge of the shoreward boundary condition at grid point  $i = 1$ . The current velocities are then calculated in a backward sweep from point  $N - 1$  by using Equation 84 and the seaward boundary condition at  $i = N$ .

#### Boundary conditions

179. Specification of the seaward boundary condition is straightforward: zero wave-induced current velocity at the end of the grid, i.e., only a wind-induced current if a wind is blowing. This specification requires that the seaward-most calculation cell ( $i = N$ ) be located sufficiently distant from the break point to truly have negligible wave-induced current. If the seaward grid boundary is located too close to the break point, the current profile will be artificially skewed toward the low side. One surf zone width seaward of the break point is considered sufficient distance for the situation of no wind. If a strong wind that has a substantial cross-shore component is blowing, the seaward-most calculation cell must be located much farther offshore since setup or setdown may extend to deeper water.

180. The most frequently specified shoreward boundary condition in the literature is zero current at the shoreline, although this contradicts field observations, which commonly show a longshore current in the swash zone. The equations used in the present and other longshore current models have limited validity in the swash zone, where complex fluid motion and strong fluid-sediment-bed interactions not described by the conventional governing equations employed here take place. To improve the current prediction in shallow water close to the shoreline or swash zone, a different boundary condition is employed in the present models. A finite-valued current at the shoreward boundary is determined from the governing equation neglecting mixing, which then allows an explicit solution to be found. The current velocity at the most shoreward grid point is determined for the linear case as,

$$V_1 = - \frac{1}{\rho B_1} \frac{(S_{xy})_2 - (S_{xy})_1}{\Delta x} \quad (88)$$

in which the subscript "1" refers to the most shoreward cell. By using Equation 84, the shoreward boundary condition can be expressed in terms of the double-sweep coefficients. It is found that  $EE_1 = 0$  and  $FF_1 = V_1$ .

#### Nonlinear model

181. If the nonlinear bottom friction term is used, a double-sweep solution is not directly applicable since terms arise containing  $V^2$  which prevents deriving a simple recursive formula such as Equation 84. However, if an iterative technique is employed and the quadratic friction term approximated using velocity values from the preceding iteration, the double-sweep scheme can still be employed. Initially, the current profile calculated with a linear friction term is used as a first approximation in the iteration for the nonlinear current profile. The only difference as compared with the previously discussed solution scheme is the quantity  $B$  (Equation 77), which is replaced by,

$$B = c_f \left( Z + \frac{w^2}{Z} \sin^2 \theta \right) \quad (89)$$

where  $Z$  and  $w$  are defined in Equations 62 and 63, respectively, and the current velocity  $V$  needed in  $Z$  is taken from the previous iteration. The current profile is recalculated in this manner until the maximum difference between consecutive iterations at any point is less than some predefined percentage of the current, typically 1 percent.

182. The shoreward boundary condition requires an iterative approach in the nonlinear model. (The seaward boundary condition also requires iteration if a wind-induced current is present.) Equation 88 is still applicable, but the factor  $B_1$  contains the velocity  $V_1$ , a quantity that is required as part of the solution. A Newton-Raphson solution method is used to determine this velocity at the shoreward boundary with a starting value from the linear solution.

183. To reduce the number of iterations required to obtain the solution to the nonlinear equation, values obtained from the linear solution are multiplied by a correction factor  $\alpha$  as given in Appendix A to provide the initial approximation. Multiplication by  $\alpha$  typically saves one to three iterations out of typically four to eight total iterations, a reduction of about one third to one half the number of required calculations. If both waves and wind generate the longshore current and if the wind contribution is dominant in some areas of the surf zone, the number of iterations may increase to 10 or 20. Such a situation is rare, because a strong wind will ordinarily be accompanied by high waves.

#### Wave-current interaction

184. If the wave-current interaction is included, calculations of wave properties and the current become coupled and must be solved iteratively. Because the effect of the current on the wave height distribution was found to be small for all current velocities tested, the calculation is started by assuming no wave-current interaction. After the current computation is made, the wave height distribution is updated, and a new current profile is obtained. The calculation including wave-current interaction normally converges after two or three iterations of this outer loop to satisfy a 1 percent tolerance for the wave height and current at each grid point.

## PART VI: VERIFICATION OF LONGSHORE CURRENT MODEL

185. The present model is a generalized version of other analytic and numerical models of the wave-induced current which have many times been demonstrated to provide accurate descriptions of the form and magnitude of the longshore current; therefore, verification is assured for the situation of regular waves shoaling on beaches with monotonically increasing depths and with no wind present. Since the model has more capabilities than previous ones, the more germane questions to be addressed in verification are:

- a. What is the difference in predictions between the linear and nonlinear current models?
- b. Are predictions reasonable for the longshore current (and waves) generated over a barred bottom profile?
- c. Are values of empirical parameters in the current models sufficiently stable that the model can be used in engineering applications with minimal or no changes?
- d. Are the wind-induced current and effect of wind on the mean water level properly calculated, and does the representation of the wind produce reasonable results?
- e. How important is the wave-current interaction?
- f. Is the model sufficiently efficient to be implemented in a desk-top computer environment?

186. To verify the applicability of the linear and nonlinear longshore current models and to establish parameter values, the models were tested to reproduce measurements from both laboratory and field. The advantage of a laboratory environment is collection of data under controlled conditions with high resolution in time and space. In the field the forcing conditions change continuously, making it difficult to quantify the relationship between cause and effect, and processes unaccounted for in the model may be acting. However, field data sets provide the ultimate test of numerical models and are thus of greatest importance.

187. The numerical models were verified using three data sets: the wave-induced longshore current, wave height, and mean water level from the laboratory experiment of Visser (1982); the field data on the current from Kraus and Sasaki (1979); and the field data on the waves and current from Thornton and Guza (1989). Example calculations were also made for a case involving the hypothetical barred topography used by Ebersole and Dalrymple

(1980) in their nearshore modeling simulation. For the field data simulations, the random wave model was used to drive the longshore current model. The influence of wind on the predicted longshore current and mean water surface elevation was also investigated in sensitivity tests.

#### Laboratory Data from Visser (1982)

188. The numerical current model was first applied to simulate four cases from the high-quality measurements reported by Visser (1982). This excellent data set provides a wide range of wave and current conditions for longshore current model testing. Visser conducted his experiments in a large rectangular wave basin with a plane-sloping beach using waves with fixed height, period, and incident wave angle. Extraordinary care was taken to minimize boundary effects through use of lateral discharge controls to minimize circulation in the basin, and it is believed that artificial processes associated with the finite size of the basin were reduced to a negligible level in the middle section of the basin. Seven cases were performed with different values of one or more of the quantities of wave height, period, incident angle, beach slope, and bed roughness. Four cases were chosen in the present study as representative of the variation in the above-mentioned variables, namely, Cases 1, 3, 4, and 7 in Visser's notation.

189. Table 3 summarizes the four cases, and Appendix B gives a listing of the corresponding wave height and current data that were compared with model simulation results. The current profile data in Appendix B were obtained by averaging Visser's measurements from transects located in the middle of the wave basin, located far from the basin boundaries, where the waves and current were most uniform alongshore.

190. Since the primary objective in the present verification was to assess the performance of the current and setup/setdown calculations and not the wave calculation, the breaker index  $\gamma_b$  in the wave model was set to the value measured by Visser (1982) to eliminate an additional model parameter. A comparison is given in Table 3 between measured breaker indices and the indices predicted by Equation 29, which could be used as an option in the wave model. The magnitude and the trend in values with wave steepness is reasonably well reproduced. It is interesting to note the difference between the

measured  $\gamma_b$  in Cases 4 and 7, which have the same wave conditions and beach slope, differing only with respect to the beach roughness. Visser did not measure the mean water level in Case 7, assuming that it was the same as in Case 4.

191. In the wave calculation, the two empirical parameters in the breaker decay model were assigned the recommended values of  $\kappa = 0.15$  and  $\Gamma = 0.40$ . The calculation grid was extended to the horizontal portion of the wave basin to make the current computation independent of the location of the most seaward grid point.

Table 3  
Summary of Experimental Cases from Visser (1982)

Case No.	H* m	T sec	$\theta$ deg	Beach Slope	$\gamma_{meas}$	$\gamma_{calc}$	Comment
1	0.072	2.01	31.1	0.101	1.00	1.09	Large wave angle
3	0.089	1.00	15.4	0.101	0.85	0.95	Large wave height
4	0.078	1.02	15.4	0.050	0.83	0.83	Smooth bottom
7	0.078	1.02	15.4	0.050	0.74	0.83	Rough bottom

\* Wave conditions refer to the horizontal portion of the basin.

192. The two empirical parameters in the current model, the bottom friction coefficient  $c_f$  and the coefficient  $\Lambda$  in the lateral mixing term, were optimized to provide the best fit to the data. As a criterion for the best fit, the sum of squares of the difference between the measured and predicted current velocities was used. Both the linear and nonlinear bottom friction terms were used in the simulations to evaluate the friction formulation. As described by Visser (1982), the assumption of a weak current with respect to the bottom orbital velocity was to a great extent violated in his experiments. Thus, in principle, the linearized friction model should produce inferior predictions of the current distribution. However, as will be shown, the difference between optimal modeling results for the linear and nonlinear models is not significant.

193. The modeling results for the four cases are shown in Figures 14 to 17. Each figure contains the measured and calculated wave height distribution across-shore and measured and calculated current profiles calculated using the linear and nonlinear models. Table 4 summarizes the modeling efforts in terms of the optimal parameter values for the linear and nonlinear models. In the following, a summary of results for each case is given.

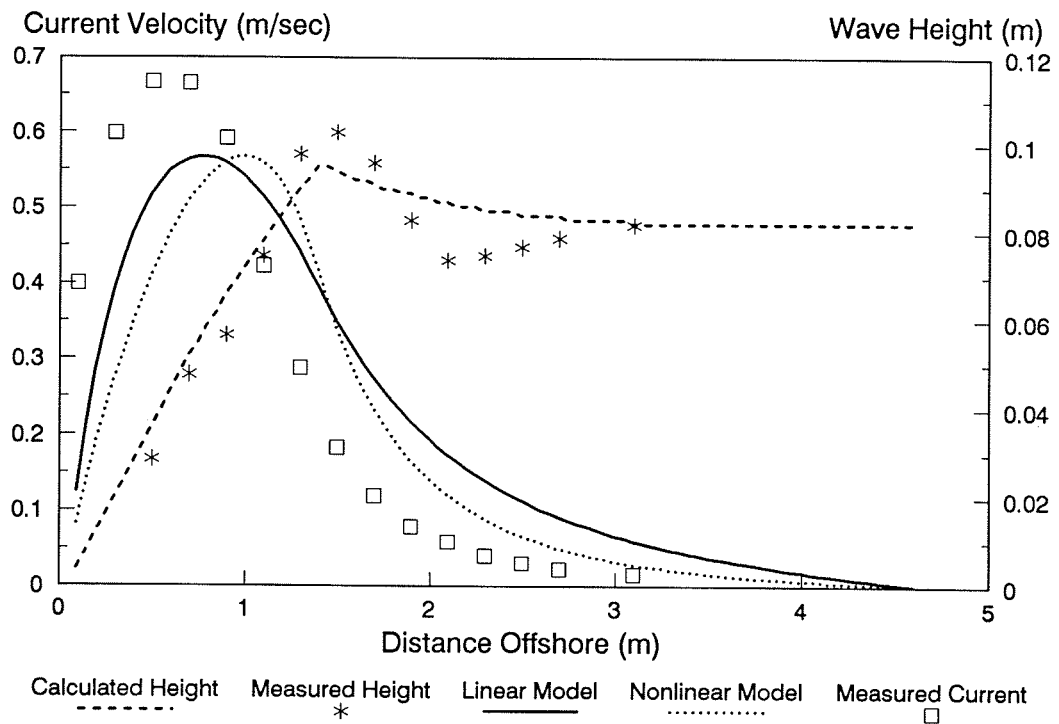
Table 4  
Optimal Model Parameters for the Visser (1982) Cases

Case No.	$(c_f)_{lin}$	$\Lambda_{lin}$	$(c_f)_{non}$	$\Lambda_{non}$
1	0.014	0.60	0.009	0.20
3	0.012	0.30	0.007	0.15
4	0.009	0.60	0.005	0.30
7	0.019	0.60	0.014	0.50

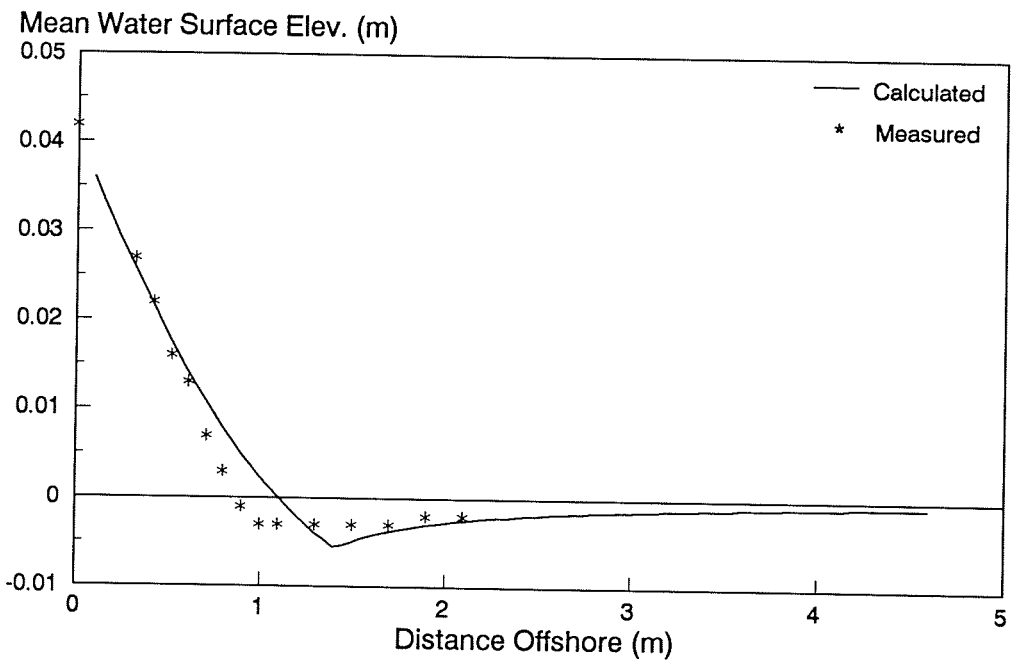
Case 1 (Figure 14)

194. This case proved the most difficult to reproduce because the maximum in the measured current profile was located far shoreward of the break point in the inner half of the surf zone, shoreward of the region where maximum decay in the wave height occurred. Visser (1984a, b) developed a numerical model of the current which incorporated the assumption that the energy dissipation starts at the plunge point, not at the break point. However, this concept introduces at least one additional parameter in a model, the plunge distance, which is related to the breaker type or how the transfer of kinetic turbulent energy occurs.

195. Smith and Kraus (1990) found that the plunge distance for barred profiles was approximately half that for a plane slope with the same incident wave conditions. Breaker type was also different between barred profile and plane slope. Reliable prediction of plunge distance is at present difficult, but recent progress holds promise that advances will be made for use in engineering models.



a. Wave height and longshore current distributions



b. Mean water surface elevation

Figure 14. Model simulations for Visser (1982) Case 1

196. Model simulations for Case 1 thus have the maximum in the current profile located seaward of the measured maximum, although the wave height distribution is well predicted, especially in the surf zone. The results shown in Figure 14a illustrate the applicability of the breaker decay model modified to include wave refraction. The prediction of the nonlinear model had an overall inferior least squares fit as compared with the linear model. However, the tail of the current profile outside the surf zone is better reproduced by the nonlinear model. The general trend for the nonlinear model is to place the maximum in the current somewhat more seaward than does the linear model, but to have a more rapid decay in current magnitude seaward of the break point.

197. By employing a smaller value of the mixing coefficient, a current distribution more similar to the measured distribution was obtained with the models, but the main body of the distribution was located too far seaward. This location produces a larger least squares error compared with the higher value of the mixing coefficient. The optimal mixing coefficient for the nonlinear model is significantly smaller than for the linear model, which is typical for all cases studied. The optimum for the parameter values is located in a rather flat region in mixing/friction coefficient space, implying that slight changes in the optimum parameter values cause only small changes in the sum of squares. As an example, increasing or decreasing the mixing coefficient by 50 percent from the optimal value of 0.2 for the nonlinear model produced a change in the sum of squares of about 1 percent. The sensitivity to the friction factor is somewhat greater since this parameter determines the magnitude of the current distribution. Overall, predictions of the longshore current model were not particularly sensitive to small variation in the two empirical parameters  $c_f$  and  $\Lambda$  about the optimum.

198. The calculation of the mean water surface elevation is well reproduced (Figure 14b), particularly in the inner surf zone. The point of calculated maximum setdown occurs somewhat seaward of the measured location, causing the setup to begin more seaward. The general trend in the setup and setdown is well reproduced.

### Case 3 (Figure 15)

199. The current measurements are well reproduced by the models, although the position of the calculated maximum lies slightly seaward of the measured maximum. The wave height calculation agrees with the trend in the measurements up to the break point and for some distance into the surf zone, but the measured wave height decay is steeper closer to shore. A better fit could have been achieved by optimizing parameter values in the breaker decay model. Compared with the linear model, the nonlinear current model required a smaller valued optimum mixing coefficient, giving a maximum in the current located more seaward than for the linear model. The linear model calculation has an overall better visual fit than the nonlinear model. The optimal friction coefficient for the nonlinear model is considerably smaller than the linear model (Table 4).

200. The calculated point of maximum setdown again lies seaward of the measured point, and the more seaward start of setup in the model causes the mean water surface elevation to be slightly overestimated in the surf zone.

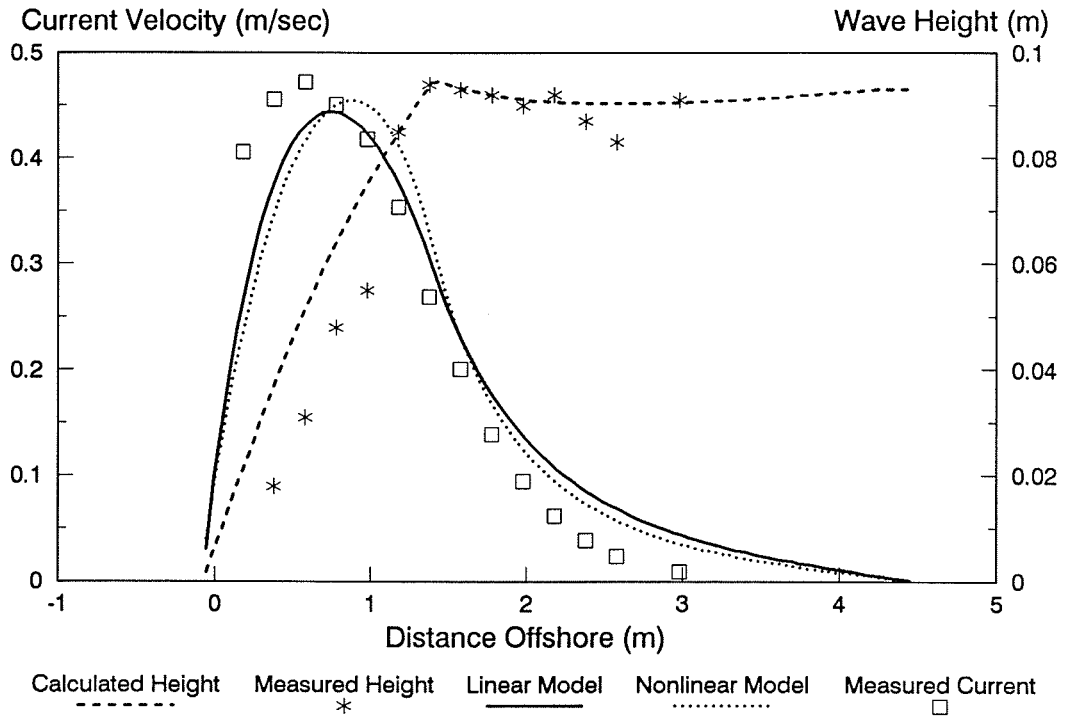
### Case 4 (Figure 16)

201. In this case the bottom was smoother than for Cases 1 and 3, and the location of the maximum current is better reproduced by the current models than in those cases. The measured wave height distribution decays more rapidly than the calculated distribution, as in Case 3. Overall, the wave and current models well simulate the respective measurements.

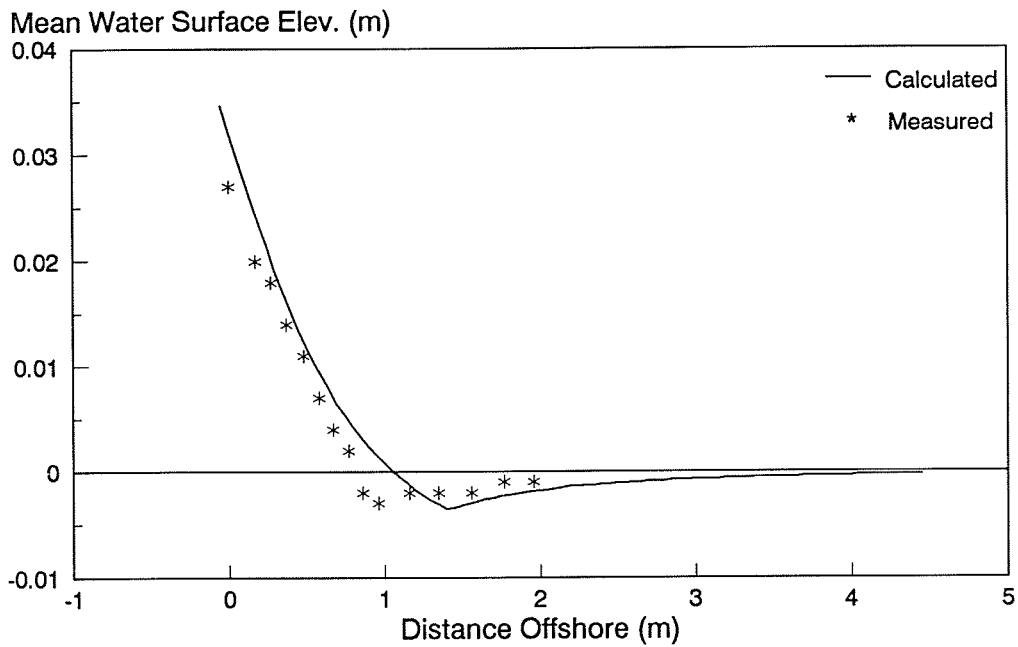
202. The measured setdown was remarkably flat in this case, whereas the numerical model gave the typical sharp minimum. The measured setup was well predicted by the model, including the value at the mean shoreline.

### Case 7 (Figure 17)

203. The bottom roughness was increased for this case as compared with Case 4, and a larger value of the optimum friction coefficient (Table 4) was required in the models. Best agreement between measurements and model predictions for all four Visser (1982) data cases was found for this case with the simulated maximum in the current lying almost on top of the measured maximum. The wave height distribution showed the least agreement for the four cases, with the predicted decay beginning shoreward of the measured decay.

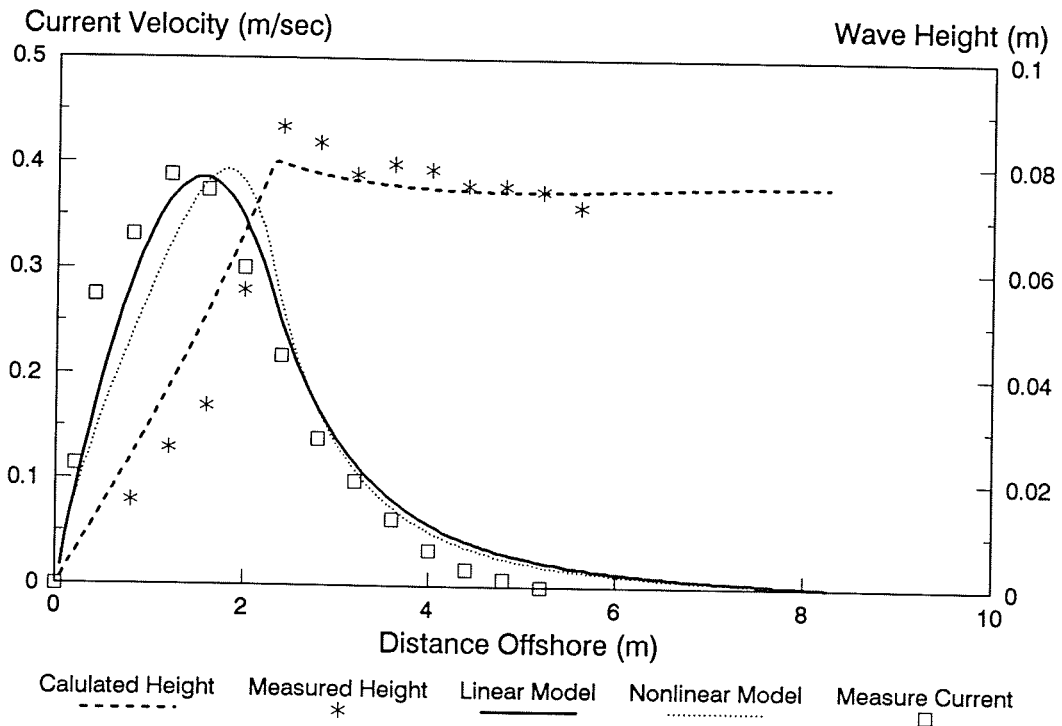


a. Wave height and longshore current distributions

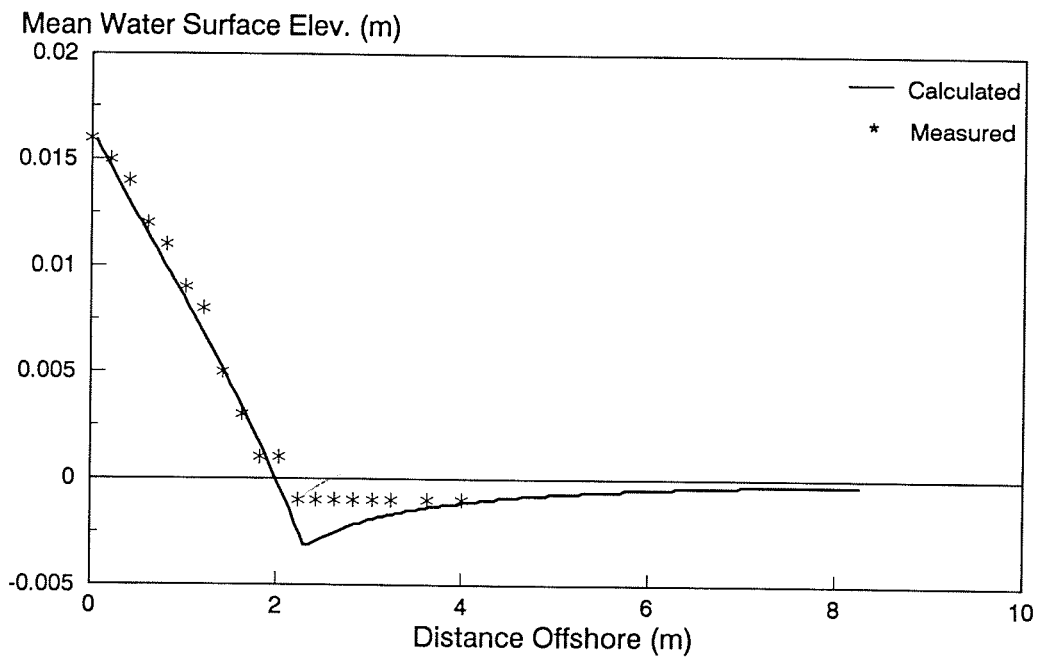


b. Mean water surface elevation

Figure 15. Model simulations for Visser (1982) Case 3



a. Wave height and longshore current distributions



b. Mean water surface elevation

Figure 16. Model simulations for Visser (1982) Case 4

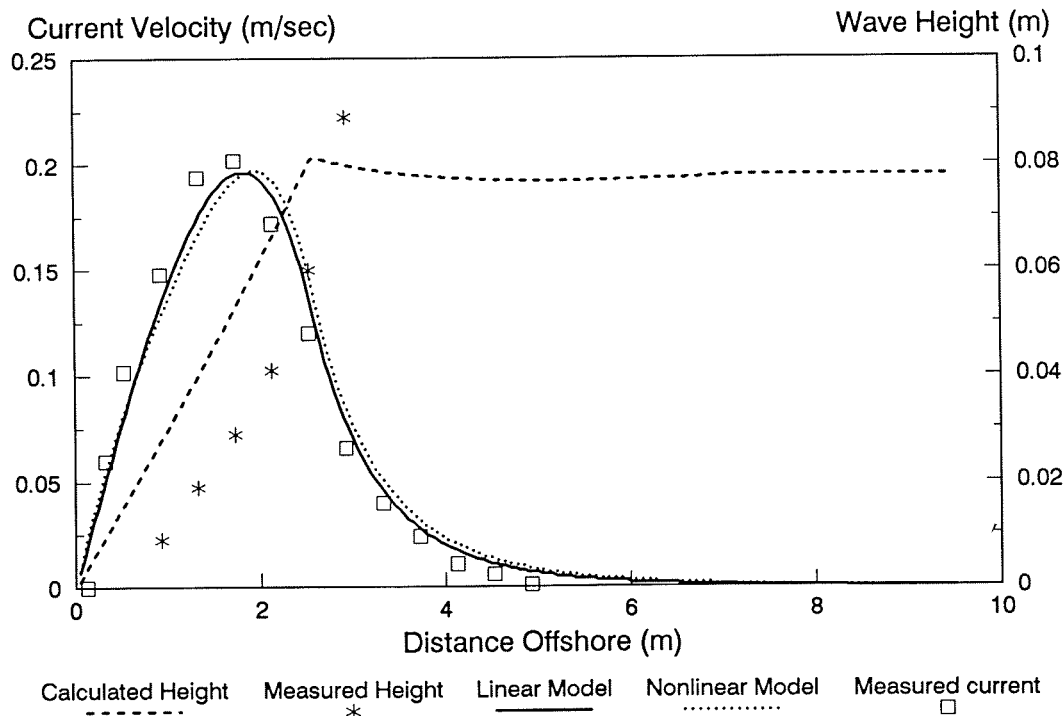


Figure 17. Model simulations for Visser (1982) Case 7

This offset in the wave height distribution promoted the better agreement in the current calculations, similar to Visser's (1984a, b) use of the plunge point rather than the break point to start wave dissipation. The difference between the optimum mixing coefficient in the linear and nonlinear models was smaller than in the previous cases. Accordingly, the tail of the current distribution for the nonlinear model is located slightly seaward of the linear model as opposed to the other cases.

#### Summary

204. In conclusion, the following summarizes model validation for the wave height distribution, longshore current profile, and water surface elevation using laboratory measurements of Visser (1982):

- a. The longshore current profile was well reproduced by the linear and nonlinear models, but the maximum in the measured current is located farther inshore than predicted by the numerical models, probably related to the wave breaker type and location of the plunge point, which are not parameters in the models.

- b. The wave height distribution was well predicted with the breaker decay model modified to include refraction and using previously established parameter values for all simulations (no calibration).
- c. The overall fit of the linear model was somewhat better than for the nonlinear model even though the weak-current approximation was violated.
- d. The optimum friction coefficient for the nonlinear model was significantly smaller for all cases, on the average of about 35 percent less than that of the linear model (Table 4). Values for the friction coefficient for the linear model were 0.012 (Cases 1, 3, and 4) and 0.019 (Case 7), whereas respective values for the nonlinear model were 0.0070 and 0.014.
- e. The optimum mixing coefficient for the nonlinear model was significantly smaller for all cases, on the average of about 45 percent less than that of the linear model. The average optimum mixing coefficient was 0.5 for the linear model and 0.3 for the nonlinear model.
- f. The optimum mixing and friction parameter values in the current models were located in relatively flat regions, implying that model predictions are insensitive to slight changes around the optimum.
- g. The measured change in mean water surface elevation produced by the obliquely incident waves was well reproduced by the model.

205. The linear current model gave a somewhat overall better fit than the nonlinear model. This result is not considered to reflect a physically better description of the phenomenon, but indicates that the linear model is more flexible in calibration. Smaller values of the mixing coefficient obtained with the nonlinear model could be interpreted as less necessity for smoothing, implying a better physical description.

#### Field Data from Kraus and Sasaki (1979)

206. Kraus and Sasaki (1979) measured the longshore current profile along seven transects on a sandy beach facing the Japan Sea. The measurements were made simultaneously on a transect by divers positioned at 5-m intervals. After completing measurements on one transect, the divers moved to the next transect, located 25 m away. The current was measured by timing the movement of almost neutrally buoyant floats with current-sensing fins located at about middepth; the floats were tethered to the wrists of the divers by a 2-m-long

line. An average current velocity was formed of three successive measurements at each location. The incident waves arrived as clean swell, and repeated visual measurements of the breaking waves using a graduated rod gave a significant height of 1.0 m, period of 4.1 sec, and angle of 9 deg. The water depth at each sampling location was measured by rod and transit. For the numerical simulations performed in the present study, average values of the water depth and current velocity were used. Appendix B contains a summary of the measurements. The bottom topography had a step-type shape, and secondary breaking was observed far shoreward of the main break point located in about 1-m water depth.

207. As shown in Figure 18, the measured current profile for the average bottom bathymetry had a peak located somewhat inshore of the main break point but was otherwise uniform throughout the surf zone. A flat profile is difficult to reproduce in a model using only monochromatic waves unless strong mixing is applied; in contrast, inclusion of wave reformation and secondary breaking can improve modeling results in such a situation. A secondary break point produces a second local maximum in the current velocity inshore, producing the uniform-like current profile inshore between the two break points. On the other hand, since the depth monotonically increases with distance offshore, wave reformation will not occur unless forced by a lower value of  $\Gamma$  in Equation 24 (Dolan and Dean 1984, Larson and Kraus 1989).

208. If a distribution of wave heights is employed to drive the longshore current model, breaking will occur more uniformly over the surf zone and produce a more uniform current profile. As described in Part III, one procedure for obtaining such a distribution is to randomly select wave heights from a Rayleigh distribution specified at some depth offshore and transform the individual waves with the breaker decay model. At each point across the shore the probability density function of the wave height can be constructed from all the individual transformed wave heights.

209. An intuitive method for obtaining the mean longshore current distribution is to calculate a current corresponding to each randomly picked wave height and average these distributions. Although statistically appealing, this approach is questionable from a physical point of view since a single wave cannot develop a steady current; a large number of consecutive identical waves are required. However, for a long averaging interval or

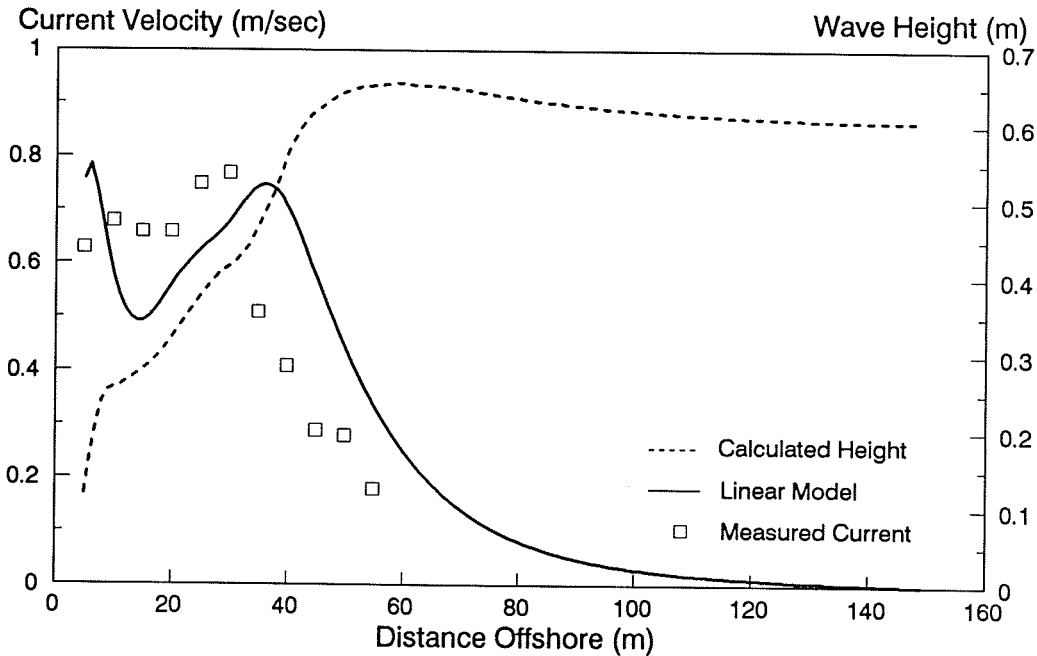


Figure 18. Simulations for the Kraus and Sasaki (1979) data; linear model

measurement period with little correlation between consecutive waves, a Monte-Carlo simulation technique is considered a valid procedure for obtaining an average current value. Concerning the equation for calculating the mean water surface elevation (Equation 15), the question can also be raised about the physical meaning of an average based on different individual waves. Nevertheless, as an engineering expedient, this procedure is used in NMLONG.

210. Kraus and Sasaki (1979) did not measure the wave height across the shore, but only at the break point. In the present work, the significant wave was transformed seaward to about 4-m depth using linear-wave theory, where no waves in a distribution would break and the wave calculation could be started. The rms wave height was determined, and wave heights were randomly picked from a Rayleigh distribution defined by this wave height. It is noted that since conditions at the break point were used to derive the offshore wave height, uncertainty was introduced in the wave height calculations. The incident wave period and angle were kept constant throughout the simulation, together with the breaker index  $\gamma_b$ . Randomization of wave direction and period in a joint

probability distribution would be an extension of this procedure; for the present, the assumption was made that a variation in wave height captures the main effect of wave randomness. A constant breaker index  $\gamma_b$  of individual waves was chosen as opposed to Equation 29 because this equation was developed for monochromatic waves and involves a moderately strong dependence on wave period. Since in the present approach wave period was constant and wave height varied, low wave steepnesses will occur that produce unrealistically high values of  $\gamma_b$  by Equation 29. Thus, a constant value ( $\gamma_b = 1.0$ ) was chosen since this was the measured breaker index for the visually significant wave at the break point.

#### Linear model

211. Both the linear and nonlinear current models were tested against the data, and optimum parameter values were sought with respect to minimizing the sum of squares as described for the laboratory tests above. The current distribution was taken as an average for 500 waves, giving a stable estimate of the mean current at points across the shore. The simulations started by seeking the optimum value of the friction coefficient for a value of the mixing coefficient corresponding to the average value ( $\Lambda = 0.5$ ) determined from the laboratory data of Visser (1982). For the linear model, a friction coefficient of 0.0042 gave the best agreement with the field measurements. This value is significantly lower than what was obtained for the laboratory measurements of Visser (1982), but close to the value  $c_f = 0.0061$  obtained by Kraus and Sasaki (1979) using an analytic model of the longshore current and fitting the location of the maximum in the profile. Figure 18 shows the measured and calculated current distributions for the linear model together with the calculated rms wave height across the shore.

212. In a true optimization with the friction coefficient and mixing parameter allowed to range freely, a significantly higher value of  $\Lambda$  was obtained, namely,  $\Lambda = 1.2$ , whereas  $c_f$  remained the same. However, these calculations with higher valued mixing coefficients showed that the "improvement" in an rms sense of defining error was an artifact of extreme flattening of the entire distribution and prolongation of the tail in deeper water where no measurements were available. In contrast, extrapolation of the measurements to deeper water shows a sharp decrease in the current. Thus, additional

measurement points in this area would degrade the solution with greater mixing and translate the optimum mixing coefficient toward a lower value.

213. As noted by Battjes (1972) and Thornton and Guza (1986), the need for lateral mixing to smooth the current distribution near the break point is reduced for random waves as compared with monochromatic waves. There is a difference, however, between obtaining a smooth velocity profile and obtaining the distribution that shows best agreement with measurements. Since Thornton and Guza (1986) found little difference in their random longshore current model whether or not lateral mixing was incorporated in simulations of their field data, calculations were carried out with the present model with a small value of  $\Lambda$  to investigate this effect. Using the linear current model, the sum of squares increased significantly for the weak-mixing case ( $\Lambda = 0.05$ ), and the value of the optimal friction coefficient increased to  $c_f = 0.0050$ . The conclusion is that lateral mixing should be included in the present model to obtain good agreement with field measurements.

#### Nonlinear model

214. Predictions with the nonlinear model were also compared with the current measurements (Figure 19), starting the series of simulations using the value of the mixing coefficient given by the laboratory data, that is,  $\Lambda = 0.3$ . A  $c_f$ -value of 0.0022 gave the best least squares agreement and had a sum of squares about 40 percent greater than the linear model. Similar to the linear model case, the optimum fit occurred for a larger mixing coefficient value, but the difference in the sum of squares was only slightly less, because the  $c_f$  and  $\Lambda$  surface was relatively flat.

#### Summary

215. The linear and nonlinear models predicted the general two-peaked form of the longshore current field measurements of Kraus and Sasaki (1979), providing a much superior fit than possible with analytic models. The calculated current profile was somewhat low in the shoreward part of the surf zone and too high seaward of the maximum current. The fit could be improved by increasing the value of the breaker index  $\gamma_b$  to 1.1, but it was desired to minimize the number of free parameters. Using a value for the mixing coefficient determined by the laboratory data in finding the optimal friction coefficient gave reasonable results. In the laboratory experiments, monochromatic waves were used, thus facilitating evaluation of the mixing

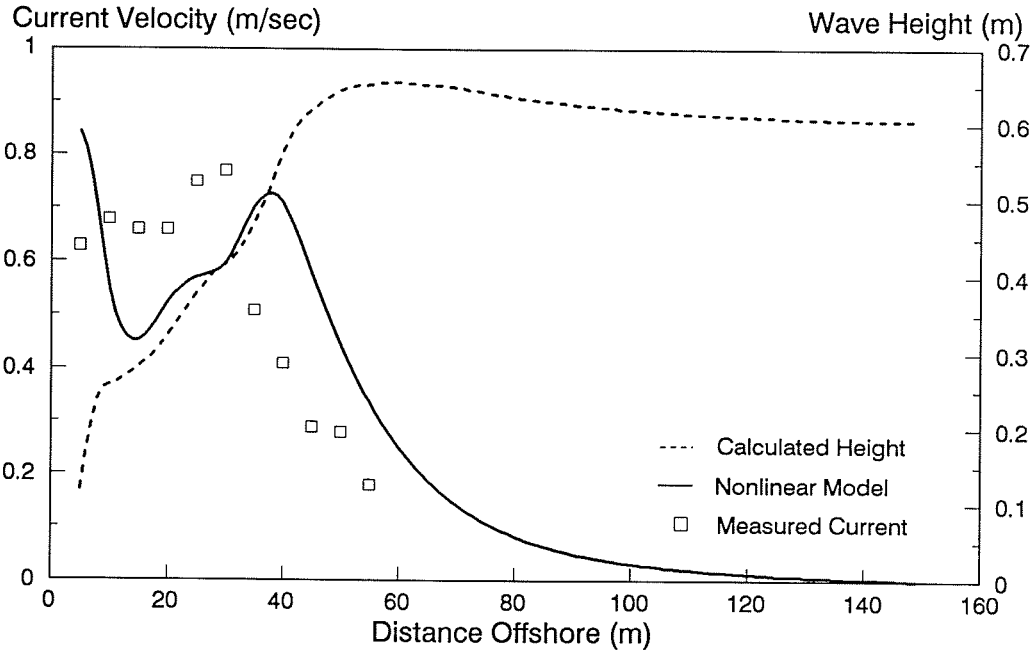


Figure 19. Simulations for the Kraus and Sasaki (1979) data; nonlinear model

coefficient under ideal conditions. For the field comparison, where the method of averaging many current distributions was employed and each distribution generated by different wave conditions, inferences about appropriate values of  $\Lambda$  through calibration are probably less reliable than for the Visser (1982) laboratory data.

216. The technique of averaging a large number of current distributions obtained from randomly generated wave heights was successful in reproducing a uniform current distribution across the beach. In general, it was possible to achieve a better fit to the measurements with the linear model as compared with the nonlinear model for the same reasons as discussed for the laboratory data.

Field Data from Thornton and Guza (1986)

Previous work

217. To further verify the applicability of the longshore current models to describe field conditions and to establish model parameter values relevant

to the field, the wave and longshore current data of Thornton and Guza (1986, 1989) were used. The random wave model is tested by predicting the transformation of the rms wave height measured at fixed points across the profile in the experiment. The data were collected during a field experiment conducted at Leadbetter Beach, Santa Barbara, California, as a part of the Nearshore Sediment Transport Study. At this site the bottom contours are relatively straight and parallel (and with no appreciable bars and troughs), thus making the data suitable for applying a current model that assumes uniform conditions alongshore. The data used for the simulations in this report derive primarily from Thornton and Guza (1989).

218. Four cases were used in the present study originating from data collected on 3-6 February 1980. These cases will be referred to in this report by the date of data collection. Table 5 provides a summary of the general wave characteristics for each case, and a complete listing of the data is given in Appendix B. The data from 2 February presented in Thornton and Guza (1986) were excluded from the present model tests with reference to "the lack of observations at the nearshore" stated by Thornton and Guza (1986). Wave information presented in Thornton and Guza (1986) was used and provided wave characteristics in about the 4-m water depth as opposed to information given in Wu, Thornton, and Guza (1985) which refers to a water depth of about 9 m. The bathymetry, measured rms wave height, and measured current velocity across-shore are listed in Thornton and Guza (1989).

219. Several model simulation studies have used the data set of Wu, Thornton, and Guza (1985) and Thornton and Guza (1986, 1989). For example, Wu, Thornton, and Guza used the data to test a 2-D model based on the steady-state momentum equations (Equations 32 and 33) with a linearized bottom friction term and without wind forcing. The rms wave height was taken as the representative measure and transformed as a monochromatic wave. In the surf zone, the wave height was simply taken as being proportional to the water depth ( $H_{rms} = \gamma_b h$ ). In another use of the data, Thornton and Guza (1986) verified a 1-D random wave and current model based on ensemble-averaged governing equations. The percentage of broken waves was assumed to be proportional to the ratio between wave height and water depth. Neither of these modeling studies described wave reformation in the surf zone.

Table 5  
Wave Conditions from the Thornton and Guza (1986) Data

Case	$H_{rms}$ m	T sec	$\theta$ deg	h m
3 Feb	0.55	14.3	7.8	4.0
4 Feb	0.56	14.2	9.0	3.8
5 Feb	0.45	12.8	8.4	3.6
6 Feb	0.26	11.6	8.3	3.5

Present modeling

220. In the following, a short description is given of the modeling procedure, and Figures 20 to 23 present the simulation results for the wave and longshore current models together with the measurements. For all cases, the parameter values  $\kappa = 0.15$  and  $\Gamma = 0.40$  were used in the breaker decay model, and a breaker index of  $\gamma_b = 0.78$ . Only values of  $c_f$  and  $\Lambda$  were changed in the longshore current models to find an optimal solution. The cell length was 1 m, and the numerical grid extended to a point where no influence on the current distribution was expected (6-m water depth). To start the simulation, offshore wave measurements were transformed to the seaward end of the grid using linear-wave theory and neglecting setdown.

221. The general approach in the simulations was to assume a Rayleigh distribution for the wave height at the seaward end of the grid and randomly select 500 waves for transformation across the beach. The rms wave height at each point across-shore was then obtained together with the current velocity for each wave, and the current velocities for the 500 waves were averaged. The optimum parameter values in the current model were first estimated using the mixing value from the laboratory simulations and determining the friction coefficient yielding the smallest sum of squares. Thereafter, the true optimum was sought, and the sensitivity of the model to changes in the parameter values established. The response of the current model to very small mixing values was also investigated. Table 6 summarizes the simulation

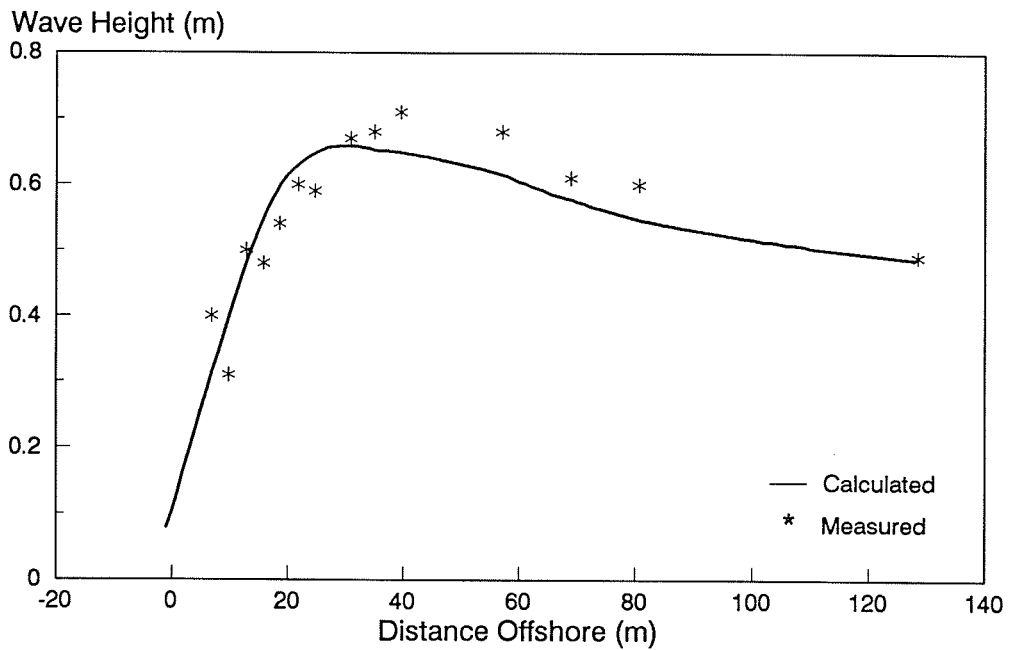
results for optimum parameter values using mixing values from the laboratory simulations.

Table 6  
Optimum Parameter Values for the Thornton  
 and Guza (1986) Data

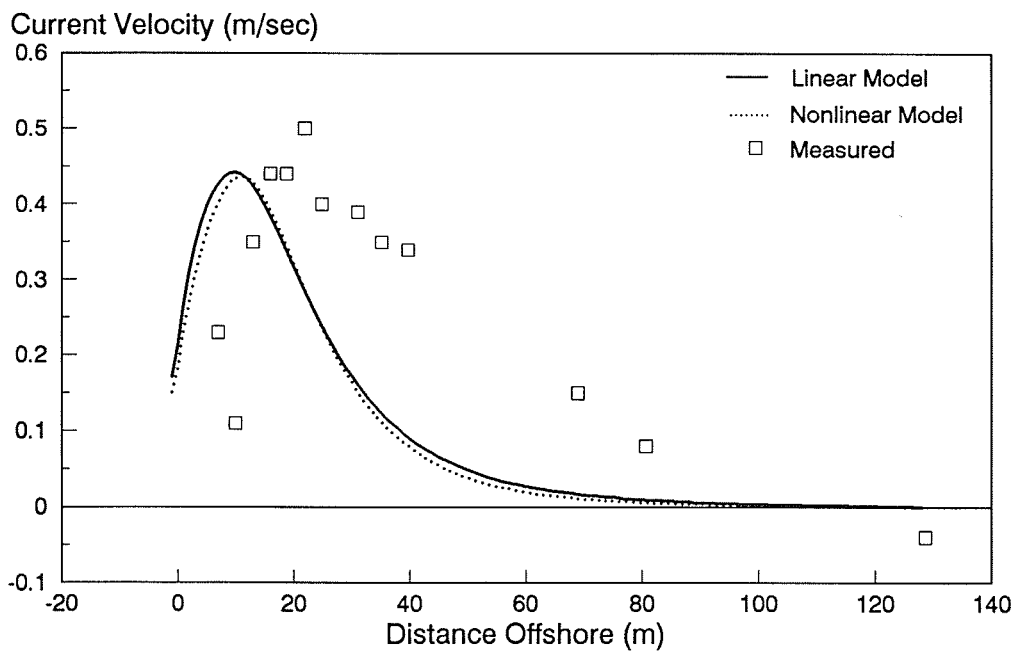
Case	Linear model		Nonlinear Model	
	$c_f$	$\Lambda$	$c_f$	$\Lambda$
3 Feb	0.0060	0.50	0.0050	0.30
4 Feb	0.0050	0.50	0.0035	0.30
5 Feb	0.0040	0.50	0.0030	0.30
6 Feb	0.0040	0.50	0.0035	0.30

222. 3 February case. This was the most difficult case to reproduce and had the largest deviation between calculation and measurements. The case clearly displays differences between model predictions and measurements that occurred to some extent in all simulations with this data set. Figure 20a shows the simulated and measured rms wave height across-shore, and Figure 20b gives the calculated and measured current distribution. The wave height across the profile is rather well predicted.

223. The predicted current profile for this case has an overall shape in agreement with the measurements, but is translated shoreward. This tendency was true for the linear and nonlinear models, with both models giving about the same sum of squares error estimate. The trend is opposite to what was noted for the laboratory cases of Visser (1982), for which the predicted maximum in the current was always located seaward of the measured maximum. Thus, in this case introduction of a plunge point concept as used by Visser (1984a, b) would degrade the fit. Optimum values of the friction coefficient for the linear and nonlinear models were 0.0060 and 0.0050, respectively, for the mixing parameter set to values determined in the laboratory tests. The optimum for freely varying combinations of  $c_f$  and  $\Lambda$  was located at a higher value of the mixing coefficient and was in a very flat region.



a. Wave height distribution across-shore



b. Longshore current profile

Figure 20. Simulations for Thornton and Guza (1986) data (3 February)

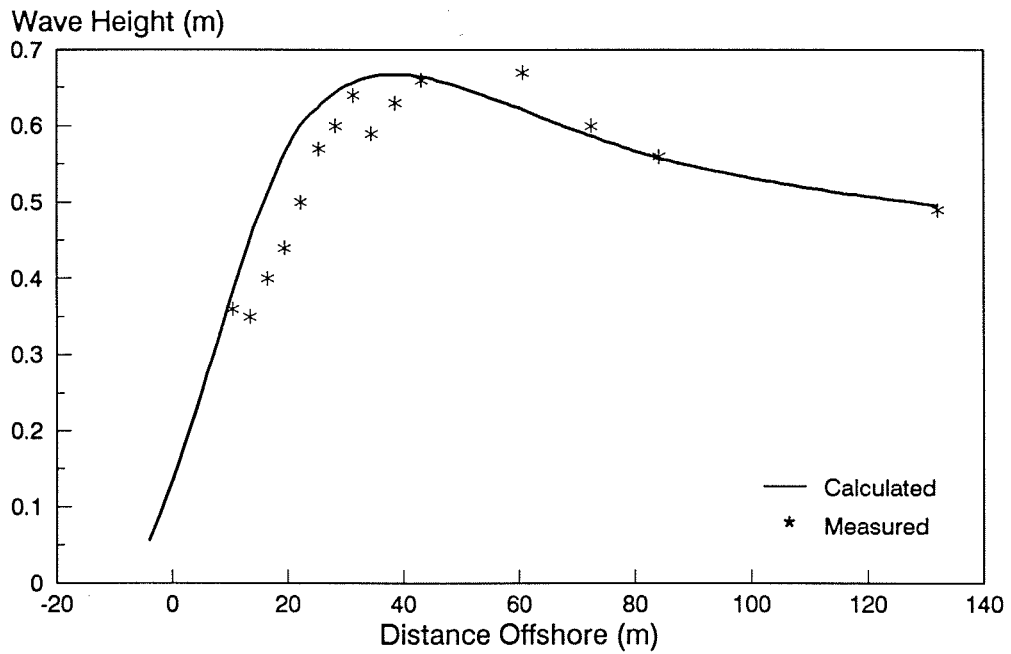
224. 4 February case. The optimum friction coefficient was smaller than for 3 February case with  $c_f = 0.0050$  and  $0.0035$  for the linear and nonlinear models using optimum mixing values from the respective laboratory simulations. The comparison between linear- and nonlinear-model calculations and measured wave height distributions and current profiles is shown in Figures 21a and b. The wave height distribution is well reproduced, although it is overestimated in the shoreward half of the surf zone. The maximum in the calculated current profile was located shoreward of that in the measurements. A small value of the mixing coefficient gave an inferior fit, but the increase in the sum of squares was not as marked as for the Kraus and Sasaki (1979) data set simulations. The linear and nonlinear models gave an almost identical fit according to the sum of squares.

225. 5 February case. Model predictions and measurements are compared in Figures 22a and b. The tails of the velocity profiles show good agreement, but the calculated peak currents lie closer to shore than the measurements, and the peak magnitudes are overpredicted. Optimum values of the friction coefficient were  $0.0040$  and  $0.0030$  for the linear and nonlinear models, respectively, with mixing coefficients as determined in the laboratory tests. Thus, smaller values for the friction coefficient were obtained than for the previous cases in the data set.

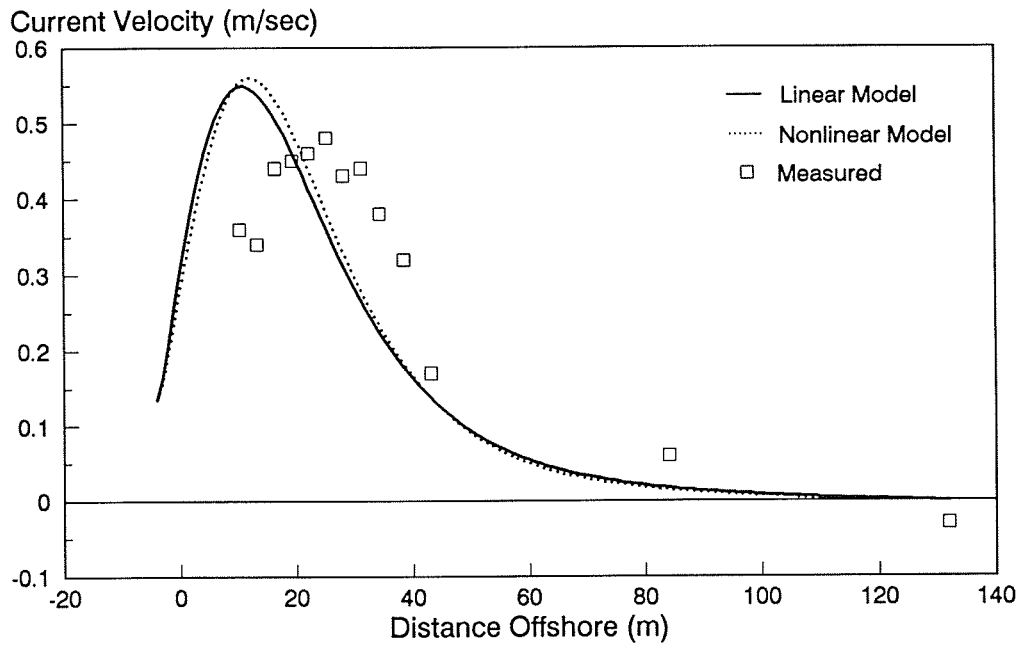
226. 6 February case. For this case, the wave height was quite small ( $H_{rms} = 0.26$  m), and the associated current was weakest of the four cases studied. Figures 23a and b show the simulation results from the wave and current models, respectively. The value of the optimum friction coefficient was identical to the 5 February case for the linear model, but somewhat higher for the nonlinear model, namely,  $c_f = 0.0035$ , with the mixing coefficients as determined from the laboratory tests. The true optimum with respect to both  $c_f$  and  $\Lambda$  was located at a higher  $\Lambda$  value, but gave little improvement in the fit. Smaller values of the mixing parameter gave a larger sum of squares, with the optimum occurring for a larger value of the friction coefficient.

#### Discussion

227. For the Thornton and Guza (1986) data set, the most notable difference between model predictions and measurements was not the shape of the current profile, but the strength and location of the peak current, where the

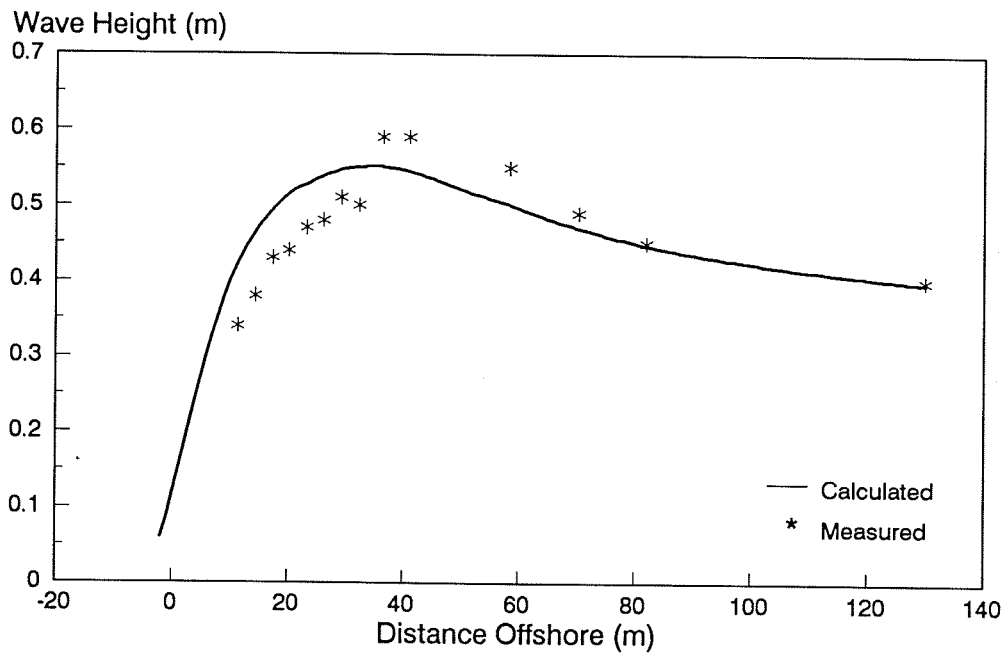


a. Wave height distribution across-shore

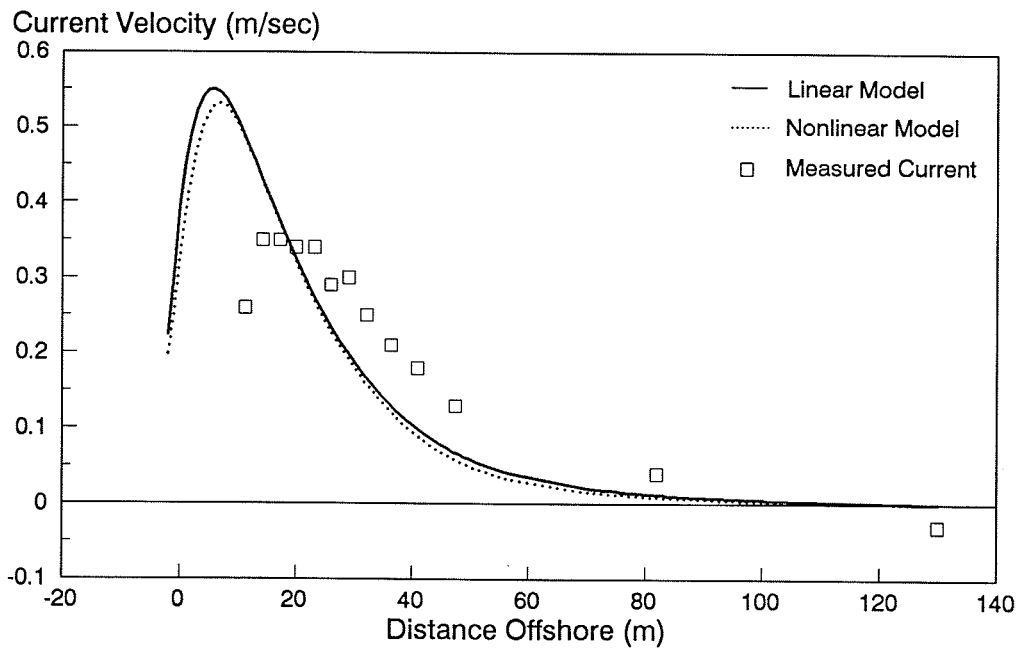


b. Longshore current profile

Figure 21. Simulations for Thornton and Guza (1986) data (4 February)

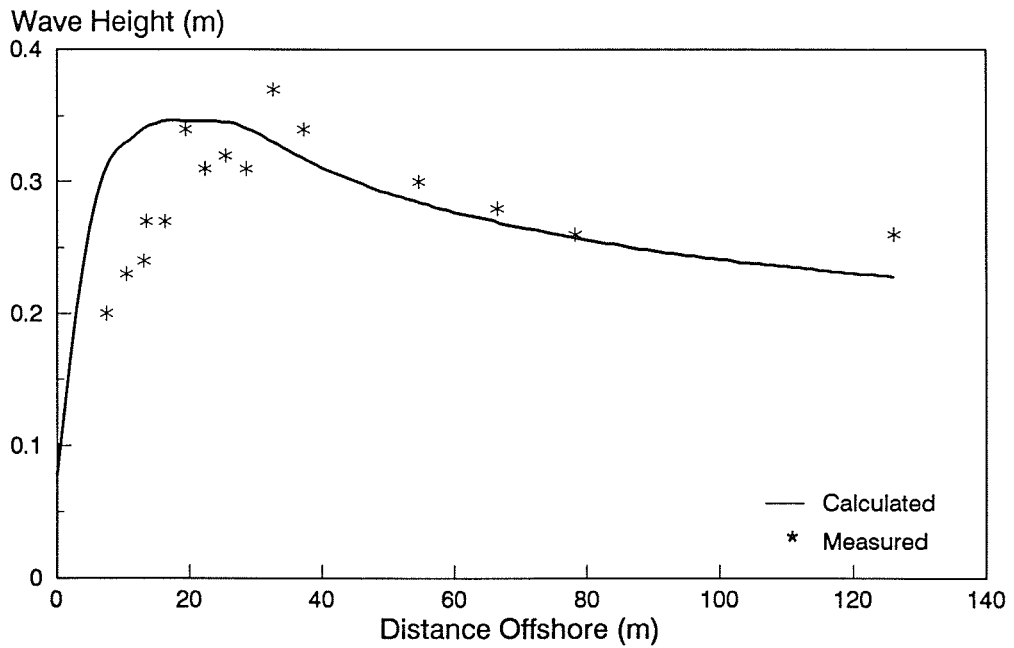


a. Wave height distribution across-shore

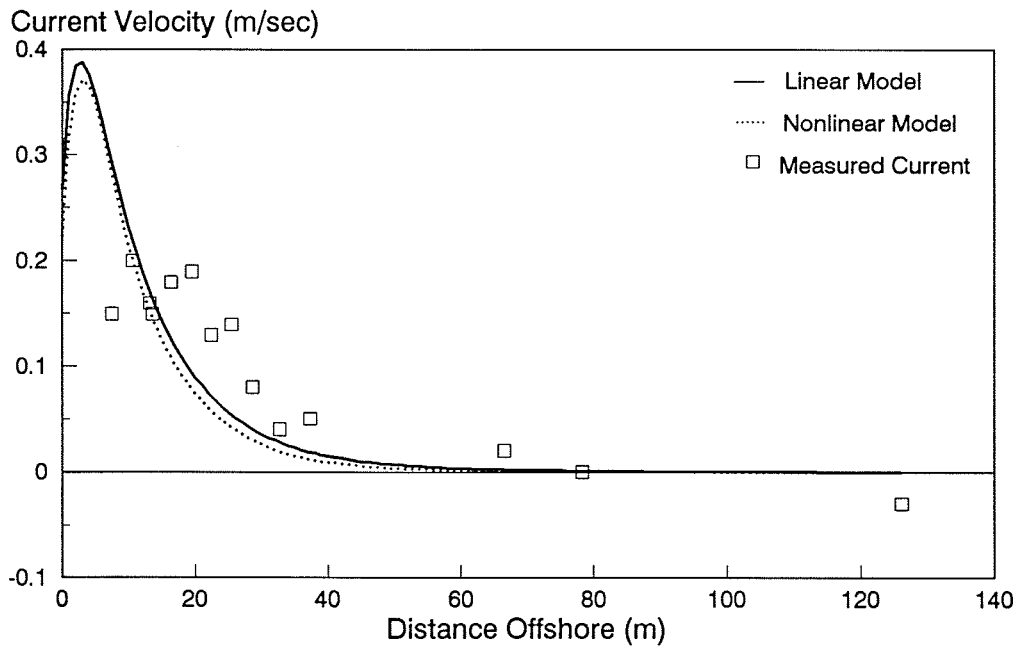


b. Longshore current profile

Figure 22. Simulations for Thornton and Guza (1986) data (5 February)



a. Wave height distribution across-shore



b. Longshore current profile

Figure 23. Simulations for Thornton and Guza (1986) data (6 February)

maximum in the predicted current profile for all four cases was located shoreward of the peak in the measurements. The calculated wave height across the profile was in reasonable agreement with the measurements. The agreement between wave model and measurements could be improved by reducing the breaker index to about 0.4 to 0.5; however, this reduction is physically unrealistic because  $\gamma_b$  represents the breaker index for a monochromatic wave in the present context. In contrast to the definition of  $\gamma_b$  used here, Thornton and Guza (1983, 1986) defined a quantity that might be denoted as  $\gamma$  (without the subscript b) to express the average ratio between wave height and water depth of all waves, breaking, broken, and unbroken, in the surf zone. Thus, this ratio is a kind of integrated description of wave conditions after the broken wave has stabilized in the form of a bore, in some sense comparable to the stable wave height concept included in the Dally (1980) breaker decay model, and is not equivalent to the breaker index of an individual wave.

228. It should be kept in mind that the field environment may have contributions that influence the current measurements in ways not accounted for in the present models. For example, the tidal current, atmospheric pressure differences, small changes in offshore and nearshore bathymetry and bottom roughness, and limitations in the measurements are all unquantified. In this respect, very close agreement between numerical calculations and field measurements should not be sought by unrealistic manipulation of model parameters.

229. One way of improving the predictive capability of the longshore current models is to manipulate parameters in the breaker decay model. A larger wave energy dissipation rate would produce a steeper decay in wave height and translate the peak of the wave height distribution seaward, and the body of the current profile would accordingly move seaward. The effect of moderate changes in wave model parameters was not considered significant enough to warrant calibration.

230. In the random wave selection process from a Rayleigh distribution, a certain number of small waves that break close to shore are produced. These waves create narrow surf zones only a few, perhaps even one, calculation cells wide. In the longshore current model, wave breaking very close to shore can create a sharp peak in the current profile and unduly influence the averaging of all current distributions. Trial simulations were carried out where wave

conditions were neglected if the number of surf zone cells was less than a predetermined value. A criterion up to five cells was used (in other words, a surf zone of at least 5-m width was required), which marginally improved the fit of the calculation to the measurements. Because of the relatively small effect of the cutoff, it was not used in the simulations, and the calculations described above were carried out with all waves obtained from the Rayleigh distribution. However, the phenomenon of very small wave heights appearing in the Monte-Carlo process should be kept in mind in application of the random wave procedure.

231. In summary the following observations were made concerning model simulations for the Thornton and Guza (1989) data set:

- a. The rms wave height variation across-shore was in general well predicted, with the greatest discrepancy in the region of steep decay.
- b. The overall longshore current profile was correctly reproduced by the models, but the predicted location of the maximum current was more shoreward than in the measurements.
- c. The linear and nonlinear models gave about the same agreement in a least squares sense in calibration against the measurements.
- d. The average value of the optimum friction coefficient for the linear model was  $c_f = 0.0050$  and  $c_f = 0.0040$  for the nonlinear model using mixing values given from the laboratory simulations.
- e. The true optimum with for free variation of both  $c_f$  and  $\Lambda$  was located at higher  $\Lambda$ , but the decrease in the sum of squares was small as compared with using mixing values from the laboratory cases.
- f. A mixing value of  $\Lambda = 0$  gave a smooth velocity profile but increased the sum of squares. The optimum value of the friction coefficient increased if  $\Lambda = 0$  was employed, giving  $c_f = 0.0065$  for the linear model and  $c_f = 0.0041$  for the nonlinear model.

232. Compared with previous independent modeling attempts, the present model gives agreement similar to that in the Thornton and Guza (1986) study, but not as good as that in the Wu, Thornton, and Guza (1985) study. The reason for the good agreement obtained by Wu, Thornton, and Guza is believed to be the small value of the breaker index employed ( $\gamma_b = 0.44$ ), causing the waves to break farther offshore. In the present work, tests indicated that equally good fits resulted with this value of the breaker index, but such a

small value of  $\gamma_b$  in a monochromatic wave model is not justified. In Thornton and Guza, the monochromatic wave approach used in Wu, Thornton, and Guza was abandoned and a randomized model presented. The random wave model as a driving model resulted in maxima in the current profiles located shoreward of those of the measured profiles, similar to the present results.

233. Values of friction coefficients obtained with the present models differ from those of Thornton and Guza (1986), being on the average about 50 percent smaller. One possible explanation may lie in the method of ensemble averaging of the governing momentum equation. Neglecting lateral mixing (which would tend to require increased values of the bottom friction coefficient), Thornton and Guza (1986) averaged the multiplying factor in the linearized friction term (Equation 58), which is a function of wave height, separately from the driving term. If instead, the driving term is divided by the factor that multiplies the current velocity in the bottom friction term and the averaging procedure then performed, the calculated current would be a factor of 1.5 smaller. The latter approach is considered by the authors of this report to be the statistically appropriate method and results if the Monte-Carlo simulation is employed. Thus, for the two averaging methods to yield the same current magnitude, the friction coefficient in the present model should be taken as approximately two-thirds that obtained by Thornton and Guza (1986) (for the simple case of no mixing and use of a linearized friction term). Inclusion of lateral mixing or use of a nonlinear friction term precludes specification of a simple factor connecting the two methods, but does not change the qualitative relation between the methods.

#### Hypothetical Case from Ebersole and Dalrymple (1980)

234. Because the available data sets for which the current models were evaluated encompassed only beach profiles with monotonically increasing depth with distance offshore or a step-type beach, a hypothetical case was chosen to qualitatively investigate the performance of the model on more complex topographies. A simple bar-type profile was selected as presented by Ebersole and Dalrymple (1980), and the same deepwater wave conditions were employed: wave height of 2.0 m, period of 8.0 sec, and incident angle of 30 deg. The breaker

index was set to  $\gamma_b = 0.78$ , and the calculation grid extended out to 7-m water depth. The depth values for the bottom topography are given in Appendix B.

235. The incident monochromatic waves broke on the bar, reformed in the trough shoreward of the bar, and broke a second time farther inshore.

Figure 24 illustrates changes in the longshore current distribution over the

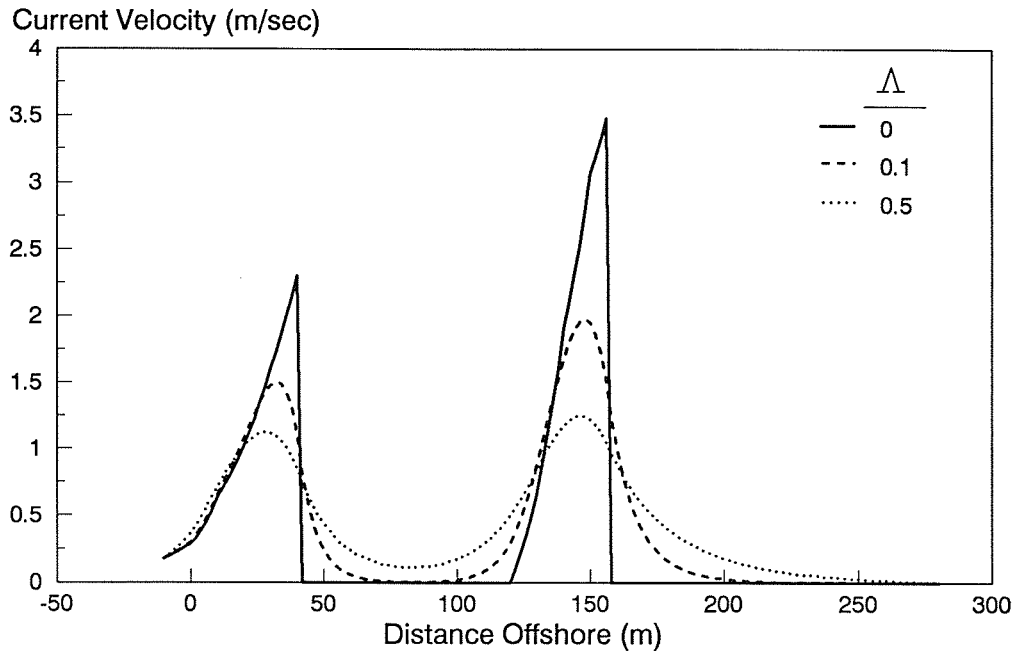


Figure 24. Influence of lateral mixing for a barred profile

barred profile for different values of the lateral mixing coefficient in the linear model. A friction coefficient of  $c_f = 0.01$  was specified to agree with Ebersole and Dalrymple (1980). For the typical wave height distribution over a barred profile, reference is made to Part III where the wave model was investigated. An increase in the lateral mixing coefficient lowers the peak in the current profile and elongates the tail. For moderate changes in  $\Lambda$ , the difference is small, not being notable until very low values of the mixing coefficient are reached. For the case of no mixing ( $\Lambda = 0$ ), two distinct peaks result with the outer one displaying a larger maximum current velocity. The simulation with the limiting case  $\Lambda = 0$  with monochromatic waves, which yields an almost discontinuous current profile, also demonstrates the numerical stability of the model.

236. Figure 25 shows the difference in predictions between the linear and nonlinear models for the same value of the friction and lateral mixing coefficients ( $c_f = 0.01$ ,  $\Lambda = 0.5$ ). As expected, the quadratic friction term lowers the velocity profile. Apart from the difference in magnitude between the two distributions, the general shapes are similar. However, the effect of the nonlinear stress term on the velocity profile is greater for the larger current velocities because of quadratic dependence on current magnitude. In deeper water, as the velocity goes to zero, the linear and nonlinear model calculations gradually converge.

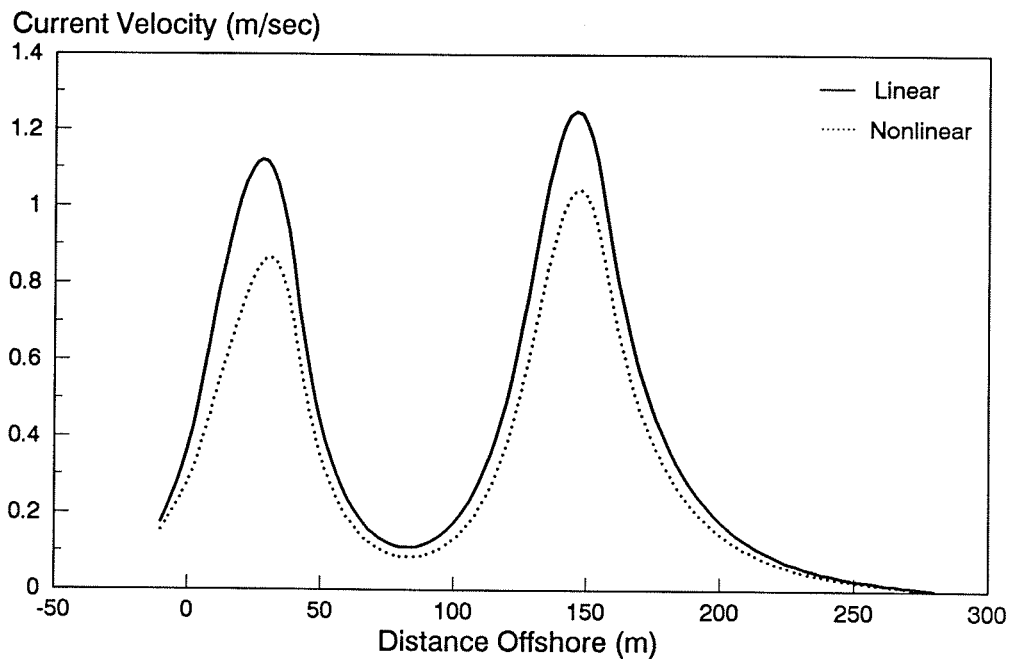


Figure 25. Model simulations for a barred profile

### Longshore Current Driven by Wind

#### Longshore current

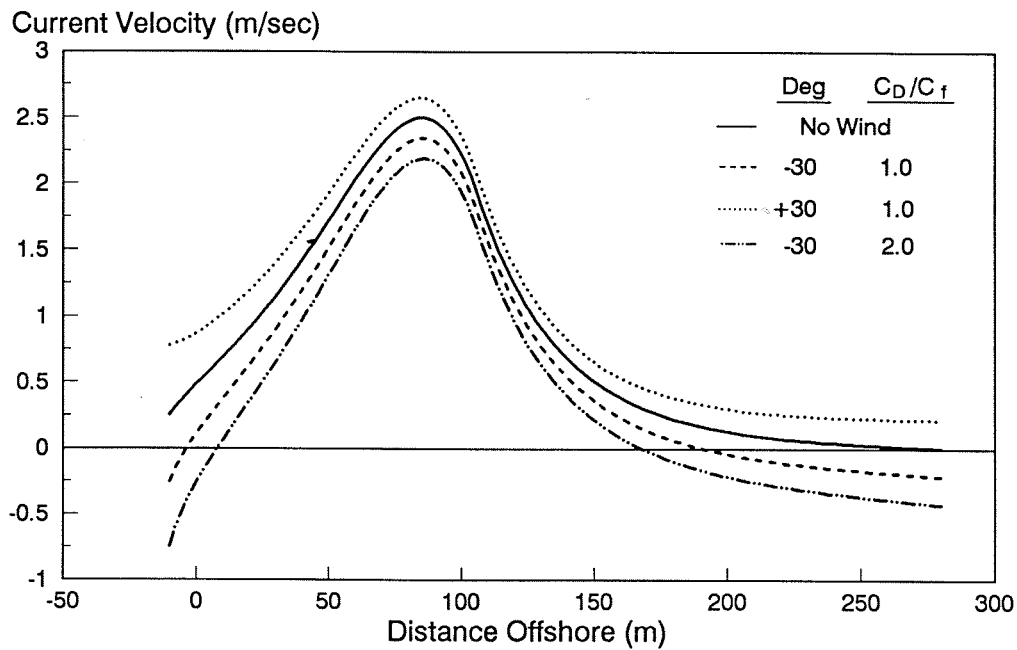
237. To examine the direct influence of wind on the longshore current profile and mean water surface elevation in the model, several hypothetical cases were simulated. Two different basic profile shapes were used, a plane-sloping beach and a barred beach. The barred profile and incident wave

conditions (deepwater wave height  $H_o = 2.0$  m,  $T = 8.0$  sec, and deepwater wave angle  $\theta_o = 30$  deg) were taken from Ebersole and Dalrymple (1980), and the plane beach was given a slope  $\tan\beta = 0.024$ . The wave model was applied with the same parameter values used in previous simulations, and the linear and nonlinear current models were applied with ( $c_f = 0.0050$ ,  $\Lambda = 0.50$ ), and ( $c_f = 0.0040$ ,  $\Lambda = 0.30$ ), respectively. The smaller value of the friction coefficient in the nonlinear model produced current velocities comparable to the linear model, facilitating comparison of model predictions.

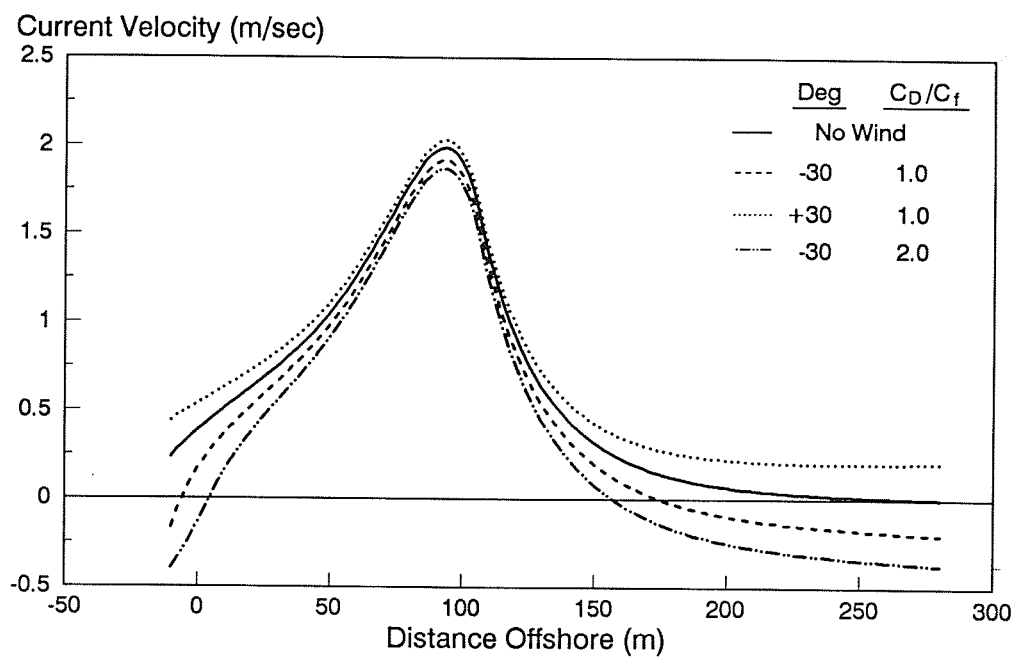
238. A wind speed of 15 m/sec was used, and the incident angle of the wind  $\phi$  was taken as +30 and -30 deg to obtain conditions that reinforced and opposed the wave-induced longshore current (negative incident wave angle), respectively. Different ratios of  $C_D/c_f$  were investigated, and monochromatic wave conditions were employed. Figures 26a and b show the influence of wind forcing on the calculated longshore current distribution for the plane-sloping beach as predicted by the linear and nonlinear current models. The distribution occurring without wind is also shown for comparison. In the figures, the current distributions for  $C_D/c_f$  ratios of 1.0 and 2.0 are shown for selected incident wind angles.

239. A wind with an alongshore component in the same direction as the current induced by breaking waves simply produces an overall increase in current speed. The linear model predicts a change in current similar in magnitude across the shore, whereas the nonlinear model shows relatively smaller changes in the vicinity of maximum in the distribution, a result of the quadratic dependence of the velocity in the friction term. Similar behavior is seen for the opposing wind and current situation, with the nonlinear model showing less reduction in current velocity around the peak in the distribution. If the opposing wind is sufficiently strong, it may dominate the wave-induced contribution and reverse the current. A change in current direction in the opposing wind and wave situation is particularly likely at the shoreward and seaward ends of the current where the wave-induced current is weak, as shown in Figures 26a and b for some of the simulations.

240. As is discussed in the following paragraphs, the modification of the boundary conditions to include wind results in a slightly increasing current velocity with distance offshore for the linear model, whereas the nonlinear model produces a constant current offshore. This trend is seen in



a. Linear model



b. Nonlinear model

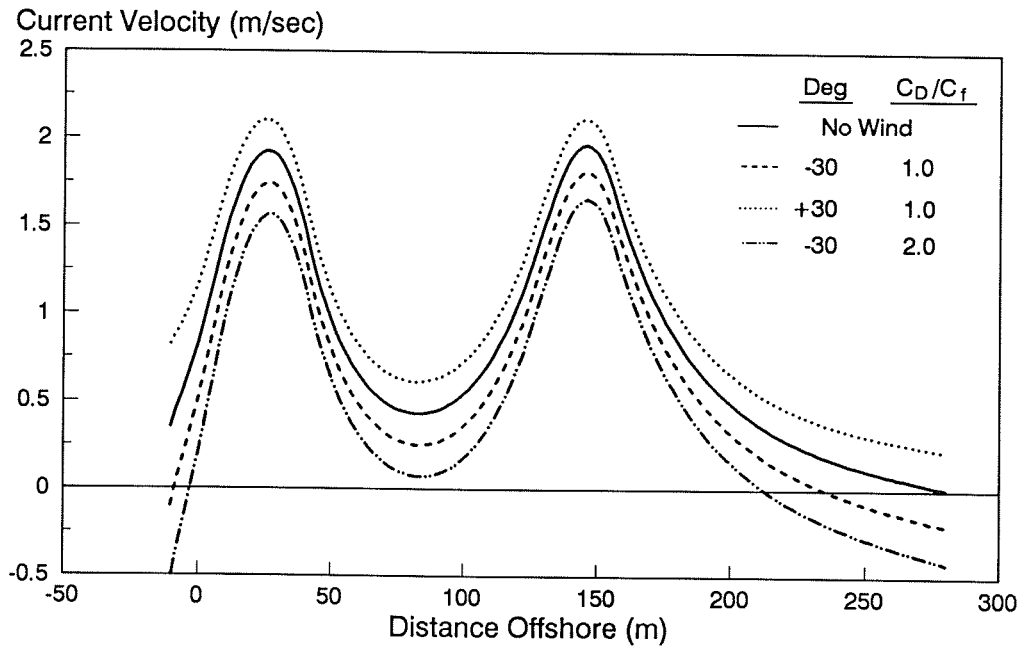
Figure 26. Effect of wind on the longshore current (plane beach)

Figures 26a and b in the seaward tail of the profiles where the linear model result displays a larger gradient than the nonlinear model. The current increases almost in proportion to the ratio  $C_D/c_f$  in the linear model with a relatively larger increase at the ends of the distributions. For the nonlinear model, the dependence of the friction term on the velocity squared makes the effect of an increase in  $C_D/c_f$  somewhat nonuniform.

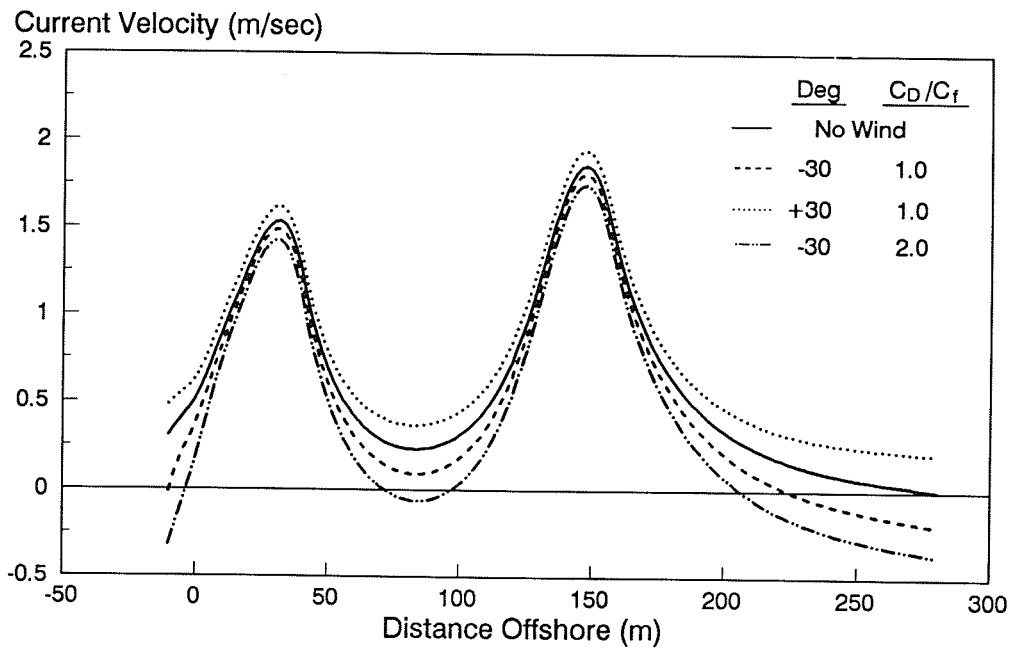
241. The same simulations as for the plane-sloping beach were carried out for the barred profile introduced by Ebersole and Dalrymple (1980). Figures 27a and b show the simulation results for the linear and nonlinear models, respectively. The influence of the wind on the current distribution exhibits the same general characteristics found for the plane-sloping beach. However, the current distribution is bimodal because the bars produce multiple wave breaking and subsequent reformation. The trough behind the bar reduces the wave energy dissipation and thus the change in the alongshore-directed radiation stress driving the wave-induced longshore current. Because of the change in radiation stress gradient, a minimum in the current profile is located just shoreward of the bar, and a second peak is produced closer to shore as the energy dissipation again becomes larger. The relatively large wave-induced contribution nearshore makes it difficult for the opposing wind to reverse the current near the shoreline. For the nonlinear model, the wind effect on the current profile is relatively small around the peaks, but becomes important in the trough region and seaward of the breaker zone. The larger valued drag coefficient giving  $C_D/c_f = 2.0$  reverses the current in the trough area for the opposing wind.

#### Mean water surface elevation

242. The wind not only enters as a forcing term in the longshore momentum equation, but also contributes to the cross-shore momentum equation. For example, a wind blowing onshore will tilt the water surface shoreward to balance the stress at the air-sea interface. Wind setup is a menacing phenomenon during storms as it allows waves to attack high on the beach, leading to severe erosion and inundation. In a numerical model, the effect of the wind on the mean water surface elevation will be underestimated unless the grid extends seaward much farther than the distance typically covered in a longshore current calculation, and the model allows opening of "wetted" cells on the previously dry beach (as allowed in NMLONG).



a. Linear model



b. Nonlinear model

Figure 27. Effect of wind on the longshore current (barred profile)

243. To estimate the importance of wind-induced setup, the simple case of an onshore-blowing wind without waves is examined. If the wind setup is small in comparison with the water depth, in the absence of waves the momentum equation (Equation 54) may be written,

$$\rho gh \frac{d\eta}{dx} = -\rho_a C_D |W| W \cos \phi \quad (90)$$

Equation 90 expresses a force balance between the surface shear stress and the hydrostatic pressure caused by the tilt of the water surface. For a wind blowing onshore, the setup decreases going seaward, according to the definition of sign given in Figure 1. For simple bottom topographies, Equation 90 is readily integrated to yield an analytic solution for  $\eta$ . In the case of a plane beach of bottom slope  $\tan\beta$ , Equation 90 gives,

$$\eta = \frac{\rho_a}{\rho} \frac{C_D}{g \tan\beta} W^2 \cos \phi \ln\left(\frac{x_0}{x}\right) \quad (91)$$

where  $x_0$  denotes the seaward location where the wind stress starts to act. Equation 91 can only be applied to within a certain distance from the shoreline since at the shoreline  $h$  equals zero, giving infinite setup. This is simply a consequence of assuming that  $\eta$  is negligible in comparison with  $h$ ; at the shoreline this assumption is inapplicable.

244. In the previous case of a plane-sloping beach and a moderate onshore-blowing wind with  $W = 15$  m/sec and  $\phi = 30$  deg, wind-induced setup over a 500-m-long grid was calculated by Equation 91 to be only about 3.0 cm at a point 1 m from the shoreline. In the example  $C_D = 5 \cdot 10^{-3}$  was used. To reproduce realistic wind setup, it is necessary to describe wind conditions over a longer stretch than what is normally used in calculating wave-induced longshore currents.

#### Numerical solution

245. Numerical solution of the momentum equations incorporating wind driving requires no special techniques; only values of the drag coefficient

and wind speed and direction must be specified. However, the boundary conditions must be modified since a wind stress is now acting at these two points. Boundary conditions are obtained by explicitly solving for the current velocity without lateral mixing. Thus, the bottom friction force is equated to the driving force, including wind. At the seaward boundary, the wind-induced current calculated by the linear model can take an unreasonably high value if the grid is located in deep water compared with the wavelength, because the current is inversely proportional to the wave orbital velocity at the bottom, which approaches zero. For a nonlinear friction term, the bottom resistance approaches the familiar velocity-squared dependence if the orbital velocity is small.

246. Figure 28 shows calculated results for the aforementioned wind and beach conditions for onshore and offshore winds. The numerical results agree well with the simple analytic model solution (simple because the total water depth is approximated by the still-water depth). The numerical solution is asymmetric because the total water depth is used.

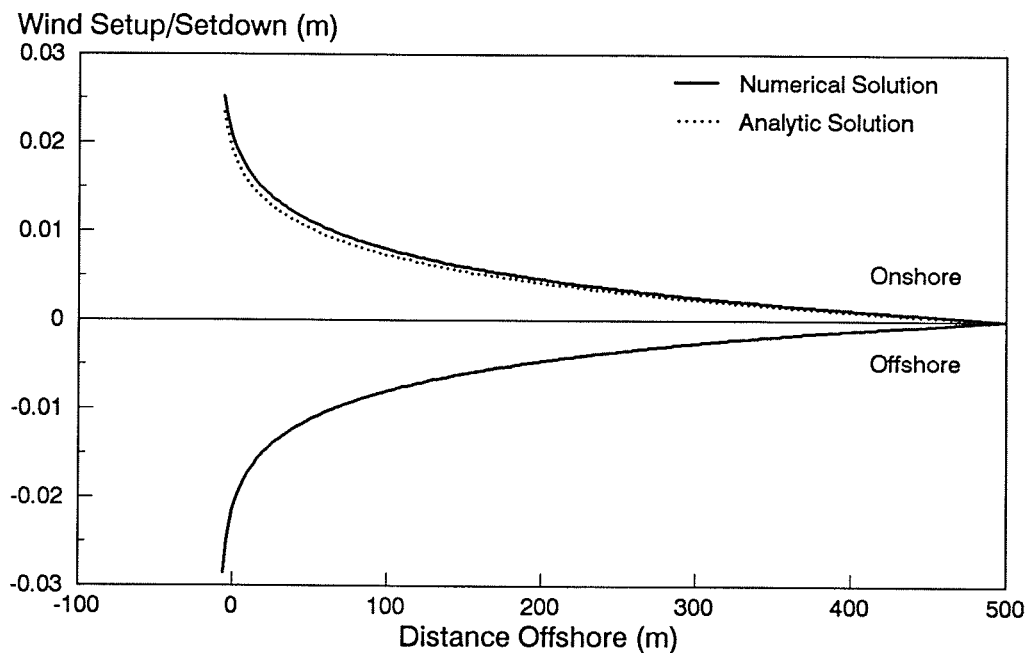


Figure 28. Simulation of wind-induced setup and setdown

## Wave-Current Interaction

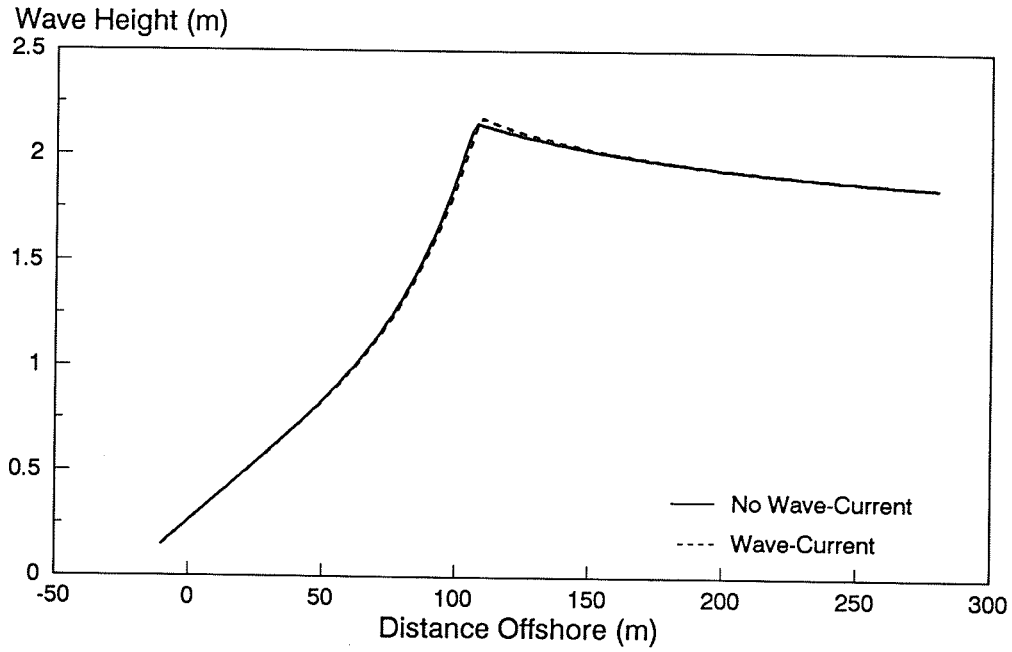
247. If the wave-current interaction is activated in the model, the wave height and current distributions cannot be obtained independently, and an iterative technique must be employed. Wave-current interaction terms appear in the wave energy flux equation (Equation 7) and wave refraction equation (Equation 19). Selected results are described here from the calculations to quantify the importance of wave-current interaction and how it influences the wave height and current profiles.

248. Both a plane beach and the barred profile of Ebersole and Dalrymple (1980) were used to evaluate the influence of the wave-current interaction on the profile. Empirical parameters in the wave model were set to default values, and the current was computed with the nonlinear model with  $c_f = 0.01$  and  $\Lambda = 0.5$  as in some of the previous simulations for the hypothetical barred profile (Figure 25). The plane-sloping beach was identical to the previous case. A breaker index of 0.78 was employed in both examples, following Ebersole and Dalrymple.

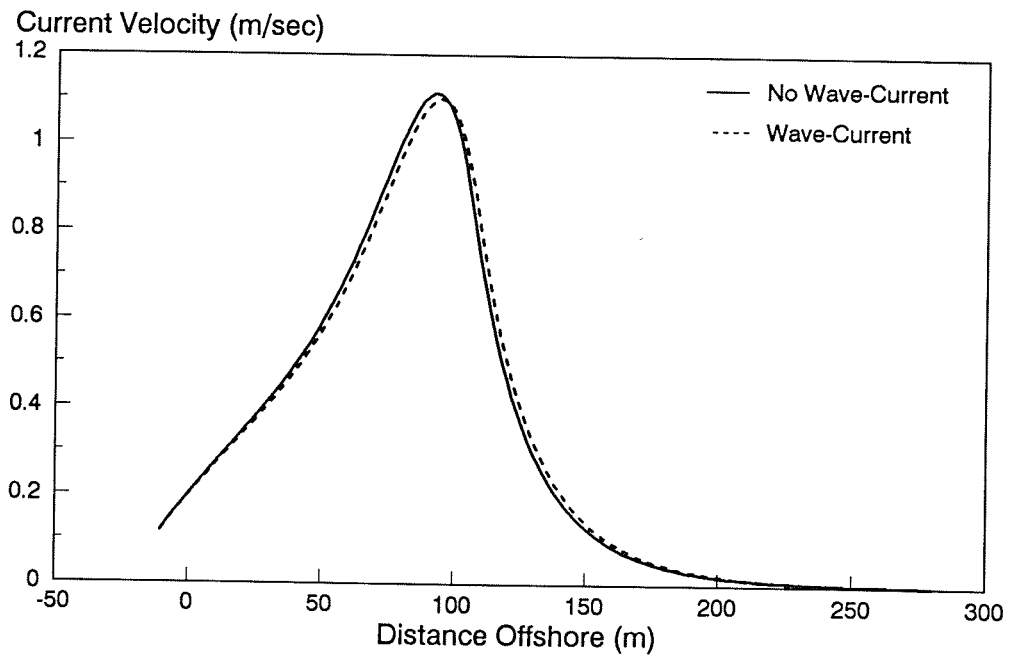
249. The current velocity was set to zero to calculate the wave height at the first iteration, and subsequent calculations of the wave height included the current velocity determined at the previous iteration. This procedure continued until two consecutively calculated distributions of the wave height and current respectively differed by less than 1 percent at every grid point. The calculation normally converged in two to three iterations, the small number of iterations indicating that the wave-current interaction was weak.

### Plane-sloping beach (Figure 29)

250. The difference in wave height incorporating the wave-current interaction is noticeable only near the break point, where the wave height is increased slightly. The effect of the interaction on the longshore current is somewhat greater, but still weak, being most pronounced around the maximum in the current and extending both shoreward and seaward of the maximum. The wave-current interaction raises the tail of the current profile, lowers the current velocity at the maximum while translating the location of the maximum current seaward, and slightly decreasing the current magnitude in the surf zone.



a. Wave height



b. Longshore current

Figure 29. Wave-current interaction on a plane-sloping beach

### Barred profile (Figure 30)

251. In this example, wave breaking occurs on the bar with reformation where the energy flux falls below the stable energy flux in the deeper part of the trough. The wave-current interaction increases the wave height slightly around the break points, similar to the plane-sloping beach case, and most notably at the seaward break point where the current velocity is greatest. The magnitude of the current is decreased slightly in the vicinity of the two maxima, and changes negligibly in the trough behind the bars.

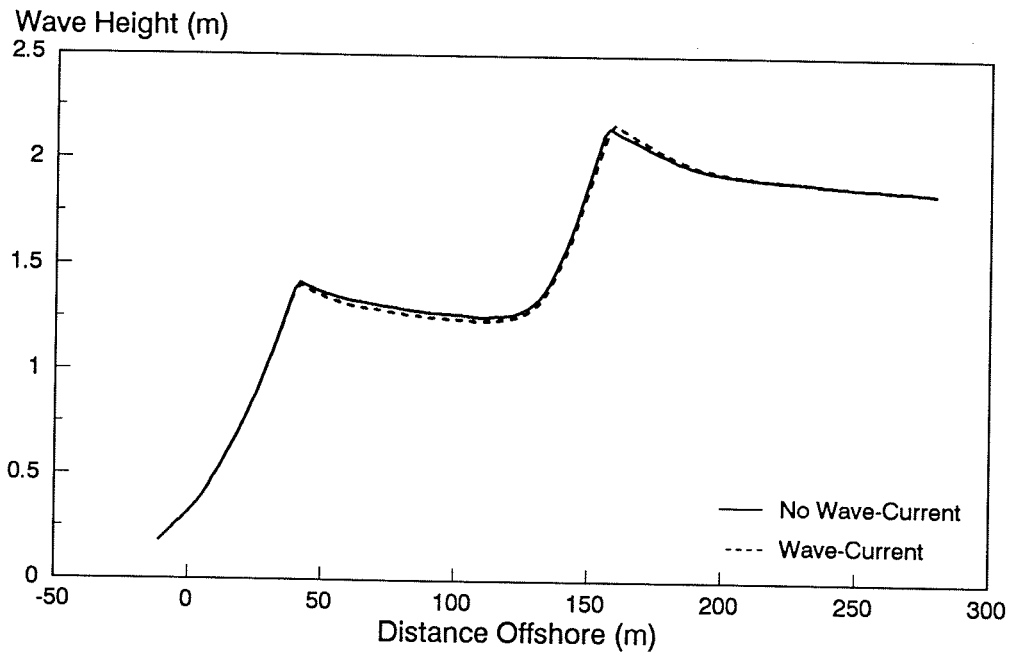
### Separate effects (Figure 31)

252. The wave-current interaction enters in two ways in NMLONG: through the wave energy flux equation (Equation 7) as an interaction term with the radiation stress and through wave refraction (current refraction) (Equation 19). To quantify the influence of these terms, their individual and combined effects were studied by example with the previous plane-sloping beach case. Figure 31a shows that refraction negligibly modifies the wave height distribution and can for all practical purposes be neglected. This conclusion holds only for the wave-current interaction for an alongshore system; even casual observation shows that localized strong seaward flow in rip current throats can greatly change wave properties and even prematurely break the waves before they become depth limited.

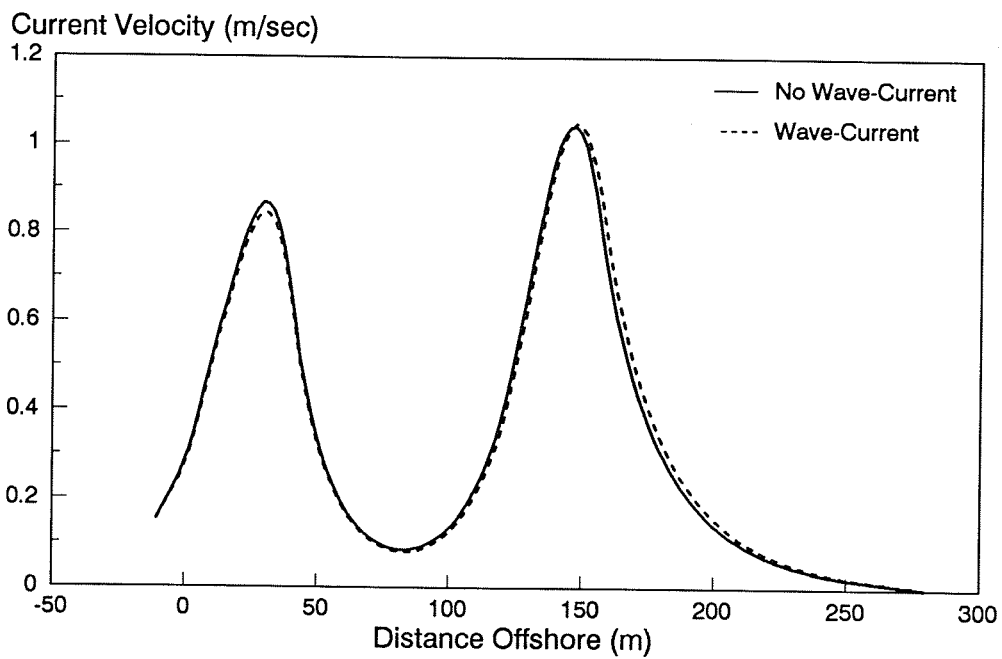
253. Calculations showed that modifications of the current by the refraction and radiation stress terms were of the same order of magnitude for the test cases (see Figure 31b). In addition, the two terms counteract each other, the radiation stress term increasing the current around the peak and decreasing the current along the tail, and the refraction term acting in the opposite way.

### Discussion

254. The calculated examples demonstrated that the wave-current interaction has relatively minor influence on the wave height and longshore current profiles for the situation of longshore uniformity with no strong offshore-directed flows such as would occur at a rip current. The examples pertained to current velocities reaching slightly more than 1 m/sec, which is considerably greater than the current on most beaches under average wave conditions. Storm waves and waves approaching at unusually large incident angles, as well as high winds, could produce significantly greater current velocities. For

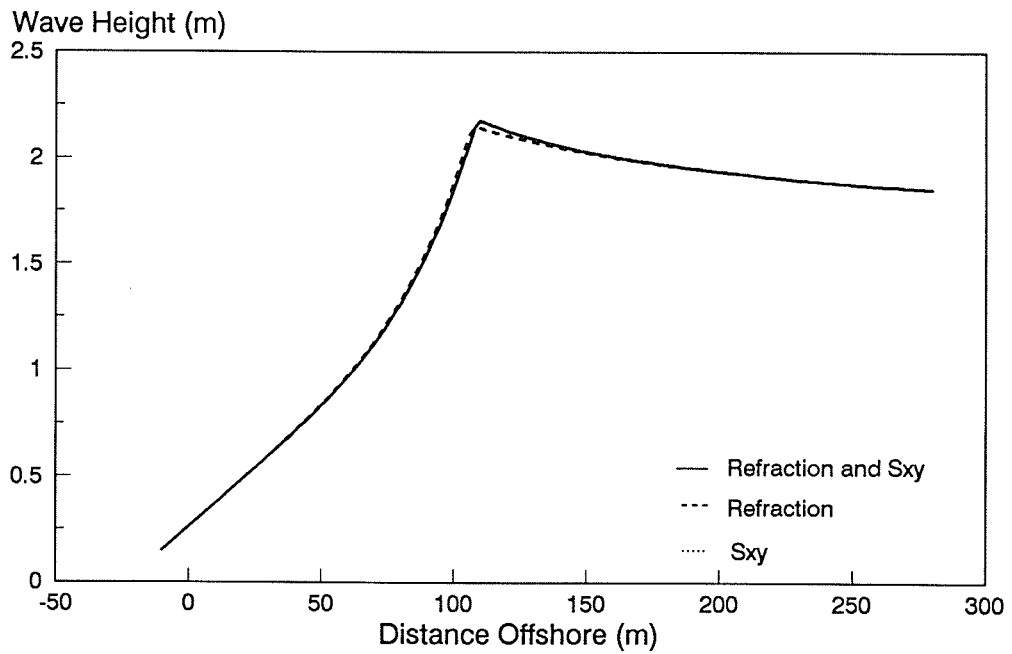


a. Wave height

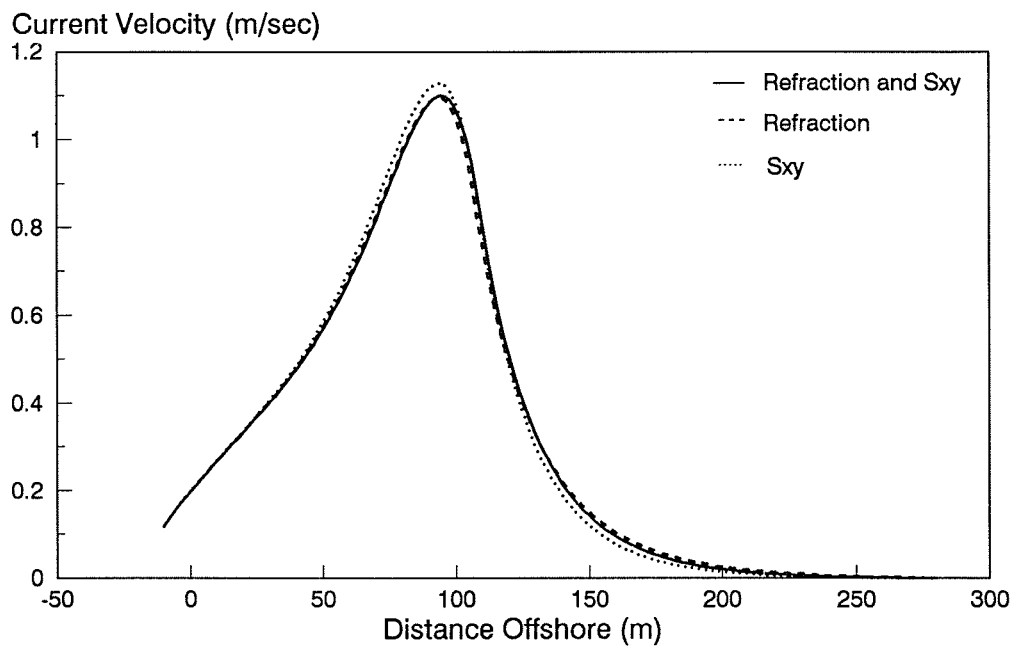


b. Longshore current

Figure 30. Wave-current interaction on a barred beach



a. Wave height



b. Longshore current

Figure 31. Evaluation of the wave-current interaction

example, longshore current velocities recorded at the FRF have reached the range of 3 to 5 m/sec in large storms. In these cases, inclusion of the wave-current interaction may be necessary. Otherwise, the increased calculation time required for solution with the wave-current interaction does not appear warranted in light of the predictive accuracy of a model driven by engineering data. The weakness of the wave-current interaction terms in the wave energy flux and longshore current governing equations, combined with the fact that the wave height decay depends on two empirical parameters, makes it doubtful whether these particular interaction terms need ever be activated. The standard implementation of NMLONG does not iterate between the wave and current models.

## PART VII: SUMMARY AND CONCLUSIONS

### Modeling System Capabilities

255. A numerical modeling system called NMLONG was developed that has the capability to calculate the wave height, wave direction, mean water level, and longshore current across a multiple bar and trough beach profile. The calculated longshore current is time-averaged and depth-integrated. A major practical restriction on the modeling system is the requirement of longshore uniformity, meaning that the beach topography, water level, and wave conditions should be uniform alongshore.

256. Major features of NMLONG may be summarized as follows:

- a. Efficient numerical solution of both the wave and longshore current equations, while maintaining general forms of linear-wave theory expressions for arbitrary depth.
- b. Capability to calculate the wave height, wave direction, and longshore current over a beach profile consisting of multiple longshore bars and troughs.
- c. Incorporation of either linear or quadratic (nonlinear) bottom friction stresses as options.
- d. Incorporation of wave and wind driving for both the longshore current and mean water level.
- e. Incorporation of a rational formulation for lateral mixing.
- f. Wide-ranging verification and sensitivity testing.
- g. Extension of the regular-wave model to random wave height as an option, and calculation of the associated longshore current.
- h. Implementation on a desk-top computer (not described in the present report).

257. The three major calculation components of the modeling system were verified separately. The wave height calculation was verified with data from small-scale laboratory experiments involving regular waves incident at an angle to the beach, prototype-scale tank data involving regular wave transformation over an irregular bottom, and with high-quality field data for which a Monte-Carlo random wave calculation procedure was successful. The mean water level calculation was verified with laboratory measurements, and the longshore current calculation was verified with laboratory measurements and two field data sets.

258. Sensitivity tests were performed on all model components, particularly those components for which verification data were not available such as the wind-induced setup and setdown and the wind-induced longshore current. Tests were also made of components operating in combination, such as longshore current generation by combined wind and waves. These tests gave physically reasonable results and also verified the stability of the numerical solution algorithms in examination of general as well as limiting cases.

259. Calculation efficiency was an important design requirement for the modeling system, because a major goal of this study is implementation of NMLONG on desk-top computers. Calculation speed of the combined wave and mean water level calculation was optimized by adopting the procedure of Dally (1980) for estimating the mean water level, thereby eliminating the necessity of iteration between the waves and water level. An explicit numerical solution scheme for the wave height and water level is more efficient and convenient than an implicit scheme, because the shoreward boundaries cannot be precalculated, being controlled by wave breaking and reformation criteria which must be evaluated cell by cell. The profile of the mean longshore current is obtained by an implicit double-sweep solution procedure. Although such algorithms are commonly used in large 2-D numerical circulation models, this appears to be the first application to the simple 1-D case. The double-sweep solution technique is stable, accurate, and much superior in efficiency to time-stepping, relaxation, and "shooting" solution procedures that have been used in other numerical models.

260. Execution time of the linear model for a barred profile discretized with 150 grid points including realistic wave and wind forcing is approximately 1 sec on a 20-MHz desk-top computer. This solution yields the wave height, water level, and longshore current velocity at all grid points. Execution time of the nonlinear friction model for the same condition is approximately 5 sec and is related to the product of the number of iterations and the execution time of the linear model solution, with great computational cost savings made by implementation of the Nishimura (1982) square-wave approximation. By use of a correction factor for estimating the nonlinear solution based on the linear solution, typically only three to five iterations are required to obtain a solution with the nonlinear friction force.

## Fundamental Processes

261. Although the major objective of this study was development of a general pragmatic model of the longshore current for engineering use, several fundamental governing processes had to be investigated.

### Nonlinear bottom friction

262. The finding of Thornton and Guza (1986) was confirmed that a quadratic friction law acts mainly to reduce the value of the average bottom friction coefficient compared with the value obtained with a linear friction law. A correction factor was developed to estimate the nonlinear current velocity by multiplication of the linear solution. Alternatively, the correction factor can be interpreted as relating the friction coefficients in the nonlinear and linear solutions. An approximation for this factor (Equation A13) was obtained as a function of the wave angle and ratio of current velocity of the linear solution and magnitude of the wave orbital velocity.

263. The Nishimura (1982) square-wave approximation of the quadratic friction force was investigated and found to be an accurate and efficient method for replacing computation-intensive time-integration of the friction term. This technique provides considerable savings in computation time, although iteration is still required in obtaining a solution of the nonlinear current model.

264. Generally speaking, the linear current model provided as good or superior agreement with measurements of the current in the surf zone as the nonlinear model, with the nonlinear model giving better agreement seaward of the breaker line because the calculated current decreased more steeply. For engineering use, at the present stage of understanding of bottom friction factors and sediment transport in the surf zone, the linear model is considered sufficiently accurate.

### Wave-current interaction

265. Numerical experimentation confirmed previous results (Dalrymple 1980, Thornton and Guza 1986) that the wave-current action is, for practical purposes, negligible for an alongshore current system except, perhaps, for extreme conditions of very large wave angles and wave heights. The radiation stress interaction term and the current-refraction term are of the same magnitude and act to cancel each other.

### Lateral mixing

266. It was found necessary to include lateral mixing in the current models to reproduce current profiles measured in a carefully controlled laboratory experiment using monochromatic regular waves as well as profiles measured in the field produced by random waves. The value of the empirical mixing coefficient was approximately the same for the laboratory and field tests. A rational form of the eddy viscosity coefficient was introduced (Equation 48) and appears to be more applicable to barred profiles than other commonly used expressions.

### Random waves

267. A Monte-Carlo approach based on a Raleigh distribution was developed to give the wave height probability distribution of random waves transforming by shoaling, refraction, breaking, and reformation at intervals across a surf zone with a bar and trough bottom profile. In this approach, between 100 and 500 waves are randomly selected from a Rayleigh distribution defined by the rms wave height and then transformed individually. Statistical properties are then obtained by invoking superposition. In this procedure, a true breaker index corresponding to regular monochromatic waves is employed. Calculation results were compared with high-quality measurements, and good agreement was found. The Monte-Carlo random wave model drove the longshore current model, and favorable results were obtained in reproducing current measurements in five field data sets.

268. The Monte-Carlo approach is computation intensive because on the order of 100 model runs must be made to obtain a reasonable representation of the wave height probability distribution and resultant current. The advantage is that the method is applicable to a bar and trough profile without invoking *a priori* assumptions about the shape of the transformed probability distribution.

### Wind drag coefficient

269. The order of magnitude of the wind drag coefficient was estimated to be the same as the bottom friction coefficient in a crude empirical analysis correlating measured winds and longshore current at one site. Several formulas for the drag coefficient were reviewed for use in the longshore current model, and the WAMDI Group (1988) formula was selected as being most appropriate for the nearshore zone.

### Future Work

270. The next stage in this study program will transfer all model developments to the desk-top computer environment. The existing prototype desk-top model will be completed and integrated with a convenient user interface that includes structured data input, automatic data cleaning and error messages, and graphical output. The results will be presented in a user's manual to be distributed with the model.

271. A research effort is required to understand the role of the wind in generating the longshore current and changing the mean water surface level. Of particular importance is how the wind changes the location of the break point and type of breaking, processes that are not represented in existing models, including NMLONG.

272. The availability of the present general model of waves, mean water level, and longshore current in the surf zone should stimulate further field data collection. The field program should include synoptic measurements of the profile topography, wave height and direction, wind speed and direction, mean water level, and longshore current for a wide range of conditions. One possible use of a well-verified model would be to infer information on the form of lateral mixing eddy viscosity coefficient, which is difficult to obtain by direct measurement.

#### REFERENCES

- Amoroch, J., and DeVries, J. J. 1980. "A New Evaluation of the Wind Stress Coefficient Over Water Surfaces," Journal of Geophysical Research, Vol 85, No. C1, pp 433-442.
- Basco, D. R. 1982. "Surf Zone Currents," Miscellaneous Report No. 82-7 (I), US Army Engineer Waterways Experiment Station, Coastal Engineering Research Center, Vicksburg, MS.
- Basco, D. R., and Coleman, R. A. 1982. "Surf Zone Currents," Miscellaneous Report No. 82-7 (II), US Army Engineer Waterways Experiment Station, Coastal Engineering Research Center, Vicksburg, MS.
- Battjes, J. A. 1972. "Set-Up Due to Irregular Waves," Proceedings of 13th Coastal Engineering Conference, American Society of Civil Engineers, pp 1993-2004.
- \_\_\_\_\_. 1974. "Surf Similarity," Proceedings of 14th Coastal Engineering Conference, American Society of Civil Engineers, pp 466-480.
- \_\_\_\_\_. 1975. "Modeling of Turbulence in the Surf Zone," Proceedings of Symposium on Modeling Techniques, American Society of Civil Engineers, pp 1050-1061.
- Battjes, J. A., and Janssen, J. P. F. M. 1978. "Energy Loss and Setup Due to Breaking of Random Waves," Proceedings of the 16th Coastal Engineering Conference, American Society of Civil Engineers, pp 569-587.
- Baum, S. K., and Basco, D. R. 1986. "A Numerical Investigation of the Longshore Current Profile for Multiple Bar/Trough Beaches," Proceedings of 20th Coastal Engineering Conference, American Society of Civil Engineers, pp 971-985.
- Birkemeier, W. A., and Dalrymple, R. A. 1975. "Nearshore Water Circulations Induced by Wind and Waves," Proceedings of Symposium on Modeling Techniques, American Society of Civil Engineers, pp 1062-1081.
- Birkemeier, W. A., Strider, J. B., Baron, C. F., and Hathaway, K. K. 1987. "Field Data from the Duck85 Field Experiment for the Evaluation of Nearshore Numerical Models," in: de Graauw, A., and Hamm, L., "Prototype Measurements to Validate Numerical Models of Coastal Processes," SOGREAH Consulting Engineers, Grenoble, France.
- Bishop, J. M. 1984. Applied Oceanography, Wiley, New York.
- Bowen, A. J. 1969. "The Generation of Longshore Currents on a Plane Beach," Journal of Marine Research, Vol 27, No. 1, pp 206-215.
- Bowen, A. J., and Holman, R. A. 1990. "Shear Instability of the Mean Longshore Current, 1. Theory," Journal of Geophysical Research, Vol 94, No. C12, pp 18,023-18,030.

- Bretschneider, C. L. 1966. "Engineering Aspects of Hurricane Surge," in: A. T. Ippen, ed., Estuary and Coastline Hydrodynamics, McGraw-Hill Book Co., New York, pp 231-256.
- Collins, J. I., and Wier, W. 1969. "Probabilities of Wave Characteristics in the Surf Zone," Report No. TC-149, Tetra Tech Corporation, Pasadena, CA.
- Dally, W. R. 1980. "A Numerical Model for Beach Profile Evolution," M.S. Thesis, Department of Civil Engineering, University of Delaware, Newark, DE.
- \_\_\_\_\_. 1987. "Wave Transformation in the Surf Zone," Ph.D. Thesis, Department of Oceanographic and Coastal Engineering, University of Florida, Gainesville, FL.
- \_\_\_\_\_. 1990. "Random Breaking Waves: A Closed-Form Solution for Planar Beaches," Coastal Engineering, Vol 14, 233-263.
- Dally, W. R., and Dean, R. G. 1988. "Closed-Form Solutions for the Probability Density of Wave Height in the Surf Zone," Proceedings 21st Coastal Engineering Conference, American Society of Civil Engineers, pp 807-821.
- Dally, W. R., Dean, R. G., Dalrymple, R. A. 1985. "Wave Height Variation Across Beaches of Arbitrary Profile," Journal of Geophysical Research, Vol 90, No. C6, pp 11917-11927.
- Dalrymple, R. A. 1980. "Longshore Current with Wave Current Interaction," Journal of the Waterway, Port, Coastal and Ocean Division, Vol 106, No. WW3, pp 414-420.
- Dean, R. G. 1977. "Equilibrium Beach Profile: U.S. Atlantic and Gulf Coasts," Ocean Engineering Report 12, Department of Civil Engineering, University of Delaware, Newark, DE.
- DeVries, J. J., and Amorocho, J. 1980. "Wind Setup Effects in Large Open Channels," Journal of Waterway, Port, Coastal and Ocean Division, Vol 106, No. WW3, pp 319-334.
- Dolan, T. J., and Dean, R. G. 1984. "Multiple Longshore Sand Bars in the Upper Chesapeake Bay," Estuarine Coastal and Shelf Science, Vol 21, No. 5, pp 727-743.
- Douglas, S. A., and Weggel, J. R. 1988. "Laboratory Experiments on the Influence of Wind on Nearshore Wave Breaking," Proceedings of 21st Coastal Engineering Conference, American Society of Civil Engineers, pp 632-643.
- Ebersole, B. A. 1987. "Measurements and Prediction of Wave Height Decay in the Surf Zone," Proceedings of Coastal Hydrodynamics, American Society of Civil Engineers, pp 1-16.

Ebersole, B. A., Cialone, M. A., and Prater, M. D. 1986. "Regional Coastal Processes Numerical Modeling System; Report 1, RCPWAVE - A Linear Wave Propagation Model for Engineering Use," Technical Report CERC-86-4, US Army Engineer Waterways Experiment Station, Coastal Engineering Research Center, Vicksburg, MS.

Ebersole, B. A., and Dalrymple, R. A. 1980. "Numerical Modeling of Nearshore Circulation," Proceedings of 17th Coastal Engineering Conference, American Society of Civil Engineers, pp 2710-2725.

Ebersole, B. A., and Hughes, S. A. 1987. "DUCK85 Photopole Experiment," Miscellaneous Paper CERC-87-18, US Army Engineer Waterways Experiment Station, Coastal Engineering Research Center, Vicksburg, MS.

Galvin, C. J. 1967. "Longshore Current Velocity: A Review of Theory and Data," Reviews of Geophysics, Vol 5, No. 3, pp 287-304.

\_\_\_\_\_. 1969. "Breaker Travel and Choice of Design Wave Height," Journal of Waterways and Harbors Division, Vol 95, No. 2, pp 175-200.

Garratt, J. R. 1977. "Review of Drag Coefficients Over Oceans and Continents," Monthly Weather Review, Vol 105, pp 915-929.

Goda, Y. 1975. "Irregular Wave Deformation in the Surf Zone," Coastal Engineering in Japan, Vol 18, pp 13-26.

Gourlay, M. R. 1976. "Nonuniform Alongshore Currents," Proceedings of 15th Coastal Engineering Conference, American Society of Civil Engineers, pp 701-720.

\_\_\_\_\_. 1982. "Nonuniform Alongshore Currents and Sediment Transport; A One-Dimensional Approach," Research Report No. CE31, Department of Civil Engineering, University of Queensland, St. Lucia, Australia.

Greenwood, B., and Sherman, D. J. 1986. "Longshore Current Profiles and Lateral Mixing Across the Surf Zone of a Barred Profile," Coastal Engineering, Vol 10, 149-168.

Guza, R. T., and Thornton, E. B. 1978. "Variability of Longshore Currents," Proceedings of 16th Coastal Engineering Conference, American Society of Civil Engineers, pp 756-775.

Hardy, T. A., and Kraus, N. C. 1988. "Coupling Stokes and Cnoidal Wave Theories in a Nonlinear Refraction Model," Proceedings of 21st Coastal Engineering Conference, American Society of Civil Engineers, pp 588-601.

Harris, T. F. W. 1969. "Nearshore Circulations; Field Observations and Experimental Investigations of an Underlying Cause in Wave Tanks," Proceedings of Symposium on Coastal Engineering, Stellenbosch, South Africa.

- Horikawa, K., and Kuo, C. 1966. "A Study on Wave Transformation Inside the Surf Zone," Proceedings of 10th Coastal Engineering Conference, American Society of Civil Engineers, pp 217-233.
- Hsu, S. A. 1972. "Wind Stress on a Coastal Water Surface," Proceedings of 13th Coastal Engineering Conference, American Society of Civil Engineers, pp 2531-2541.
- \_\_\_\_\_. 1988. Coastal Meteorology. Academic Press, Inc., San Diego, CA.
- Huang, N. E., Bliven, L. F., Long, S. R., and DeLeonibus, P. S. 1986. "A Study of the Relationship Among Wind Speed, Sea State, and the Drag Coefficient for a Developing Wave Field," Journal of Geophysical Research, Vol 91, No. C6, pp 7733-7742.
- Hubertz, J. M. 1984. "Modeling of Nearshore Wave Driven Currents," Proceedings of 19th Coastal Engineering Conference, American Society of Civil Engineers, pp 2208-2219.
- \_\_\_\_\_. 1986. "Observations of Local Wind Effects on Longshore Currents," Coastal Engineering, Vol 10, pp 275-288.
- \_\_\_\_\_. 1987. "A Wind- and Wave-Driven Nearshore Current Model," The One-Dimensional Model, Miscellaneous Paper CERC-87-4, US Army Engineer Waterways Experiment Station, Coastal Engineering Research Center, Vicksburg, MS.
- Hubertz, J. M., Long, C. E., Rivers, P., and Brown, W. A. 1987. "Duck '85 Nearshore Waves and Current Experiment: Data Summary Report," Miscellaneous Paper CERC-87-3, US Army Engineer Waterways Experiment Station, Coastal Engineering Research Center, Vicksburg, MS.
- Hughes, S. A., and Borgman, L. E. 1987. "Beta-Rayleigh Distribution for Shallow Water Wave Heights," Proceedings of Coastal Hydrodynamics '87, American Society of Civil Engineers, pp 17-31.
- Hunt, J. F. 1979. "Direct Solution of the Wave Dispersion Relation," Journal of Waterways, Port, Coastal, and Ocean Division, Vol 105, No. WW4, pp 457-459.
- Inman, D. L., Tait, R. J., and Nordstrom, C. E. 1971. "Mixing in the Surf Zone," Journal of Geophysical Research, Vol 76, pp 3493-3514.
- Inman, D. L., and Quinn, W. H. 1952. "Currents in the Surf Zone," Proceedings of 2nd Coastal Engineering Conference, American Society of Civil Engineers, pp 24-36.
- James, I. D. 1974. "A Non-Linear Theory of Longshore Currents," Estuarine and Coastal Marine Science, Vol 2, No. 3, pp 235-249.
- Jonsson, I. G. 1966. "Wave Boundary Layers and Friction Factors," Proceedings of 10th Coastal Engineering Conference, American Society of Civil Engineers, pp 127-148.

Jonsson, I. G., Skovgaard, O., and Jacobsen, T. S. 1974. "Computation of Longshore Currents," Proceedings of 14th Coastal Engineering Conference, American Society of Civil Engineers, pp 699-714.

Kajima, R., Saito, S., Shimizu, T., Maruyama, K., Hasegawa, H., and Sakakiyama, T. 1983b. "Sand Transport Experiments Performed by Using a Large Water Wave Tank," Data Report No. 4-1, Central Research Institute for Electric Power Industry, Civil Engineering Division (in Japanese).

Kajima, R., Shimizu, T., Maruyama, K., and Saito, S. 1983a. "Experiments of Beach Profile Change with a Large Wave Flume," Proceedings of 18th Coastal Engineering Conference, American Society of Civil Engineers, pp 1385-1404.

Keely, J. R., and Bowen, A. J. 1977. "Longshore Variation in Longshore Currents," Canadian Journal of Earth Science, Vol 14, No. 8, pp 1897-1905.

Komar, P. D. 1975. "Nearshore Currents: Generation by Obliquely Incident Waves and Longshore Variations in Breaker Wave Height," in Nearshore Sediment Dynamics and Sedimentation, J. Hails and A. Carr, eds., Wiley, London, pp 19-45.

Komar, P. D., and Oltman-Shay, J. 1990. "Nearshore Currents," in Handbook of Coastal and Ocean Engineering, J. Herbich, ed., Gulf Publishing Co., Houston, TX.

Kraus, N. C. 1980. "Lateral Mixing in the Nearshore Area," NERC Report No. 10, Cooperative Research on Surf Zone Dynamics, Part 2, Natural Beaches, Nearshore Environment Research Center, Tokyo, Japan, pp 161-177.

Kraus, N. C., Cialone, M. A., and Hardy, T. A. 1987. "Numerical Model of Finite-Amplitude Wave Refraction," Proceedings of Coastal Hydrodynamics, American Society of Civil Engineers, pp 46-59.

Kraus, N. C., Mimura, N., and Horikawa, K. 1980. "Measurements and Investigations of the Mixing Coefficient in and near the Surf Zone," Proceedings of the 27th Japanese Conference on Coastal Engineering, Japan Society of Civil Engineers, pp 173-177 (in Japanese).

Kraus, N. C., and Sasaki, T. O. 1979. "Influence of Wave Angle and Lateral Mixing on the Longshore Current," Marine Science Communications, Vol 5, No. 2, pp 91-126.

Large, W. G., and Pond, S. 1981. "Open Ocean Momentum Flux Measurements in Moderate to Strong Winds," Journal of Physical Oceanography, Vol 11, pp 324-336.

Larson, M., and Kraus, N. C. 1989. "SBEACH: Numerical Model for Simulating Storm-Induced Beach Change, Report 1: Empirical Foundation and Model Development," Technical Report CERC-89-9, US Army Engineer Waterways Experiment Station, Coastal Engineering Research Center, Vicksburg, MS.

- Le Mehaute, B. 1962. "On Non-Saturated Breakers and the Wave Runup," Proceedings of 8th Coastal Engineering Conference, American Society of Civil Engineers, pp 77-92.
- Leont'ev, I. O. 1988. "Randomly Breaking Waves and Surf-Zone Dynamics," Coastal Engineering, Vol 12, pp 83-103.
- Liu, P. L-F., and Dalrymple, R. A. 1978. "Bottom Frictional Stresses and Longshore Currents Due to Waves with Large Angles of Incidence," Journal of Marine Research, Vol 36, No. 2, pp 357-375.
- Long, C. E., and Hubertz, J. M. 1988. "Nearshore Wind-Stress Measurements: Background, Preliminary Field Work, and Experiment Design," Miscellaneous Paper CERC-88-14, US Army Engineer Waterways Experiment Station, Coastal Engineering Research Center, Vicksburg, MS.
- Longuet-Higgins, M. S. 1970a. "Longshore Currents Generated by Obliquely Incident Sea Waves, 1," Journal of Geophysical Research, Vol 75, No. 33, pp 6778-6789.
- \_\_\_\_\_. 1970b. "Longshore Currents Generated by Obliquely Incident Sea Waves, 2," Journal of Geophysical Research, Vol 75, No. 33, pp 6790-6801.
- \_\_\_\_\_. 1972. "Recent Progress in the Study of Longshore Currents," in Waves on Beaches, R. E. Meyer, ed., Academic Press, New York, pp 203-248.
- Longuet-Higgins, M. S., and Stewart, R. W. 1962. "Radiation Stress and Mass Transport in Gravity Waves with Application to 'Surf Beats,'" Journal of Fluid Mechanics, Vol 13, pp 481-504.
- \_\_\_\_\_. 1963. "A Note on Wave Set-up," Journal of Marine Research, Vol 21, pp 4-10.
- \_\_\_\_\_. 1964. "Radiation Stresses in Water Waves; A Physical Discussion with Applications," Deep Sea Research, Vol 11, No. 4, pp 529-562.
- Madsen, O. S., Ostendorf, A. S., and Reyman, A. S. 1978. "A Longshore Current Model," Proceedings of Coastal Zone '78, American Society of Civil Engineers, pp 2332-2341.
- McDougal, W. G., and Hudspeth, R. T. 1983. "Wave Setup/Setdown and Longshore Current on Non-Planar Beaches," Coastal Engineering, Vol 7, pp 103-117.
- \_\_\_\_\_. 1986. "Influence of Lateral Mixing on Longshore Currents," Ocean Engineering, Vol 13, No. 5, pp 419-433.
- \_\_\_\_\_. 1989. "Longshore Current and Sediment Transport on Composite Beach Profiles," Coastal Engineering, pp 315-338.

- McLellan, T. N. 1990. "Nearshore Mound Construction Using Dredged Material," Journal of Coastal Research, Special Issue No. 7, pp 99-107.
- Meadows, G. A. 1976. "Time Dependent Fluctuations in Longshore Currents," Proceedings of 15th Coastal Engineering Conference, American Society of Civil Engineers, pp 660-680.
- Mei, C. C. 1983. The Applied Dynamics of Ocean Surface Waves, John Wiley & Sons, New York.
- Miller, C. D. 1987. "Longshore Current and Wave Decay in the Surf Zone," Proceedings of Coastal Hydrodynamics, American Society of Civil Engineers, pp 140-154.
- Mizuguchi, M. 1980. "An Heuristic Model of Wave Height Distribution in Surf Zone," Proceedings of 17th Coastal Engineering Conference, American Society of Civil Engineers, pp 278-289.
- Mizuguchi, M., Oshima, Y., and Horikawa, K. 1978. "Longshore Currents," Proceedings of the 25th Japanese Conference on Coastal Engineering, Japan Society of Civil Engineers (in Japanese).
- Murden, W. R. 1988. "Berm Concept Could Solve Disposal Problems," International Dredging Review, Vol 7, No. 1, pp 6-7.
- Nairn, R. B. 1988. "Prediction of Wave Height and Mean Return Flow in Cross Shore Sediment Transport Modelling," IAHR Symposium on Mathematical Modelling of Sediment Transport in the Coastal Zone, Copenhagen, Denmark, pp 193-202.
- Nishimura, H. 1982. "Numerical Simulation of Nearshore Circulations," Proceedings of the 29th Japanese Conference on Coastal Engineering, Japan Society of Civil Engineers, pp 333-337 (in Japanese).
- \_\_\_\_\_. 1988. "Computation of Nearshore Current," in Nearshore Dynamics and Coastal Processes, K. Horikawa, ed., University of Tokyo Press, Tokyo, Japan, pp 271-291.
- Noda, E. K. 1974. "Wave-Induced Nearshore Circulation," Journal of Geophysical Research, Vol 79, pp 4097-4106.
- Nummedal, D., and Finley, R. J. 1978. "Wind-Generated Longshore Currents," Proceedings of 16th Coastal Engineering Conference, American Society of Civil Engineers, pp 1428-1438.
- Oltman-Shay, J., Howd, P. A., and Birkemeier, W. A. 1990. "Shear Instabilities of the Mean Longshore Current, 2. Field Observations," Journal of Geophysical Research, Vol 94, No. C12, pp 18,031-18,042.
- O'Conner, B. A., and Yoo, D. 1987. "Turbulence Modeling of Surf Zone Mixing Processes," Proceedings of Coastal Hydrodynamics '87, American Society of Civil Engineers, pp 371-383.

- Pechon, P. 1987. "Modelling of Longshore Currents with a Non Linear Wave Theory," Proceedings of Coastal Hydrodynamics '87, American Society of Civil Engineers, pp 170-183.
- Pond, S., and Pickard, G. L. 1977. Introductory Dynamic Oceanography, Pergamon Press, New York.
- Roelvink, J. A., and Stive, M. J. F. 1989. "Bar-Generating Cross-Shore Flow Mechanisms on a Beach," Journal of Geophysical Research, Vol 94, No. C4, pp 4785-4800.
- Shepard, F. P., Emery, K. O., and La Fond, E. C. 1941. "Rip Currents: A Process of Geological Importance," Journal of Geology, Vol 49, No. 4, pp 337-369.
- Shepard, F. P., and Inman, D. L. 1950. "Nearshore Circulation Related to Bottom Topography and Wave Refraction," Transactions of American Geophysical Union, Vol 3, No. 2, pp 196-212.
- Singamsetti, S. R., and Wind, H. G. 1980. "Breaking Waves Characteristics of Shoaling and Breaking Periodic Waves Normally Incident to Plane Beaches of Constant Slope," Delft Hydraulics Laboratory, Report M 1371, Delft, The Netherlands.
- Smith, E. R., and Kraus, N. C. 1990. "Laboratory Study on Macro-Features of Wave Breaking over Bars and Artificial Reefs," Technical Report CERC-90-12, US Army Engineer Waterways Experiment Station, Coastal Engineering Research Center, Vicksburg, MS.
- Smith, J. M., and Kraus, N. C. 1987. "Longshore Current Based on Power Law Wave Decay," Proceedings of Coastal Hydrodynamics '87, American Society of Civil Engineers, pp 155-169.
- \_\_\_\_\_. 1988. "An Analytic Model of Wave-Induced Longshore Current Based on Power Law Wave Height Decay," Miscellaneous Paper CERC-88-3, US Army Engineer Waterways Experiment Station, Coastal Engineering Research Center, Vicksburg, MS.
- Sonu, C. J. 1972. "Field Observation of Nearshore Circulation and Meandering Currents," Journal of Geophysical Research, Vol 77, No. 18, pp 3232-3247.
- Southgate, H. N. 1989. "A Nearshore-Profile Model of Wave and Tidal Interaction," Coastal Engineering, Vol 13, pp 219-245.
- Sunamura, T. 1980. "A Laboratory Study of Offshore Transport of Sediment and a Model for Eroding Beaches," Proceedings of 17th Coastal Engineering Conference, American Society of Civil Engineers, pp 1051-1070.
- Svendsen, I. A. 1984. "Wave Heights and Set-Up in a Surf Zone," Coastal Engineering, Vol 8, pp 303-329.

The WAMDI Group. 1988 (Dec). "The WAM Model — A Third Generation Ocean Wave Prediction Model," Journal of Physical Oceanography, pp 1775-1810.

Thornton, E. B. 1970. "Variation of Longshore Current Across the Surf Zone," Proceedings of 12th Coastal Engineering Conference, American Society of Civil Engineers, pp 291-308.

Thornton, E. B., and Guza, R. T. 1983. "Transformation of Wave Height Distribution," Journal of Geophysical Research, Vol 88, No. C10, pp 5925-5938.

\_\_\_\_\_. 1986. "Surf Zone Longshore Currents and Random Waves: Field Data and Models," Journal of Physical Oceanography, Vol 16, pp 1165-1178.

\_\_\_\_\_. 1989. "Models for Surf Zone Dynamics," in Nearshore Sediment Transport, R. J. Seymour, ed., Plenum Press, New York, pp 337-369.

Visser, P. J. 1982. "The Proper Longshore Current in a Wave Basin," Report No. 82-1, Department of Civil Engineering, Delft University of Technology, Delft, The Netherlands.

\_\_\_\_\_. 1984a. "A Mathematical Model of Uniform Longshore Currents and the Comparison with Laboratory Data," Report No. 84-2, Department of Civil Engineering, Delft University of Technology, Delft, The Netherlands.

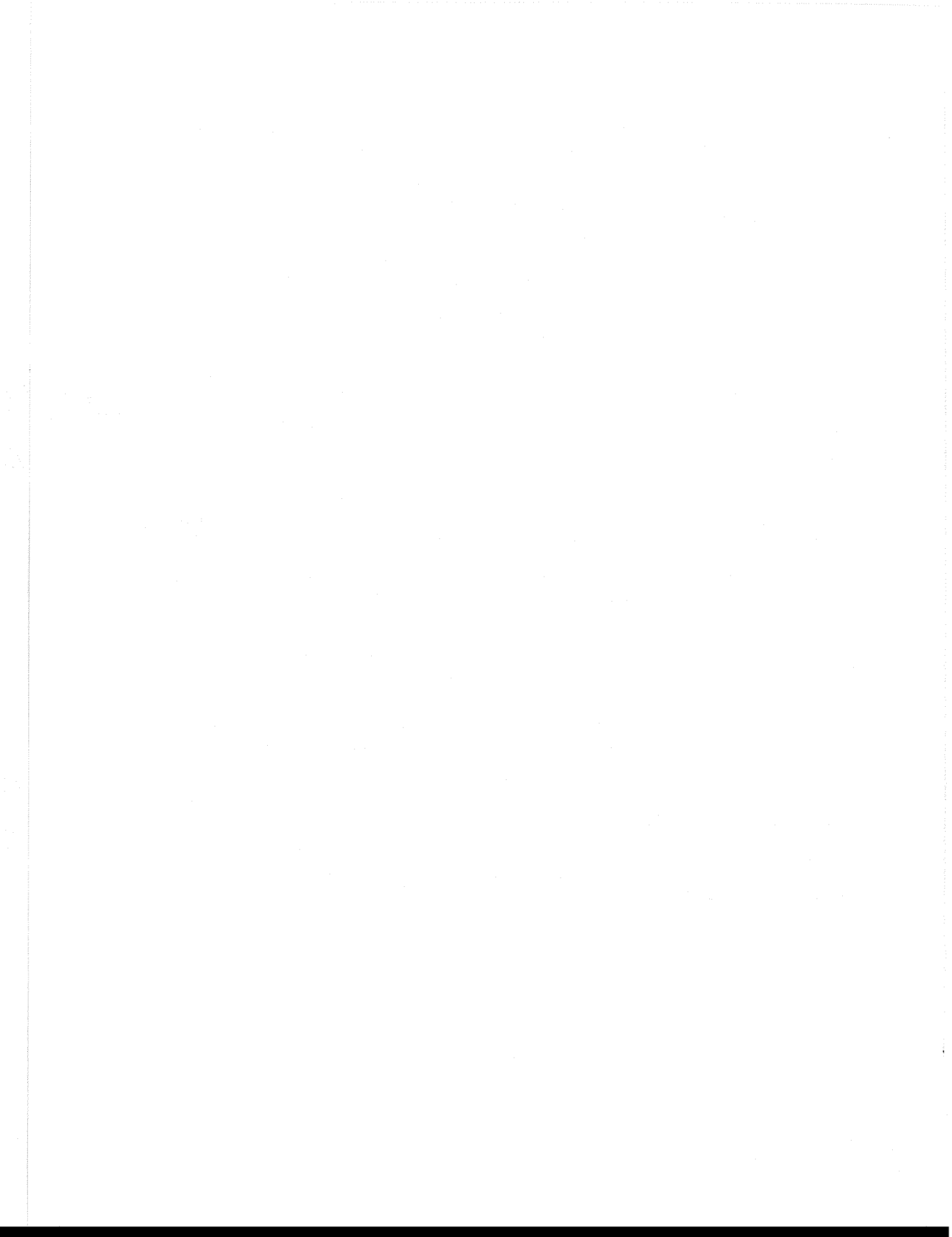
\_\_\_\_\_. 1984b. "Uniform Longshore Current Measurements and Calculations," Proceedings of 19th Coastal Engineering Conference, American Society of Civil Engineers, pp 2192-2207.

Weggel, R. J. 1972. "Maximum Breaker Height," Journal of the Waterways, Harbors and Coastal Engineering Division, American Society of Civil Engineers, Vol 98, No. 1, pp 529-547.

Whitford, D. J., and Thornton, E. B. 1988. "Longshore Current Forcing at a Barred Beach," Proceedings of 21st Coastal Engineering Conference, American Society of Civil Engineers, pp 77-90.

Wood, W. L., and Meadows, G. A. 1975. "Unsteadiness in Longshore Currents," Geophysical Research Letters, Vol 2, No. 11, pp 503-505.

Wu, C-S., Thornton, E. B., and Guza, R. T. 1985. "Waves and Longshore Currents: Comparison of a Numerical Model with Field Data," Journal of Geophysical Research, Vol 90, No. C3, pp 4951-4958.



APPENDIX A: NISHIMURA'S SQUARE-WAVE APPROXIMATION

1. Nishimura (1982, 1988) introduced an approximate method for numerically evaluating the time integration of the full bottom friction term in Equation 57 (see main text). In this method, the sinusoidally varying horizontal component of the wave orbital velocity  $u_o = u_m \cos(2\pi t/T)$  is replaced by a square wave having the same area as the original sinusoid. The velocity is then expressed as:

$$u_o = \begin{cases} \frac{2}{\pi} u_m, & 0 < t < \frac{T}{4}, \frac{3}{4} T < t < T \\ -\frac{2}{\pi} u_m, & \frac{T}{4} < t < \frac{3}{4} T \end{cases} \quad (\text{A1})$$

Equation A1 represents the least squares fit of a square wave to the original  $\cos(2\pi t/T)$  term in Equation 57. By this approximation, the bottom orbital velocity becomes time independent in the different intervals indicated above, and the integration is readily carried out for each interval. The time integration may thus be written,

$$f_{by} = \frac{1}{T} \left( \int_0^{\frac{T}{4}} \frac{1}{\rho} \tau_{by} dt + \int_{\frac{T}{4}}^{\frac{3T}{4}} \frac{1}{\rho} \tau_{by} dt + \int_{\frac{3T}{4}}^T \frac{1}{\rho} \tau_{by} dt \right) \quad (\text{A2})$$

where

$$\frac{\tau_{by}}{\rho} = c_f \sqrt{u_o^2 + V^2 + 2u_o V \sin\theta} (V + u_o \sin\theta) \quad (\text{A3})$$

2. To evaluate Equation A2, the expression for  $u_o$  in Equation A3 should be evaluated for the respective time interval according to Equation A1. Since the integrand is constant within each interval, the three integrals in Equation A2 may be evaluated as:

$$\frac{1}{\rho} \int_0^{\frac{T}{4}} \tau_{by} dt = c_f \sqrt{w^2 + V^2 + 2wV\sin\theta} (V + w\sin\theta) \frac{T}{4} \quad (\text{A4})$$

$$\frac{1}{\rho} \int_{\frac{T}{4}}^{\frac{3T}{4}} \tau_{by} dt = c_f \sqrt{w^2 + V^2 - 2wV\sin\theta} (V - w\sin\theta) \frac{T}{2} \quad (\text{A5})$$

$$\frac{1}{\rho} \int_{\frac{3T}{4}}^T \tau_{by} dt = c_f \sqrt{w^2 + V^2 + 2wV\sin\theta} (V + w\sin\theta) \frac{T}{4} \quad (\text{A6})$$

The definition  $w = (2/\pi)u_m$  was introduced in Equations A4 to A6 following the notation of Nishimura (1982, 1988). Thus, Equation A2 may be written,

$$f_{by} = \frac{c_f}{2} [Z_1(V + w\sin\theta) + Z_2(V - w\sin\theta)] \quad (\text{A7})$$

where

$$Z_1 = \sqrt{w^2 + V^2 + 2wV\sin\theta} \quad (\text{A8})$$

$$Z_2 = \sqrt{w^2 + V^2 - 2wV\sin\theta} \quad (\text{A9})$$

3. Rearrangement of Equation A7 yields:

$$f_{by} = \frac{c_f}{2} [V(Z_1 + Z_2) + w\sin\theta(Z_1 - Z_2)] \quad (\text{A10})$$

The conjugate expression  $(Z_1 + Z_2)$  is used to multiply (and divide) the last term within the bracket of Equation A10, and, after carrying out the multiplication, the following simplified equation is obtained:

$$f_{by} = c_f V \left( Z + \frac{w^2}{Z} \sin^2 \theta \right) \quad (\text{A11})$$

where

$$Z = \frac{Z_1 + Z_2}{2} \quad (\text{A12})$$

4. Equation A11 is the square-wave approximation for the time-averaged friction term as presented by Nishimura (1982, 1988) if no cross-shore current is present. It can be shown that Equation A11 reduces to the formal expressions for the linear bottom friction term for weak mean current (Equation 59) and a pure quadratic form for strong mean current (Equation 60).

5. In the nonlinear current model developed in this report, Equation A11 is used to evaluate the bottom friction term. Nishimura (1988) states that Equation A11 deviates at most by 10 percent from the original formulation in Equation 57. Figure A1 displays a comparison between the friction term as predicted by Equation A11 and the full equation (Equation 57) for various incident wave angles and ratios  $V/u_m$ . For the range of values studied, the approximation is quite good and within Nishimura's error margin.

6. In numerical solution of the nonlinear longshore momentum equation for the current, an iterative technique is employed. To evaluate the friction term  $f_{by}$  the velocity obtained at the previous iteration is used to determine  $Z$ , thereby giving a linear dependence on  $V$ . Once the difference between two consecutively calculated velocity distributions is smaller than some predetermined tolerance at each grid point, the calculation is halted. As an initial guess, the linear solution with a friction term according to Equation 59 is used. However, depending on  $\theta$  and  $V/u_m$ , this initial estimate could still be far off, not reducing the large number of iterations required. Because reduction of execution time is one of the practical objectives of this study, improvements in the initial guess are of importance.

7. As discussed in Part V, if lateral mixing is neglected it is possible to derive a correction factor to multiply the linear solution to obtain the nonlinear solution. This factor is a function of  $\theta$  and  $V/u_m$  and cannot be expressed analytically, only graphically. To improve the initial guess for

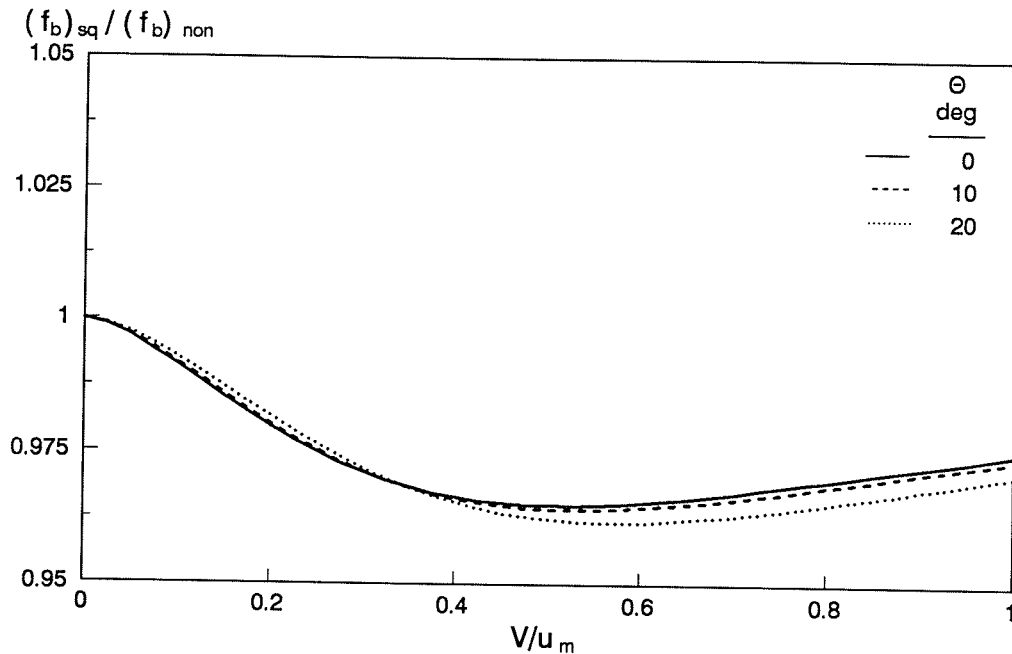


Figure A1. Evaluation of the square-wave approximation

the current distribution, a correction factor was derived based on Equation A11 and Equation 59 (used in the linear solution). This correction factor was then approximated with the following empirical equation derived for the condition  $V_{lin}/w > 0.5$ ,

$$\alpha = (0.754 + 0.00314 |\theta|) \left( \frac{|V_{lin}|}{w} \right)^{-0.333} \quad (A13)$$

where  $\theta$  is given in degrees and  $V_{lin}$  refers to the linear current solution using a friction term according to Equation 59. Thus, if  $V_{lin}/w > 0.5$ , at the first iteration the linear current solution obtained is multiplied with  $\alpha$  as given from Equation A13; if  $V_{lin}/w \leq 0.5$ , the linear solution is retained as the first guess without correction. This correction procedure saves one to three iterations from the typically four to eight iterations required for convergence of  $V$  to 1 percent of the previous value at any point on the grid.

APPENDIX B: SUMMARY OF DATA USED IN THE SIMULATIONS

Laboratory Data from Visser (1982)

1. The data for the current measurements are taken from Visser (1982). Because of observed and potential disturbances of the current at the basin boundaries, for the present simulations the current was averaged from two centrally located transects. The transects are Cases 1, 4, and 7, transects 4 and 5; Case 3, transects 8 and 9 (Tables B1, B2, B3, and B4). Mean water surface elevations were digitized from figures appearing in Visser (1984a).

Table B1  
Visser (1982) Case 1: Slope 0.101

<u>Distance Offshore</u> <u>m</u>	<u>Wave Height</u> <u>m</u>	<u>Current</u> <u>m/sec</u>	<u>Mean Water Surface Elevation</u> <u>m</u>
0.10	--	0.401	--
0.30	--	0.600	0.027
0.50	0.029	0.668	0.016
0.70	0.048	0.666	0.007
0.90	0.057	0.593	-0.001
1.10	0.075	0.424	-0.003
1.30	0.098	0.289	-0.003
1.50	0.103	0.184	-0.003
1.70	0.096	0.121	-0.002
1.90	0.083	0.080	-0.002
2.10	0.074	0.060	-0.002
2.30	0.075	0.042	--
2.50	0.077	0.032	--
2.70	0.079	0.024	--
3.10	0.082	0.017	--

Table B2  
Visser (1982) Case 3: Slope 0.101

<u>Distance Offshore</u> m	<u>Wave Height</u> m	<u>Current</u> m/sec	<u>Mean Water Surface Elevation</u> m
0.18	--	0.406	0.020
0.38	0.018	0.456	0.014
0.58	0.031	0.472	0.007
0.78	0.048	0.451	0.002
0.98	0.055	0.418	-0.003
1.18	0.085	0.354	-0.002
1.38	0.094	0.269	-0.002
1.58	0.093	0.201	-0.002
1.78	0.092	0.139	-0.001
1.98	0.090	0.095	-0.001
2.18	0.092	0.062	--
2.38	0.087	0.039	--
2.58	0.083	0.024	--
2.98	0.091	0.009	

Table B3  
Visser (1982) Case 4: Slope 0.050

<u>Distance Offshore</u> m	<u>Wave Height</u> m	<u>Current</u> m/sec	<u>Mean Water Surface Elevation</u> m
0.01	--	0.000	0.016
0.21	--	0.114	0.015
0.41	--	0.275	0.014
0.81	0.016	0.332	0.011
1.21	0.026	0.389	0.008
1.61	0.034	0.375	0.003
2.01	0.056	0.301	-0.001
2.41	0.087	0.218	-0.001
2.81	0.084	0.139	-0.001
3.21	0.078	0.099	-0.001
3.61	0.080	0.063	-0.001
4.01	0.079	0.034	-0.001
4.41	0.076	0.016	--
4.81	0.076	0.007	--
5.21	0.075	0.000	--
5.61	0.072	-0.006	--

Table B4  
Visser (1982) Case 7: Slope 0.050

Offshore Distance m	Wave Height m	Current m/sec
0.13	--	0.000
0.33	--	0.060
0.53	--	0.102
0.93	0.009	0.148
1.33	0.019	0.194
1.73	0.029	0.202
2.13	0.041	0.172
2.53	0.060	0.120
2.93	0.089	0.066
3.33	--	0.040
3.73	--	0.024
4.13	--	0.011
4.53	--	0.006
4.93	--	0.001
5.33	--	-0.004

Field Data from Kraus and Sasaki (1979)

2. These data are taken from Kraus and Sasaki (1979), who list current measurements made at Urahama Beach, Japan, at seven transects alongshore. The values in Table B5 are averages from all transects.

Table B5  
Kraus and Sasaki (1979) Field Data

<u>Distance Offshore</u> <u>m</u>	<u>Depth</u> <u>m</u>	<u>Current</u> <u>m/sec</u>
5	0.45	0.63
10	0.50	0.68
15	0.52	0.66
20	0.59	0.66
25	0.69	0.75
30	0.69	0.77
35	0.76	0.51
40	0.99	0.41
45	1.11	0.29
50	1.26	0.28
55	--	0.18

Field Data from Thornton and Guza (1986)

3. The data listed in Tables B6 to B9 are presented in Thornton and Guza (1989) and summarize measurements of wave height and longshore current made during 3-6 February 1980 at Leadbetter Beach in California. The data set is also discussed in Wu, Thornton, and Guza (1985) and Thornton and Guza (1986). The distance offshore is given with respect to the mean shoreline measured during the data collection interval. The wave height listed is the root-mean-square value, whereas the current velocity represents a mean value. Wave characteristics for the measurement events are given in Table 1 in the main

text. An asterisk in a table implies that an average value is given of two gages located close together.

Table B6  
Thornton and Guza (1989) Field Measurements of 3 February

<u>Distance Offshore</u> <u>m</u>	<u>Depth</u> <u>m</u>	<u>Wave Height</u> <u>m</u>	<u>Current</u> <u>m/sec</u>
6.93	0.37	0.40	0.23
9.93	0.50	0.31	0.11
12.99	0.65	0.50	0.35
15.95	0.80	0.48	0.44
18.75	0.94	0.54	0.44
21.88	1.11	0.60	0.50
24.80	1.24	0.59	0.40
31.00	1.48	0.67	0.39
35.12	1.65	0.68	0.35
39.70	1.77	0.71	0.34
57.16	2.28	0.68	--
68.96	3.02	0.61	0.15
80.70	3.80	0.55*	0.08
128.60	6.51	0.49	-0.04

Table B7

Thornton and Guza (1989) Field Measurements of 4 February

<u>Distance Offshore</u> <u>m</u>	<u>Depth</u> <u>m</u>	<u>Wave Height</u> <u>m</u>	<u>Current</u> <u>m/sec</u>
10.39	0.52	0.36	0.36
13.39	0.65	0.35	0.34
16.45	0.78	0.40	0.44
19.41	0.89	0.44	0.45
22.21	1.01	0.50	0.46
25.34	1.16	0.57	0.48
28.26	1.24	0.60	0.43
31.31	1.34	0.64	0.44
34.46	1.42	0.59	0.38
38.58	1.56	0.63	0.32
43.16	1.70	0.66	0.17
60.62	2.37	0.67	--
72.42	3.03	0.60	--
84.16	3.79	0.56*	0.06
132.06	6.50	0.49	-0.03

Table B8

Thornton and Guza (1989) Field Measurements of 5 February

<u>Distance Offshore</u> <u>m</u>	<u>Depth</u> <u>m</u>	<u>Wave Height</u> <u>m</u>	<u>Current</u> <u>m/sec</u>
11.36	0.65	0.34	0.26
14.42	0.78	0.38	0.35
17.38	0.88	0.43	0.35
20.18	0.97	0.44	0.34
23.31	1.07	0.47	0.34
26.23	1.12	0.48	0.29
29.28	1.18	0.51	0.30
32.43	1.26	0.50	0.25
36.55	1.37	0.59	0.21
41.13	1.52	0.59	0.18
47.60	1.78	--	0.13
58.59	2.21	0.55	--
70.39	2.90	0.49	--
82.13	3.64	0.45*	0.04
130.03	6.35	0.40	-0.03

Table B9

Thornton and Guza (1989) Field Measurements of 6 February

<u>Distance Offshore</u> <u>m</u>	<u>Depth</u> <u>m</u>	<u>Wave Height</u> <u>m</u>	<u>Current</u> <u>m/sec</u>
7.53	0.50	0.20	0.15
10.58	0.65	0.23	0.20
13.23	0.70	0.24	0.16
13.58	0.71	0.27	0.15
16.38	0.77	0.27	0.18
19.51	0.85	0.34	0.19
22.43	0.90	0.31	0.13
25.48	0.95	0.32	0.14
28.63	1.03	0.31	0.08
32.75	1.18	0.37	0.04
37.33	1.38	0.34	0.05
54.79	2.22	0.30	--
66.59	2.79	0.28	0.02
78.33	3.45	0.26*	0.00
126.23	6.16	0.26	-0.03

Barred Profile of Ebersole and Dalrymple (1980)

4. Table B10 lists the data used to generate a barred profile configuration taken from Ebersole and Dalrymple (1980). The values were digitized from a figure appearing in that reference.

Table B10

Barred Profile of Ebersole and Dalrymple (1980)

<u>Distance Offshore</u>	<u>Water Depth</u>
<u>m</u>	<u>m</u>
-10	0.00
0	-0.27
10	-0.50
20	-0.87
30	-1.24
40	-1.67
50	-2.02
60	-2.31
70	-2.50
80	-2.69
90	-2.89
100	-2.98
110	-3.16
120	-3.06
130	-2.81
140	-2.45
150	-2.45
160	-2.93
170	-3.41
180	-4.01
190	-4.63
200	-5.02
210	-5.31
220	-5.55
230	-5.72
240	-6.03
250	-6.28
260	-6.46
270	-6.66
280	-7.00

## APPENDIX C: NOTATION

- $c_f$  = bottom friction coefficient  
 $(c_f)_{lin}$  = friction coefficient associated with the linearized friction law  
 $(c_f)_{non}$  = friction coefficient associated with the nonlinear (quadratic) bottom friction law  
 $d$  = total water depth (m)  
 $f_{by}$  = formal expression for the longshore component of the bottom friction stress ( $m^2/sec^2$ )  
 $(f_{by})_{lin}$  = linearized form of  $f_{by}$  ( $m^2/sec^2$ )  
 $(f_{by})_{non}$  = complete (nonlinear) form of  $f_{by}$ , evaluated numerically ( $m^2/sec^2$ )  
 $(f_{by})_{sq}$  = evaluation of  $f_{by}$  by the square-wave approximation ( $m^2/sec^2$ )  
 $g$  = acceleration produced by gravity ( $m/sec^2$ )  
 $h$  = still-water depth (m)  
 $u$  = cross-shore component of the total current velocity (m/sec)  
 $u_b$  = cross-shore component of the horizontal water particle velocity at the bottom (m/sec)  
 $u_m$  = magnitude of the horizontal water particle velocity (m/sec)  
 $u_*$  = shear velocity (m/sec)  
 $v$  = longshore component of the total current velocity (m/sec)  
 $v_b$  = longshore component of the horizontal water particle velocity at the bottom (m/sec)  
 $w$  = auxiliary quantity entering the square-wave time-averaged friction approximation (m/sec)  
 $x$  = cross-shore coordinate directed positive seaward (m)  
 $y$  = longshore coordinate (m)  
 $z$  = vertical coordinate directed positive from still-water surface (m)  
 $z_o$  = roughness length scale, or elevation where the wind speed  $W$  is zero (m)  
 $A$  = auxiliary quantity used to simplify notation in expressing the longshore current governing equation and related to contributions from lateral mixing ( $m^3/sec$ )  
 $AH_i$  = auxiliary quantity used to simplify notation in the numerical solution of the longshore current equation and related to contributions from lateral mixing (m/sec)

- $B$  = auxiliary quantity used to simplify notation in expressing the longshore current governing equation and related to contributions from bottom friction (m/sec)
- $BH_i$  = auxiliary quantity used to simplify notation in the numerical solution of the longshore current equation and related to contributions from bottom friction (m/sec)
- $C$  = wave phase speed (m/sec)
- $C_D$  = drag coefficient for the wind-water interface
- $(C_D)_{10}$  = drag coefficient evaluated at the 10-m elevation from the water or land surface
- $C_g$  = wave group speed (m/sec)
- $CH_i$  = auxiliary quantity used to simplify notation in the numerical solution of the longshore current equation and related to contributions from lateral mixing (m/sec)
- $C_o$  = wave phase speed in deep water (m/sec)
- $EE_i$  = auxiliary quantity in the double-sweep algorithm
- $F$  = wave energy flux (Nm/m/sec)
- $F_{bx}$  = cross-shore component of the bottom friction shear stress divided by the total water depth (m/sec<sup>2</sup>)
- $F_{by}$  = longshore component of the bottom friction shear stress divided by the total water depth (m/sec<sup>2</sup>)
- $F_i$  = wave energy flux at grid cell  $i$  (Nm/m/sec)
- $F_s$  = wave energy flux corresponding to the stable wave height (Nm/m/sec)
- $F_{si}$  = wave energy flux corresponding to the stable wave height at grid cell  $i$  (Nm/m/sec)
- $FF_i$  = auxiliary quantity in the double-sweep algorithm (m/sec)
- $H$  = wave height (m)
- $H_i$  = wave height at grid boundary  $i$  (m)
- $H_p$  = wave height threshold having exceedance probability  $1-p$  (m)
- $H_{rms}$  = root-mean-square wave height (m)
- $H_s$  = wave height associated with the stable condition (m)
- $L_x$  = cross-shore component of lateral mixing term (m/sec<sup>2</sup>)
- $L_y$  = longshore component of the lateral mixing term (m/sec<sup>2</sup>)
- $N$  = number of grid cells
- $RH_i$  = auxiliary quantity used to simplify notation in the numerical solution of the longshore current equation and related to contributions from the wave and wind driving terms (m<sup>2</sup>/sec<sup>2</sup>)
- $R_{bx}$  = cross-shore component of the wave driving term (m/sec<sup>2</sup>)

- $R_{by}$  = longshore component of the wave driving term (m/sec<sup>2</sup>)  
 $R_{sx}$  = cross-shore component of the wind driving term (m/sec<sup>2</sup>)  
 $R_{sy}$  = longshore component of the wind driving term (m/sec<sup>2</sup>)  
 $S_{xx}$  = radiation stress component in the direction of the waves (N/m)  
 $S_{xy}$  = shoreward-directed radiation stress component alongshore (N/m)  
 $S_{yy}$  = radiation stress component alongshore (N/m)  
 $U$  = cross-shore component of the mean (time-averaged) current speed (m/sec)  
 $V$  = longshore current speed (longshore component of the mean (time-averaged) current speed) (m/sec)  
 $V_i$  = longshore current speed at cell  $i$  (m/sec)  
 $V_{lin}$  = longshore current speed obtained from the linear friction stress law (m/sec)  
 $V_{non}$  = longshore current speed obtained from the nonlinear (quadratic) friction stress law (m/sec)  
 $W$  = wind speed (m/sec)  
 $W_{10}$  = wind speed at the 10-m elevation from the water surface (m/sec)  
 $W_y$  =  $|W|\sin\phi$ , longshore component of wind speed (m/sec)  
 $Z$  = auxiliary quantity entering the square-wave time-average friction approximation (m/sec)  
 $Z_1, Z_2$  = auxiliary quantities entering the square-wave time-average friction approximation (m/sec)  
 $\alpha$  = longshore current speed calculated with nonlinear model divided by the speed calculated with the linear model  
 $\gamma$  = ratio of wave height to water depth for breaking and nonbreaking waves.  
 $\gamma_b$  = breaker index (ratio of wave height and water depth at incipient breaking)  
 $(\gamma_b)_c$  = calculated breaker index  
 $(\gamma_b)_m$  = measured breaker index  
 $\Gamma$  = empirical coefficient relating the stable wave height to the water depth  
 $\epsilon$  = lateral mixing eddy viscosity coefficient (m<sup>2</sup>/sec)  
 $\epsilon_{i,j}$  = components of the lateral mixing eddy viscosity coefficient tensor in which subscripts  $(i,j)$  each denote the coordinate axes components  $(x,y)$  (m<sup>2</sup>/sec)  
 $\zeta$  =  $\sin\theta$

- $\eta$  = mean displacement of the water surface from the still-water level as induced by waves and wind (called "setup" if positive displacement and "setdown" if negative) (m)
- $\eta_i$  = mean displacement of the water surface at grid cell  $i$  (m)
- $\theta$  = angle of wave crests to the bottom contours (m)
- $\theta_i$  = angle of wave crests with respect to the bottom contours at grid cell  $i$
- $\kappa$  = empirical decay coefficient in the wave dissipation term
- $\kappa$  = von Karman's constant (approximately 0.41)
- $\Lambda$  = empirical coefficient in lateral mixing eddy viscosity
- $\Lambda_{lin}$  = value of  $\Lambda$  evaluated with the linear current model
- $\Lambda_{non}$  = value of  $\Lambda$  evaluated with the nonlinear current model
- $\xi$  = surf similarity parameter
- $\pi$  = 3.14159265...
- $\rho$  = density of water (kg/m<sup>3</sup>)
- $\rho_a$  = density of air (kg/m<sup>3</sup>)
- $\tau_b$  = instantaneous total bottom shear stress (N/m<sup>2</sup>)
- $\tau_{bx}$  = cross-shore component of the instantaneous total bottom shear stress (N/m<sup>2</sup>)
- $\tau_{by}$  = longshore component of the instantaneous total bottom shear stress (N/m<sup>2</sup>)
- $\tau_s$  = magnitude of the total shear stress induced by wind at the water surface (N/m<sup>2</sup>)
- $\tau_{sx}$  = cross-shore component of the shear stress induced by wind at the water surface (N/m<sup>2</sup>)
- $\tau_{sy}$  = longshore component of the shear stress induced by wind at the water surface (N/m<sup>2</sup>)
- $\phi$  = incident angle of the wind
- $\psi$  = ratio of longshore current speed of linear model to the magnitude of the wave orbital velocity at the bottom
- $\langle \rangle$  = time-averaging operation